Chapter 3
Physical Processes

3.1 Phases and Transitions Between Them

Every transition is a crisis…
Johann Wolfgang von Goethe, Wilhelm Meister's Apprenticeship

A phase is a macroscopic amount of substance which possesses uniform chemical composition and physical properties and is confined by a boundary surface. Single-component substance can exist in four major states of matter: gas, liquid, crystal, and glass [1]. The conversion from one state to another is called a phase transition. At constant pressure, a phase transition is caused by changes in temperature. An increase in temperature intensifies molecular motion that destabilizes molecular structure of a given phase so that at a certain temperature it rearranges to the structure of another more energetically favorable phase, i.e., a phase that has lower molar Gibbs energy, G (Fig. 3.1). Normally this would be a more loosely packed (more mobile) phase. The transition happens at the temperature when two phases have the same Gibbs energy, i.e., $\Delta G = 0$. It means that at this temperature the phases can coexist in equilibrium.

When heated, a typical crystal would melt first. This happens at the temperature of melting, T_m, past which a tightly packed crystalline lattice rearranges to a loosely packed liquid phase. Further heating to the temperature of boiling, T_b, causes liquid to vaporize. At this temperature, the vapor pressure of the liquid rises to the atmospheric pressure, and the liquid structure unpacks to practically unbound molecules of the gas phase. Crystalline compounds can transform directly into the gas phase without melting, provided that the liquid phase does not exist at a given pressure. This is the sublimation transition and it occurs at the temperature, T_s. At this temperature, the vapor pressure of the crystal becomes equal to the atmospheric pressure. There are a very few crystalline compounds that can coexist in equilibrium with its vapor phase at ambient pressure. The best-known example is carbon dioxide (dry ice) for which T_s at 1 atm is −78.5 °C [2].

It should be stressed that the transition temperatures T_m, T_b, and T_s denote equilibria between the bulk phases. In other words, on crossing the transition

S. Vyazovkin, *Isoconversional Kinetics of Thermally Stimulated Processes,*
DOI 10.1007/978-3-319-14175-6_3

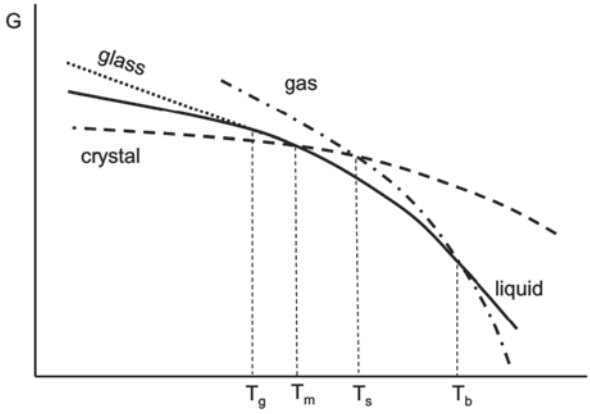

Fig. 3.1 Temperature dependence on the Gibbs free energy for solid, liquid, gas, and glass phases at constant pressure

temperature, the whole bulk of one phase would convert entirely to another phase. However, the processes of vaporization and sublimation occur to some extent well below their respective transition temperatures. This is an entirely surface phenomenon. Because the surface molecules are bound to fewer neighbors than the molecules in the bulk, they have higher mobility and through fluctuation can gain enough energy to leave the surface. As long as the condensed substance is enclosed in a container whose volume is not much larger than the volume of the substance, the process would continue until the vapor phase saturates, i.e., its pressure reaches an equilibrium value at a given temperature. Otherwise, it will continue until the condensed phase is gone. Similarly, the higher mobility of the surface layer in the crystal melts at a temperature lower than T_m, while the bulk of the crystal remains solid indefinitely.

From the equilibrium standpoint, the reverse transitions are supposed to happen at the same temperature as the forward ones, i.e., condensation of vapor to crystal at T_s, condensation of vapor to liquid at T_b, and crystallization of liquid at T_m. In reality, all these processes occur at markedly lower temperatures because of a significant energy barrier to nucleation, i.e., the energy of creating the surface of a nucleus of the new condensed phase [3, 4]. The barrier can only be overcome when ΔG (Fig. 3.1) is negative enough to outweigh the surface energy of the new phase, i.e., when the fluid phase is supercooled below the equilibrium transition temperature, at which ΔG is zero.

An important property of supercooled or metastable liquids [3] is their ability to form the glass phase. While thermodynamic drive toward crystallization increases with decreasing temperature, the molecular mobility becomes increasingly slower. At certain temperature, T_g (Fig. 3.1), the molecular mobility becomes so slow that the supercooled liquid cannot maintain the equilibrium liquid structure at a given rate of cooling. At this point, the supercooled liquid turns into a glass, and the respective temperature is taken as the glass transition temperature. The glass is a non-equilibrium phase and, thus, its Gibbs energy is larger than that of the supercooled liquid. Therefore, the glass is bound to relax continuously toward the supercooled liquid. Unlike the equilibrium phases, the glass cannot coexist in equilibrium with any other phases, and for that reason, the glass transition temperature can never be

defined with the same certainty as the transition temperatures between the equilibrium phases.

Another important difference between the glass transition and other transitions presented in Fig. 3.1 is that at T_g the G versus T curve for glass merges smoothly with the curve for liquid, whereas the G versus T curves for other transitions demonstrate a change in the slope at the transition temperature. Mathematically, a change in the slope is equivalent to discontinuity of the first derivative of G with respect to T, which, in turn, means discontinuity in the entropy, S, and enthalpy, H:

$$S = -\left(\frac{\partial G}{\partial T}\right)_P \tag{3.1}$$

$$H = \left[\frac{\partial (G/T)}{\partial (1/T)}\right]_P. \tag{3.2}$$

Per Ehrenfest's classification [5], the phase transitions that show discontinuity in the first derivative of the Gibbs energy are defined as transitions of first order. The glass transition does not show discontinuity in the first but in the second derivative of G with respect to T, which means discontinuity in the heat capacity:

$$C_P = -T\left(\frac{\partial^2 G}{\partial T^2}\right)_P = \left(\frac{\partial H}{\partial T}\right)_P. \tag{3.3}$$

Discontinuity in the second derivative classifies a phase transition as being of second order. Although the glass transition reveals this feature of a second-order transition, it is not the classical second-order transition that occurs between two phases coexisting in equilibrium with each other.

The aforementioned difference between the glass and first-order transitions has direct implication for experimental measurements of these processes by differential scanning calorimetry (DSC). The instrument measures the heat flow that has two principal contributions:

$$\Phi \equiv \frac{\mathrm{d}H}{\mathrm{d}t} = C_P\left(\frac{\mathrm{d}T}{\mathrm{d}t}\right) + \Delta H\left(\frac{\mathrm{d}\alpha}{\mathrm{d}t}\right). \tag{3.4}$$

The first term in the right-hand side represents a contribution from the sensible heat flow. This is the heat produced by substance of finite heat capacity in response to changing temperature. The second term is a contribution from the latent heat flow. This heat arises from a change in the enthalpy, ΔH, due to a phase transition or chemical reaction. Per Eq. 3.2, first-order transitions are accompanied by the latent heat. In DSC, they manifest themselves as peaks because as seen from Eq. 3.4, the heat is released in proportion to the processes rate ($\mathrm{d}\alpha/\mathrm{d}t$), which under the conditions of continuous heating (or cooling) always starts from and finishes at zero, passing some nonzero value in between. On the other hand, the glass transition is

not accompanied by the latent heat, i.e., $\Delta H = 0$ in Eq. 3.4. Then, the heat flow signal is produced by the first term in Eq. 3.4. According to Eq. 3.3, the glass transition is accompanied by a change in the heat capacity. At T_g, its value changes from C_P of the glass to C_P of the liquid, if the transition is measured on heating, or other way around when it is measured on cooling. As a result, the glass transition manifests itself as a step change between two nearly linear segments of the heat flow.

As follows from the above discussion, the solid state of matter can exist either as the crystal or as the glass phase. The issue, however, can be further complicated by the existence of more than one crystal phase for the same solid compound. This phenomenon known as polymorphism [1] is widely encountered in inorganic [6, 7] and organic [8] compounds as well as in elements, for which it is referred to as allotropy. The polymorphic solid–solid transitions can be of first and second order. They are typically easy to measure by DSC.

Different liquid phases can be encountered in a single-component liquid. The examples of the liquid–liquid transitions in isotropic liquids are quite rare [9–12]. Much more common are the transitions in liquid crystals, whose liquid state can exist in disordered (isotropic) as well as in ordered (smectic, nematic, cholesteric) phases [4]. The liquid crystalline phases are also called mesophases to emphasize their intermediate character between the solid and liquid phases. For liquids involving more than one component (i.e., mixtures or solutions), a common liquid–liquid phase transition is mixing and demixing (phase separation). The transition can be caused by heating or cooling of a solution and results in its separation in the solvent-rich and solute-rich phases. A very special case of a phase transition in a solution is gelation [4, 13]. It results in conversion of a liquid solution into a gel, which is a network of cross-linked solute molecules that entrap a solvent. A gel is a soft solid or a liquid that has lost its ability to flow. Most of the aforementioned transitions in liquids are of first order and normally appear in DSC as well-defined peaks, although some transitions [14] in liquid crystals can be of second order.

The following sections of this chapter provide a discussion about the kinetics of most of the aforementioned transitions.

3.2 Vaporization and Sublimation

All existing things soon change, and they will either be reduced to vapor, if indeed all substance is one, or they will be dispersed
Marcus Aurelius, Meditations

3.2.1 Background

Vaporization and sublimation are phase transitions in which the respective liquid and solid compounds transform to the gas phase. Both processes are promoted by heating that intensifies molecular motion and thus initiates breakage of the intermolecular (cohesive) bonds that hold a compound in the condensed state. Depending

on the strength of the inter- and intramolecular bonds, vaporization and/or sublimation may or may not be accompanied by decomposition. For example, a typical covalent compound such as a hydrocarbon is held in the condensed phase by weak van der Waals forces. It would undergo vaporization or sublimation at temperatures that are too low to break the strong covalent bonds and cause decomposition of the compound. However, decomposition may readily occur in ionic compounds that are held in the condensed phase by strong ionic forces. Decomposition can complicate significantly the kinetics of vaporization or sublimation that by itself is relatively simple.

In 1913, Langmuir [15, 16] proposed an equation that describes the rate of vaporization in vacuum:

$$-\frac{\mathrm{d}m}{\mathrm{d}t} = \gamma\ P\sqrt{\frac{M}{2\pi RT}}, \tag{3.5}$$

where $\mathrm{d}m/\mathrm{d}t$ is the rate of mass loss per unit of the surface area, M is molecular mass of the gaseous compound, P is the vapor pressure of the compound, R is the gas constant, T is the temperature, and γ is the accommodation coefficient. The latter was taken to be close to unity for reasonable molecular masses, e.g., it is 0.98 for carbon dioxide [16]. The equation was derived from the Knudsen equation [17] for the effusion rate through an orifice that lies in the foundation of the Knudsen method for determining molar mass or/and the vapor pressure from the mass loss rate data [18].

We can isolate the temperature-dependent parameters in Eq. 3.5 and write it in a more convenient form using the extent of conversion:

$$\frac{\mathrm{d}\alpha}{\mathrm{d}t} = \mathrm{Const}PT^{-0.5}, \tag{3.6}$$

where Const collects all temperature-independent parameters. The vapor pressure in Eq. 3.6 depends on temperature in accord with the Clausius–Clapeyron equation:[18]

$$\ln P = C - \frac{\Delta H}{RT}, \tag{3.7}$$

where C is a constant and ΔH is the enthalpy of vaporization or sublimation. Then with regard to Eq. 3.7, Eq. 3.6 can be used to derive the activation energy of the process as follows:

$$E = -R\left[\frac{\mathrm{d}\ln(\mathrm{d}\alpha/\mathrm{d}t)}{\mathrm{d}T^{-1}}\right] = \Delta H - \frac{1}{2}RT. \tag{3.8}$$

The second term in Eq. 3.8 does not exceed a few kilojoules in any reasonable temperature range and thus can be neglected. Therefore, Eq. 3.8 suggests that if one

fits the temperature dependence of the rate of vaporization or sublimation to the Arrhenius equation, the resulting activation energy should provide a fair estimate for the enthalpy of the process.

As fairly noticed by Price and Hawkins [19], the accommodation coefficient in Eq. 3.5 should not be assumed to be unity when the mass loss measurement is conducted in a flow of a purge gas at ambient pressure as typically is the case of regular thermogravimetric analysis (TGA) runs. The actual measurements on methylparaben by Chatterjee et al. [20] have produced an estimate of $\gamma = 5.8 \times 10^{-5}$ that is too low to be meaningful. Some rational insights into the problem have been provided by Pieterse and Focke [21], who suggested that in order to be applicable to the conditions other than vacuum, the Langmuir equation needs to account for diffusion of the vapor in surrounding gas. The equation derived by Pieterse and Focke is as follows:

$$-\frac{\mathrm{d}m}{\mathrm{d}t} = PD\frac{M}{zRT}, \tag{3.9}$$

where D is the diffusion coefficient of the vapor compound in the surrounding gas, and z is the height of the pan occupied by the gas. Comparing Eq. 3.9 with Eq. 3.5 suggests that the value of the coefficient γ is:

$$\gamma = \frac{D}{z}\sqrt{\frac{2\pi M}{RT}}. \tag{3.10}$$

Equation 3.10 affords explaining the excessively small values of γ. The order of magnitude of γ is determined primarily by the value of D whose typical order of magnitude is about $10^{-4} - 10^{-5}$ m^2s^{-1}. Substitution of the actual values *D, z, T,* and *M* for vaporization of methylparaben yields $\gamma = 4.8 \times 10^{-5}$ which is quite close to the value experimentally found by Chatterjee et al. [20].

Following the same logic as above, we can use Eq. 3.9 to derive the activation energy of vaporization or sublimation. The resulting expression is as follows:

$$E = -R\left[\frac{\mathrm{d}\ln(\mathrm{d}\alpha/\mathrm{d}t)}{\mathrm{d}T^{-1}}\right] = \Delta H + E_\mathrm{D} - RT, \tag{3.11}$$

where E_D is the activation energy of diffusion. For diffusion of gases in gases, the typical values of E_D are quite small. Figure 3.2 demonstrates the Arrhenius plots for the temperature dependence of the diffusion coefficient of several gases in helium [22]. It is seen that the plots have nearly the same slopes. The E_D values estimated from these slopes fall in the range 5–6 kJ mol^{-1}. Considering that the RT term in Eq. 3.11 has similar magnitude but its sign is opposite to E_D, we can expect these two terms to cancel each other at least partially. Therefore, we can conclude again that the activation energy of vaporization or sublimation should generally provide a reasonable estimate of the process enthalpy.

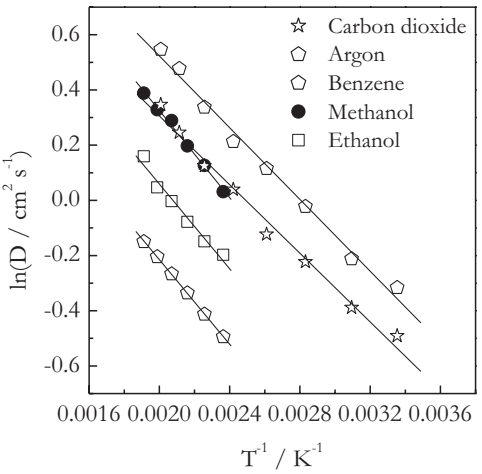

Fig. 3.2 Arrhenius plots for the temperature dependence of the diffusion coefficient of various gases in helium. (Data taken from Seager et al. [22])

3.2.2 Isoconversional Treatment

When it comes to applying an isoconversional method to treat the kinetics of vaporization or sublimation, one should notice that neither Eq. 3.5 nor Eq. 3.9 includes the value of the mass lost (m) in their respective right-hand sides. It means that if one replaces the mass with the conversion, these equations would not include in their right-hand sides any reaction model either. Although it may sound confusing, in fact these equations do include one very specific reaction model, $f(\alpha)=1$. This is called the zero-order reaction model. This model represents a process whose rate remains constant throughout the whole range of conversions from 0 to 1. However, the rate of vaporization or sublimation is proportional to the free surface area (i.e., the surface area that is in contact with surrounding gas or vacuum) of the condensed substance. Then the rate of these processes would be independent of conversion only in a specific case when the free surface area does not change with the process progress. This is a reasonable assumption when, for example, vaporization rate is measured for a liquid that fills one of cylindrical pans (Fig. 3.3a) usually used in thermal analysis studies. In this case, the free surface area of the liquid would be determined by the circular cross-sectional area of the pan until the interface reaches the pan bottom and the liquid breaks into several droplets. Nevertheless, when the condensed substance is present in the form of individual droplets or crystals (Fig. 3.3b), the free surface area as well as the process rate would be decreasing with increasing the conversion. In this situation, the rate equation for vaporization or sublimation would have to include explicitly some $f(\alpha)$ of the decelerating type such as the model of contracting sphere or cylinder.

Note that the introduction of some explicit $f(\alpha)$ in the right-hand side of Eqs. 3.5 or 3.9 would not affect the values of the isoconversional activation energy estimated as:

$$E_\alpha = -R\left[\frac{\partial \ln(\mathrm{d}\alpha/\mathrm{d}t)}{\partial T^{-1}}\right]_\alpha . \tag{3.12}$$

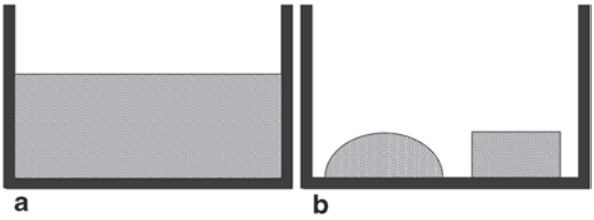

Fig. 3.3 Schematic representation of vaporization or sublimation of different form samples placed in cylindrical pan. **a** Sample in the form of continuous volume of a liquid or solid substance. **b** Sample in the form of individual droplets (*left*) or crystals (*right*)

This is because the logarithmic derivative of $f(\alpha)$ is zero at a constant value of α (Eq. 1.12). Therefore, Eqs. 3.8 and 3.11 would remain true under the isoconversional conditions. That is, for the process of vaporization or sublimation, one should generally expect the isoconversional values of E_α to be practically independent α and close to the value of the process enthalpy. Some systematic dependencies as well as deviations may occur naturally because the enthalpy depends on temperature in accord with the Kirchhoff's law:[18]

$$\Delta H^0(T_2) = \Delta H^0(T_1) + \int_{T_1}^{T_2} \Delta C_P \mathrm{d}T, \tag{3.13}$$

where ΔH^0 is the standard enthalpy change at the temperatures T_1 and T_2, and ΔC_P is the heat capacity change due to a transition from the condensed to gaseous state.

However, the issue of using proper reaction models arises when isoconversional analysis is applied to determine the preexponential factor and reaction model. An instructive example of isoconversional analysis of vaporization of 2,2′-bipyridyl is given by Vecchio et al. [23] (Figs. 3.4 and 3.5). As seen in Fig. 3.4, the E_α values do not practically depend on α. The respective average activation energy is 61±2 kJ mol^{-1}. The value agrees very well with the independently measured enthalpy of vaporization, 59±2 kJ mol^{-1} [23]. The reaction model of vaporization

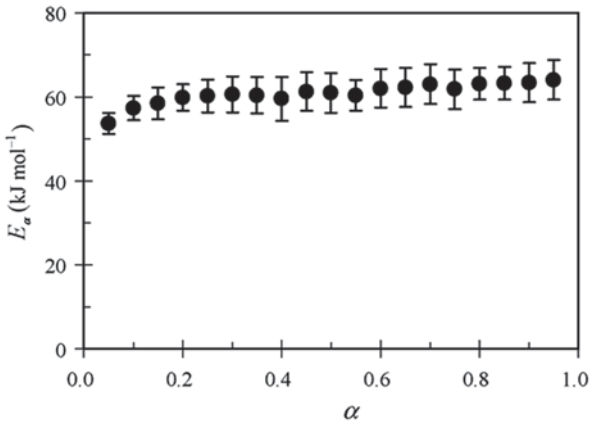

Fig. 3.4 E_α dependence for vaporization of 2,2′-bipyridyl. (Reproduced from Vecchio et al. [23] with permission of Elsevier)

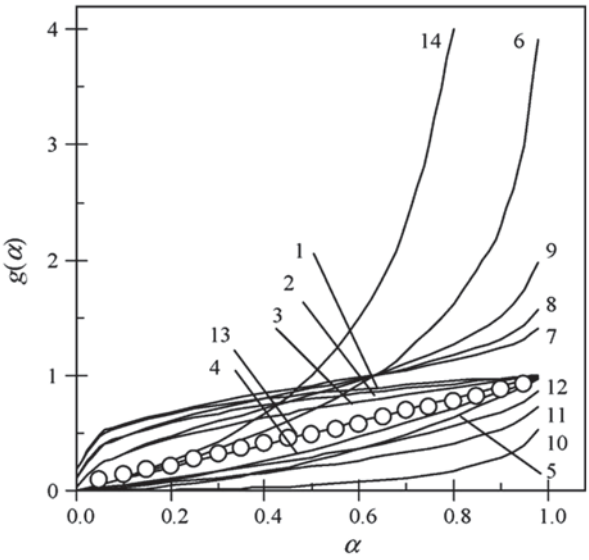

Fig. 3.5 Determination of the reaction model for vaporization of 2,2′-bipyridyl. (Reproduced from Vecchio et al. [23] with permission of Elsevier)

has been determined by using the technique described in Sect. 2.2.2. According to Fig. 3.5, the best-fitting model of this process is N13, which is $g(\alpha)=\alpha$ (i.e., $f(\alpha)=1$) or zero order [23]. This is obviously consistent with the basic assumption of Eqs. 3.5 and 3.9. However, as already mentioned, this is not always the case. For example, both vaporization and, especially, sublimation of ammonium nitrate demonstrate clear deviation from the zero order to decelerating type of kinetics [24].

The rate of diffusion of the condensed substance vapor in the surrounding gas is a very important factor when measurements are conducted under the conditions of regular thermal analysis experiments. The surrounding gas is a purge gas, such as nitrogen, that is delivered to the sample at an ambient pressure and a certain flow rate. If the forming vapor diffuses too slowly, the surrounding gas may become saturated with it. The local vapor pressure may start approaching its equilibrium values that would promote the reverse reaction of condensation. That is why the rate of vaporization or sublimation should be measured at sufficiently fast flow rates that would secure efficient removal of the forming vapor and suppress its condensation.

The effect of the purge gas flow rate on vaporization of methyl salicylate has been demonstrated by Cheng et al. [25]. It has been found that a systematic increase in the flow rate of nitrogen resulted in a small but systematic shift of TGA mass loss curves to lower temperature. This effect is typical to find in reversible processes [26]. The isoconversional activation energies of vaporization also have demonstrated a systematic shift as illustrated in Fig. 3.6. It is seen as an increase in the flow rate causes a systematic decrease in the activation energy of vaporization, bringing its value closer to the reference value of the vaporization enthalpy (52 kJ mol^{-1}).

The rate equations 3.5 and 3.9 rely on the mass loss that makes TGA a method of choice for measuring the kinetics of vaporization and sublimation. However, DSC

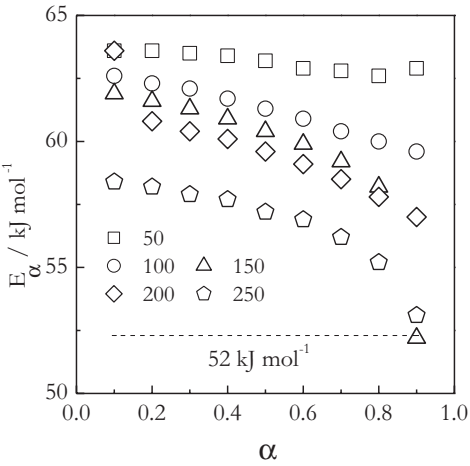

Fig. 3.6 Effect of the nitrogen gas flow rate on the activation energy of vaporization of methyl salicylate. Numbers by symbols represent the flow rate in mL min^{-1}. (Data taken from Cheng et al. [25])

can be used in such studies as well. Figure 3.7 shows a dependence of the effective activation energy estimated from DSC data on vaporization of water [27]. The isoconversional values of E_α are practically independent of α in a rather wide range. The average E_α value in the range $\alpha = 0.4–0.6$ is 43.80 ± 0.03 kJ mol^{-1}. The value is somewhat larger than the reference value [2] of the enthalpy of vaporization of water, 40.7 kJ mol^{-1}. It should be noted that this reference value corresponds to the enthalpy of vaporization at 100 °C, i.e., the boiling temperature, which is a common way of reporting the enthalpies of vaporization. However, under the conditions of DSC runs (open pan, flow of nitrogen), water is completely vaporized by 60 °C.

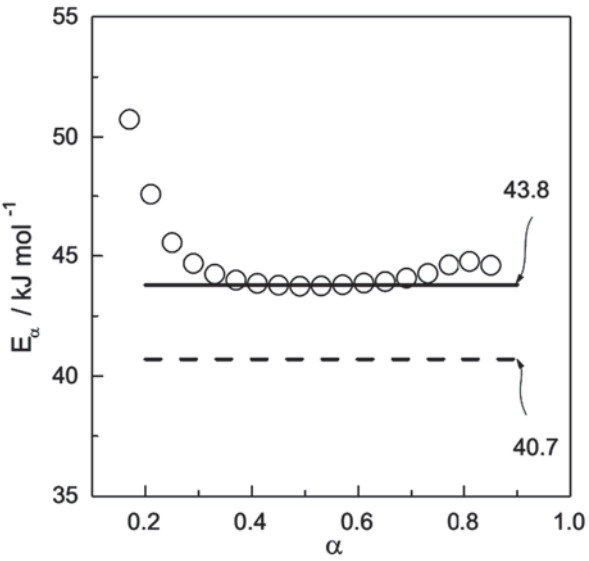

Fig. 3.7 Isoconversional values of the activation energy for vaporization of water. *Solid line* represents the average of the E_α values in the range of $\alpha = 0.4–0.6$. *Dash line* denotes the enthalpy of water vaporization at 100 °C. (Reproduced from Prado and Vyazovkin [27] with permission of Elsevier)

About 50 % of water becomes vaporized around 40 °C. The vaporization enthalpy of water at this temperature can be estimated from Kirchhoff's law (Eq. 3.13) by using the values of the heat capacity for liquid and gaseous water, which are [2] 75.29 and 33.58 J $mol^{-1}K^{-1}$, respectively. Neglecting the temperature dependence of the heat capacity, the vaporization enthalpy at 40 °C is estimated to be:

$$\Delta H^0(40^\circ\mathrm{C}) = \Delta H^0(100^\circ\mathrm{C}) + \Delta C_P(T_2 - T_1)$$

which is 43.2 kJ mol^{-1}. This value is almost identical to the average E_α value (Fig. 3.7).

Overall, the examples considered suggest that the activation energy estimated from the rates of vaporization of liquids is similar to the enthalpy of vaporization. There are many more examples in the literature that confirm this correlation. However, in the case of sublimation of solids, the correlation is not nearly as consistent. The direct application of the Langmuir equation to the mass loss data provides about equal number of examples when the correlation is good as when it is poor [28]. It is not very surprising considering that the mechanism of sublimation [29] is more complex than that of vaporization. If vaporization of a liquid involves essentially one step, in which a molecule breaks the surface tension, sublimation of a solid involves multiple steps. First, a molecule breaks away from a site where it is bound to a fewer neighbors such as a kink or ledge site. Then, it diffuses along the surface and finally desorbs from it. Schematically, it can be seen as a mechanism of three consecutive steps:

$$A_{\text{solid}} \xrightarrow{\text{breaking away}} A_{\text{surface}} \xrightarrow{\text{diffusion}} A_{\text{adsorbed}} \xrightarrow{\text{desorption}} A_{\text{vapor}}.$$

Any of these three steps can be rate limiting during sublimation. As a result, the activation energy estimated from the sublimation rate data can be the one for any of these steps. To complicate matters further, the surface molecule may undergo a chemical reaction of dissociation or association, which also can become a rate-limiting step of sublimation. However, the enthalpy of sublimation is invariably determined by the difference in the enthalpies for A_{vapor} and A_{solid}.

3.3 Glass Transition

> *Only there's no equilibrium in the world. It's just an error of some kilogram and a half over the universe as a whole, but it's really a surprising thing*
>
> Daniil Kharms, On Equilibrium

3.3.1 Background

Typically, the glass phase is formed in supercooled liquids that are cooled so fast that they do not have sufficient time to crystallize. Ultimately, any liquid can be

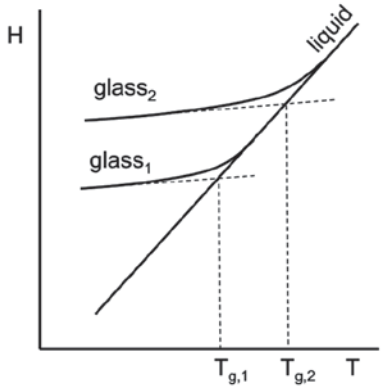

Fig. 3.8 Enthalpy versus temperature diagram for the formation of two glass phases: $glass_1$ and $glass_2$. The $glass_2$ phase is formed at faster cooling rates than $glass_1$ and thus has a larger glass transition temperature that is determined as intersection of the glass and liquid tangent lines

converted to glass subject to sufficiently fast rate of cooling. For slow crystallizing liquids such as the melts of some polymers, the glass can be formed on cooling at tens of degrees per minute. Fast crystallizing liquids such as water may have to be cooled at millions degrees per second to form the glass phase. Anyway, the key reason of the glass formation is the limited rate of the molecular mobility that slows down progressively as liquid is cooled. At certain point, the mobility becomes insufficient to maintain the equilibrium liquid structure so that a supercooled liquid becomes a glass. The respective temperature is called the glass transition temperature, T_g. Since the glass is a nonequilibrium phase, its T_g designates the transition between the supercooled liquid and a specific glassy structure that depends particularly on the cooling rate and generally on the overall thermal history. Figure 3.8 demonstrates a change in the temperature dependencies of the enthalpy for liquid and two glasses formed at different cooling rate. Obviously, the faster liquid is cooled, the sooner it falls out of equilibrium and forms the glass phase. Therefore, faster cooling produces the glass of a more nonequilibrium structure that has larger glass transition temperature.

On reheating, the glass does not follow the same enthalpic trace as on cooling (Fig. 3.9). The respective enthalpy values are lower because the glass is relaxing continuously toward the supercooled liquid state. Another important feature of the glass transition observed on heating is the "enthalpy overshoot." Upon reaching the equilibrium liquid line, the glass does not immediately convert to the liquid but continues to follow the glass line for some time. The reason is that at this point the molecular mobility of the glass is too slow to assume immediately the liquid structure. Therefore, it continues to maintain the glassy structure until the point when temperature accelerates the molecular mobility to such extent that the glass can quickly restore the liquid structure. For the glass formed at a certain cooling rate, the use of faster heating rates results in increasing the magnitude of the enthalpy overshoot. The heating and cooling traces are brought closer to each other when the heating and cooling rates are equal.

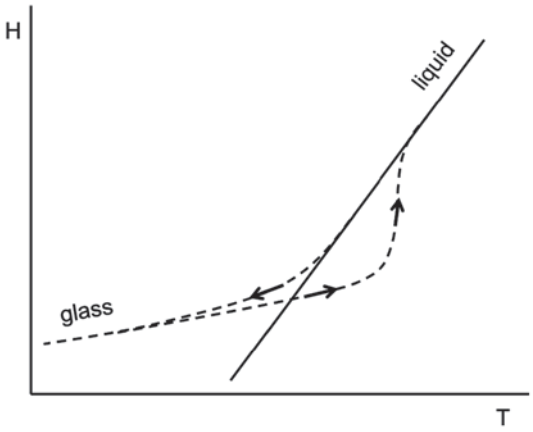

Fig. 3.9 When glass is reheated, its enthalpy crosses (overshoots) the liquid line and returns to it at higher temperature

The enthalpy plot (Fig. 3.9) is helpful in understanding the DSC (heat flow) traces measured on heating and cooling. According to Eq. 3.4, the heat flow related to the glass transition originates from a change in the heat capacity between the values for the liquid and glass phase. By virtue of Eq. 3.3, the heat capacity would change as the first derivative of the plots presented in Fig. 3.9. On cooling, DSC shows some small stepwise change in the heat flow. On the other hand, on heating, the DSC signal is complicated by a peculiar feature associated with enthalpy overshoot, which manifests itself as a relatively small endothermic peak at the end of the glass transition step. Figure 3.10 displays an example of this feature observed in the glass transition of polystyrene (PS) and PS–clay nanocomposite [30].

The nonequilibrium structure of the glass phase reveals itself in the relaxation kinetics. When the glass freezes dynamically, it conserves a heterogeneous structure

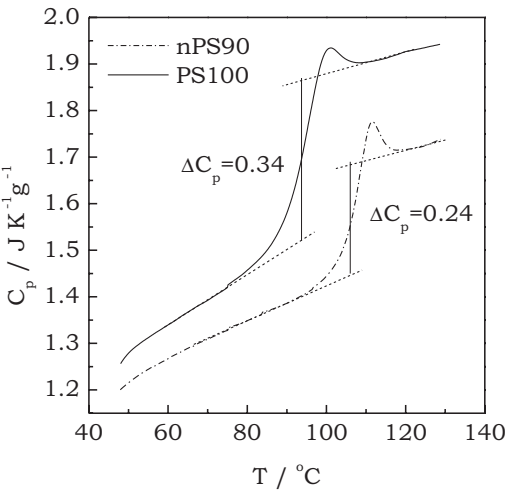

Fig. 3.10 Heat capacity change during the glass transition in polystyrene (PS100) and polystyrene–clay nanocomposite (nPS90) on heating at 10 °C min^{-1}. (Reproduced from Vyazovkin and Dranca [30] with permission of ACS)

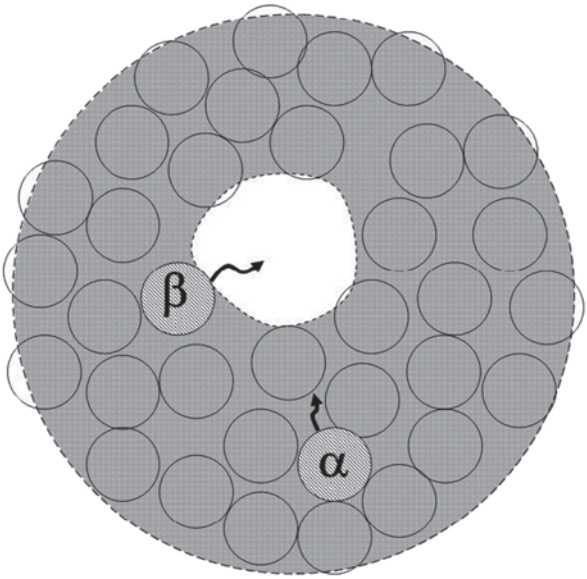

Fig. 3.11 Schematic representation of molecular mobility in the glass phase. The letters α and β represent molecules respectively involved in cooperative and noncooperative motion. The *open area* is a mobility island

that contains significant density fluctuations (Fig. 3.11). The lower density areas form the mobility islands [31] inside the glass. As a result, the molecules of the glass phase find themselves in a variety of the spatial situations of different crowdedness. Those, stuck in highly congested situations, can only move cooperatively, i.e., together with moving the closest neighbors. The respective motion is termed the α-process (relaxation). This is a slow process characterized by high activation energy whose value is typically on the order of hundreds of kilojoules per mole. On the other hand, the molecules located in the vicinity of the mobility islands can move rather freely, i.e., in a noncooperative manner. The respective motion is referred to as the β-process (relaxation) or Johari–Goldstein process. This process is fast and its activation energy amounts to several tens of kilojoules per mole.

When glass relaxes toward the equilibrium supercooled liquid structure, the overall process would occur generally via both cooperative and noncooperative motion. However, one particular mechanism may dominate depending on temperature or the stage of relaxation. Since cooperative and noncooperative processes can occur in parallel with each other, at any given temperature, the kinetics of relaxation is dominated by the fastest process, i.e., a process having the smallest relaxation time, τ. Cooperative and noncooperative processes have distinctly different temperature dependencies of the relaxation time. Noncooperative processes, such as β-relaxation, obey the Arrhenius equation:

$$\tau = C \exp\left(\frac{E}{RT}\right), \tag{3.14}$$

where C is the temperature-independent preexponential factor, E is the activation energy, and R is the gas constant. It follows from Eq. 3.14 that

$$E = R\left(\frac{\mathrm{d}\ln\tau}{\mathrm{d}T^{-1}}\right). \tag{3.15}$$

This means that for a noncooperative process, the plot of $\ln\tau$ versus T^{-1} should be a straight line whose slope is E/R.

The temperature dependence of a cooperative process, such α-relaxation, follows the Vogel–Tammann–Fulcher (VTF) equation:

$$\tau = B\exp\left(\frac{A}{T - T_0}\right), \tag{3.16}$$

where B is the temperature-independent preexponential factor, A is a constant, and T_0 is a reference temperature, typically well below T_g. By using the same principle as in Eq. 3.15, we can derive the activation energy from Eq. 3.16:

$$E = R\left[\frac{AT^2}{\left(T - T_0\right)^2}\right]. \tag{3.17}$$

Equation 3.17 suggests that the activation energy and, thus, the slope of the plot of $\ln\tau$ versus T^{-1} increase with decreasing temperature. A similar result is obtained [32] from the Williams–Landel–Ferry (WLF) equation:

$$E = 2.303R\left[\frac{C_1C_2T^2}{(C_2 + T - T_g)^2}\right], \tag{3.18}$$

where $C_1 = 17.44$ and $C_2 = 51.6$ are universal constants. Both VTF and WLF equations are applied commonly to describe the temperature dependence of viscosity of supercooled liquids. Although the equations can be used interchangeably, the WLF equation is most frequently applied to polymers, whereas the VTF equation to low molecular weight species.

The non-Arrhenius type of the temperature dependence (i.e., the VTF or WLF dependence) breaks down in the vicinity of T_g, below which the dependence takes the Arrhenius form (Fig. 3.12a). This is empirically found in a variety of liquids [3]. An explanation of this phenomenon is provided by the theoretical results of Di Marzio and Yang [33]. The change in the type of the temperature dependence around T_g has important implications for estimating experimental activation energies (Fig. 3.12b). That is, above T_g, the transition from the glass to liquid phase should demonstrate large values of the activation energy that decrease with temperature. However, when glass relaxes to supercooled liquid below T_g, one should

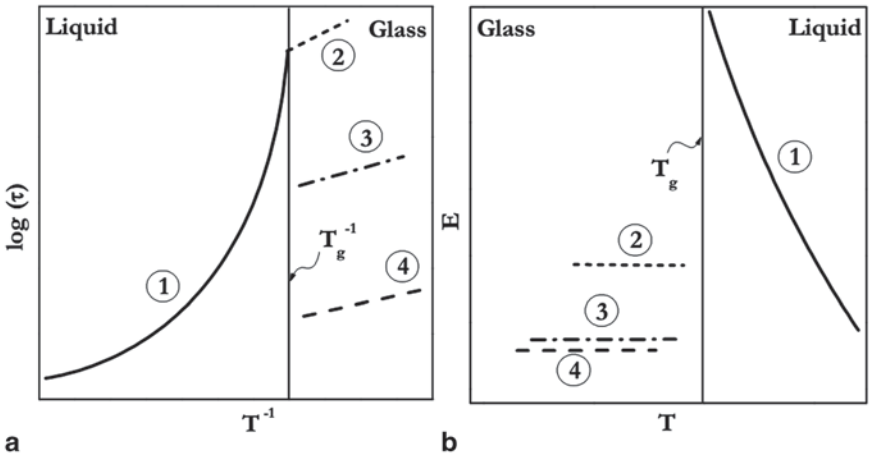

Fig. 3.12 Schematic representation of the temperature dependencies of the relaxation time (**a**) and the respective activation energies (**b**). **a** Curve 1 represents a typical VTF dependence of the α-relaxation. Straight lines 2–4 represent various processes occurring in the glassy state: 2 nonequilibrium mode of the α-relaxation; 3 α' process; 4 β-process. **b** Sub-T_g processes 2–4 have significantly lower activation energy than the α-process (1). VTF Vogel–Tammann–Fulcher. (Reproduced from Vyazovkin and Dranca [35] with permission of Elsevier)

expect the activation energy values to be markedly smaller and decreasing with decreasing temperature down to the values characteristic of the β-process.

It should be noted that beyond the β-relaxation, there are some processes that occur below T_g and similarly demonstrate the temperature dependencies of the Arrhenius type and the activation energies that are smaller than those for cooperative α-process occurring above T_g [34]. One of them is the nonequilibrium mode of the α-relaxation that manifests itself as a break point in the respective VTF dependence that occurs at T_g and gives rise to a smaller slope and, thus, lower activation energy (Fig. 3.12) [35]. The latter is either somewhat larger [36, 37] or comparable [37] to that of the β-process. Another is the so-called α'-relaxation process that is observed in metallic [38] as well as polymeric glasses [39]. It is reported [38] to be associated with the "frozen-in relaxation sites" and has small activation energies (Fig. 3.12), which makes it very similar to the regular β-relaxation. However, both nonequilibrium α-process and α'-process are detected at higher temperatures than the regular β-process.

3.3.2 Isoconversional Treatment

In order to apply an isoconversional method to the DSC data on the glass transition, one needs first to determine the extent of conversion. This can be done in a way similar to calculating the normalized heat capacity [40].

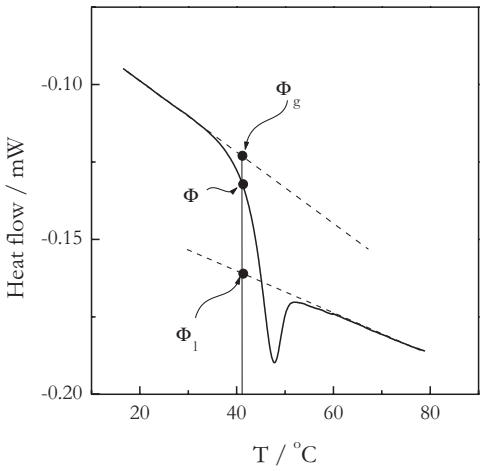

Fig. 3.13 The glass transition in amorphous indomethacin measured at 5 °C min^{-1}. Φ represents the heat flow value at a given temperature, T. Φ_l and Φ_g represent the extrapolated heat flow baselines for the liquid and glass at the same temperature T. These are the values to be substituted in Eq. 3.20 to determine α at this T

$$C_P^N = \frac{(C_P - C_{Pg})\big|_T}{(C_{Pl} - C_{Pg})\big|_T}, \tag{3.19}$$

where C_P is the current heat capacity, and C_{Pg} and C_{Pl} are the glassy and liquid heat capacity, respectively. The normalized heat capacity runs from 0 to 1, i.e., in the same way as the extent of conversion. Equation 3.19 is equally applicable to the heat flow data so that the extent of conversion is determined as follows:

$$\alpha = \frac{(\Phi - \Phi_g)\big|_T}{(\Phi_l - \Phi_g)\big|_T}, \tag{3.20}$$

where Φ is the heat flow at a given temperature T, and Φ_l and Φ_g are the heat flow values for the liquid and glass extrapolated to the same temperature T (Fig. 3.13). In practical terms, one starts by estimating the straight baseline for the glass phase and subtracting it from the whole DSC signal. Then at each given T, α is calculated as the ratio of the resulting heat flow to the heat flow obtained from extrapolation of the straight baseline for the liquid phase to this temperature.

The application of the aforementioned procedure results in α versus T curves similar to those obtained for the glass transition in amorphous drug indomethacin (IM) [41] (Fig. 3.14). The enthalpy overshoot (the endothermic peak at the end of the glass transition step) observed on heating (see Fig. 3.13), gives rise to the α-values in excess of unity. This feature does not appear when the glass transition is measured on cooling. When the glass transition kinetics is measurement on heating, each heating run has to be preceded by cooling performed from temperature significantly above T_g to significantly below T_g at the rate of cooling whose absolute value

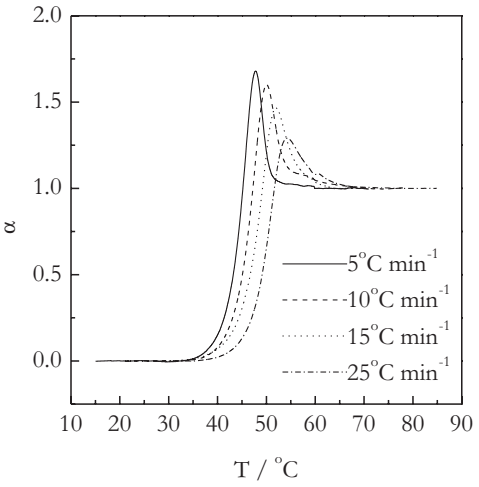

Fig. 3.14 Conversion against temperature curves for the glass transition of amorphous indomethacin at four heating rates

is equal to the rate of the following heating [42, 43]. A suitable temperature range of measurements is typically from T_g+40 to T_g-40.

For measurements performed on heating (Fig. 3.14), the isoconversional calculations need to use only the ascending part of the α versus T curves up to $\alpha=1$. The resulting dependence of the activation energy of conversion is shown in Fig. 3.15. The observed decreasing shape of the E_α versus α dependence is typical for the glass transition and has been observed in variety of other systems, including many polymers [44]. The decrease in E is easy to understand in terms of the cooperative molecular mobility discussed earlier (Fig. 3.12). The glassy phase is characterized by a small amount of free volume that permits only local noncooperatve motion (e.g., the β-process) that dominates well below T_g. As temperature rises approach-

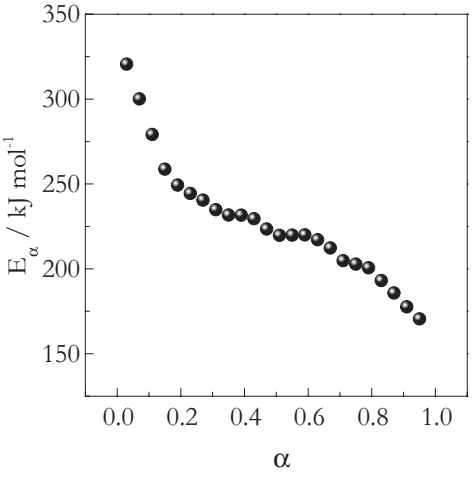

Fig. 3.15 Conversion dependence of the activation energy evaluated from the data shown in Fig. 3.14. (Adapted from Vyazovkin and Dranca [41] with permission of ACS)

ing the glass transition region, the molecular motion intensifies, and the free volume increases, initiating the α-process. The latter involves considerable cooperativity between the molecules and, thus, a large energy barrier as reflected in the large value of E at the initial stages of the transition (Figs. 3.12b and 3.15). As temperature continues to rise, the free volume continues to increase. The molecular packing becomes increasingly looser, allowing the molecules to move less dependently, i.e., in a less cooperative fashion. This relieves the energetic constrains, and the activation energy decreases.

A decrease in E is consistent with the predictions of the VTF and WLF equations (Eqs. 3.17 and 3.18). A similar trend is predicted by the Adam–Gibbs equation[45]

$$\tau = A \exp\left(\frac{z^* \Delta\mu}{k_B T} \right), \tag{3.21}$$

where k_B is the Boltzmann constant, $\Delta\mu$ is the activation energy per particle, and z^* is the number of particles that cooperatively rearrange. In Eq. 3.21, z^* is inversely proportional to the configurational entropy that increases with T so that both z^* and the effective activation energy (i.e., $z^*\Delta\mu$) decrease with T.

Note that even before the first applications [30, 46] of isoconversional methods to the glass transition kinetics, the trend for the activation energy to decrease with increasing temperature was observed in other studies [47–49]. In them, the activation energy was determined from the shift in the value of T_g with the heating rate in accord with the equation proposed by Moynihan et al.: [42, 43]

$$E = -R \frac{\mathrm{d}\ln|\beta|}{\mathrm{d}T_g^{-1}}, \tag{3.22}$$

where β can be the rate of heating or cooling. However, the value of T_g can be defined in the order of its increase as the onset temperature, the temperature of the midpoint step in the heat flow, and the endset temperature. For the glass transition of sorbitol, Angell et al. [47] have found that Eq. 3.22 gives rise to a significantly larger E when T_g is determined as the onset temperature than when T_g is estimated as the temperature of the heat capacity peak. A similar effect was reported by Lacey et al. [48] for PS oligomer and side-chain polysiloxane and by Hancock et al. [49] for some pharmaceutical glasses, including poly(vinylpyrrolidone) (PVP), IM, and several sugars. The observed temperature dependence of the activation energy suggests that the plot of $\ln\beta$ versus T_g^{-1} should be nonlinear. The nonlinearity can be quite obvious when T_g is measured in a wide range of the heating rates as illustrated in Fig. 3.16 for the glass transition in PS [30]. From this plot, we can see again that the activation energy of the glass transition decreases with increasing temperature.

Our numerous applications of the isoconversional method to the glass transition in a variety of systems indicate that the obtained activation energies are in reasonable agreement with the activation energies obtained by other techniques, such as

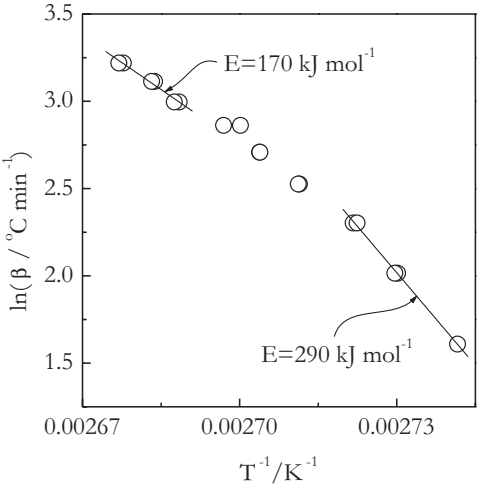

Fig. 3.16 Plot of lnβ versus T_g^{-1} measured for the glass transition in polystyrene at nine heating rates from 5 to 25 °C min^{-1}. T_g was measured twice at each heating rate and determined as the temperature at midpoint of the glass transition step. The E values of 290 and 170 kJ mol^{-1} are found respectively from the three slowest and the three fastest heating rates. (Adapted from Vyazovkin and Dranca [30] with permission of ACS)

dielectric and mechanical spectroscopy, for the α-relaxation [44, 46]. Of course, one should not expect precise agreement between the absolute values. This is not only because different techniques measure different physical properties but also because the activation energy of the α-relaxation depends on temperature and the temperature regions employed by different techniques rarely coincide. In particular, it has been reported [50] that the E values derived from DSC data obtained on cooling are markedly larger than those derived from the heating data. However, what is essential is that a variation in E is detected by different techniques, including DSC, as long as DSC data are analyzed by an isoconversional method.

Although an isoconversional method consistently produces a decreasing E versus α dependence for the transition from the glass to liquid phase, the absolute values of E and the degree of its variability with temperature change dramatically between the glassy substances. Note that an E versus α dependence (e.g., Fig. 3.15) can be converted to an E versus T dependence by replacing the values of α with the mean value of the temperatures related to this α at different heating rates (see Fig. 3.14). Figure 3.17 presents a set of the E versus T dependencies evaluated by applying an isoconversional method to the glass transition in a series of substances: poly(vinyl chloride) (PVC), poly(*n*-butyl methacrylate) (PBMA), PVP, poly(ethylene 2,6-naphthalate) (PEN), PS, poly(ethylene terephthalate) (PET), and boron oxide (B_2O_3) [44, 46]. The differences in the activation energy variability are really staggering. At one extreme, we have PVC and PET, in which the glass transition occurs in a very narrow temperature range and accompanied by a drastic change in the activation energy. At another extreme we see PBMA and B_2O_3 whose glass transition stretches over a wide temperature range with little change in the activation energy.

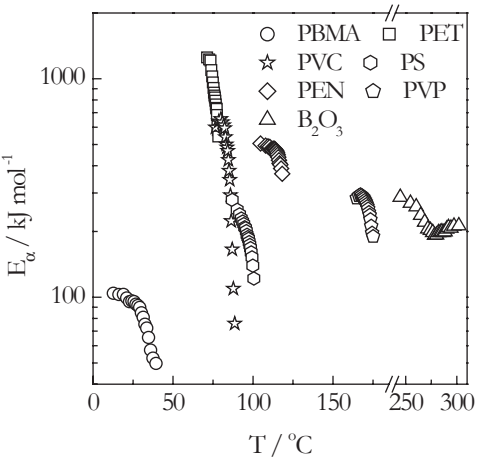

Fig. 3.17 Temperature dependencies of the activation energy for the glass transition in various substances. *PBMA* poly(*n*-butyl methacrylate), *PET* poly(ethylene terephthalate), *PVC* polyvinyl chloride, *PS* polystyrene, *PEN* poly(ethylene 2,6-naphthalate), *PVP* poly(vinylpyrrolidone). (Adapted from Vyazovkin et al. [44, 46] with permission of Wiley)

In order to characterize the variability in E numerically, we have introduced [44] a variability parameter defined as

$$\Delta_E = \frac{E_{0.25} - E_{0.75}}{T_{0.25} - T_{0.75}}, \tag{3.23}$$

where $E_{0.25}$ and $E_{0.75}$ are the E_α values at $\alpha = 0.25$ and 0.75, respectively, and $T_{0.25}$ and $T_{0.75}$ are the values of T_α for the respective values of α. The dependencies presented in Fig. 3.17 yield the Δ_E values collected in Table 3.1. In terms of the logτ versus T^{-1} plots, larger variability of E means larger curvature of the plot (Fig. 3.12). Ultimately, when the plot is linear (i.e., of the Arrhenius type), E becomes independent of T, and Δ_E turns into zero. That is, the variability parameter should correlate with the departure of the logτ versus T^{-1} plot from the Arrhenius behavior, or, in other words, with the dynamic fragility.

The concept of fragility was introduced by Angell [51] to characterize the differences in the temperature dependencies of viscosity or relaxation time of glass-forming liquids. According to this concept, the strong liquids are those that demonstrate close to linear or Arrhenius type of logτ versus T^{-1} (Fig. 3.18). The fragile liquids, on the contrary, demonstrate nonlinear plots of the VTF or WLF type. Typically, the strong liquids are inorganic glass formers, whereas polymers belong to the most fragile liquids. Deviation from the Arrhenius behavior is estimated as the fragility parameter, m. By assuming the VTF type of the temperature dependence (Eq. 3.16), the parameter is defined as:[52]

$$m = \frac{A / T_g}{\ln 10 \cdot (1 - T_0 / T_g)^2}. \tag{3.24}$$

Table 3.1 Estimated (Eq. 3.23) values of the variability parameter and literature values of the fragility parameter

Substance	Δ_E (kJ mol^{-1} K^{-1})	m
B_2O_3	−0.6	32 [53]
PBMA	−2.3	48 [55]
PEN[a]	−10.0	99 [57], 66[58]
PVP[b]	−11.1	102
PS	−11.5	139 [53], 77[54]
PVC	−73.0	191 [53], 160 [54]
PET	−110.6	156 [56]

PBMA poly(n-butyl methacrylate), *PEN* poly(ethylene 2,6-naphthalate), *PVP* poly(vinylpyrrolidone), *PS* polystyrene, *PVC* polyvinyl chloride, *PET* poly(ethylene terephthalate)

[a] The m values have been estimated from the VTF parameters reported in the respective papers

[b] For PVP, the m value has been predicted from Δ_E by the correlation shown in Fig. 3.19

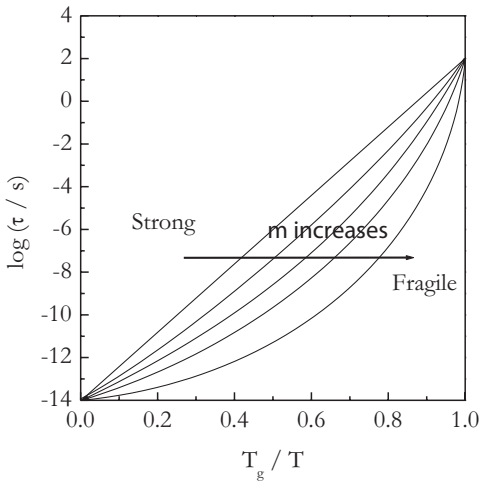

Fig. 3.18 Temperature dependencies of the relaxation time in the strong and fragile liquids

For all the compounds presented in Table 3.1, except PVP, the values of m are found in the literature [53–58]. As seen from Table 3.1, the Δ_E and m parameters are correlated. The correlation is nonlinear, but can be reduced to a linear form by replacing Δ_E with $\log(-\Delta_E)$ (Fig. 3.19). The dataset from Table 3.1 demonstrates strong correlation ($r = 0.9665$) of the following form:

$$\log(-\Delta_E) = -0.438 + 0.0145m. \tag{3.25}$$

Surmising that the correlation (3.25) holds for a wide class of glasses, one can use it to estimate the fragility parameter from Δ_E. For example, based on Eq. 3.25, the m value for PVP should be around 102.

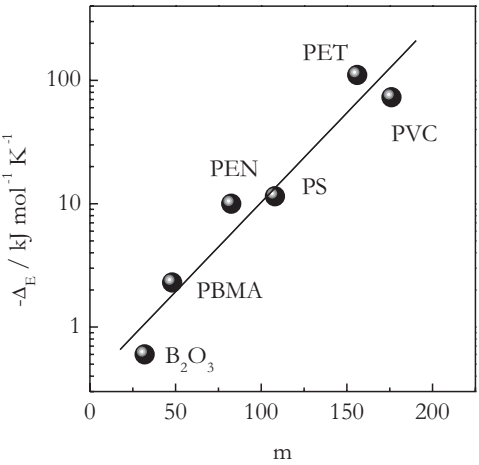

Fig. 3.19 Correlation of the parameters of variability ($-\Delta_E$) and fragility (m). The m values are from Table 3.1 (if there is more than one literature value, the mean value is used). *PET* poly(ethylene terephthalate), *PVC* polyvinyl chloride, *PS* polystyrene, *PEN* poly(ethylene 2,6-naphthalate), *PBMA* poly(*n*-butyl methacrylate). (Adapted from Vyazovkin et al. [44] with permission of Wiley)

3.4 Glass Aging

The glass is falling hour by hour, the glass will fall for ever
Louis MacNeice, Bagpipe Music

3.4.1 Background

When liquid is well above its T_g, its relaxation time is significantly shorter than the timescale of regular measurements, which typically last from minutes to hours. On such timescale, any fluctuations of the molecular structure of liquid are relaxed, i.e., liquid is at equilibrium. When temperature drops below T_g, the relaxation time of liquid exceeds the experimental timescale, and the structural fluctuations do not have enough time to relax. Instead, they become frozen kinetically as the nonequilibrium glass phase (Fig. 3.20). This phase is driven thermodynamically to relax its structure toward that of the equilibrium supercooled liquid. The relaxation can occur on heating (i.e., when temperature raises continuously) of a glass through the glass transition temperature. In this case, the process is referred to as the glass transition (Sect. 3.3).

However, this relaxation also occurs on annealing (i.e., when temperature is held constant) below the glass transition temperature. This process is called physical aging [59]. Physical aging is accompanied by a change in mechanical, dielectric, magnetic, and optical properties of a glass. Thermodynamically, the process is characterized by a decrease in three thermodynamic parameters: the enthalpy, entropy, and volume (Fig. 3.20). That is, physical aging is an exothermic process, during which the glass becomes more ordered structurally and its volume shrinks.

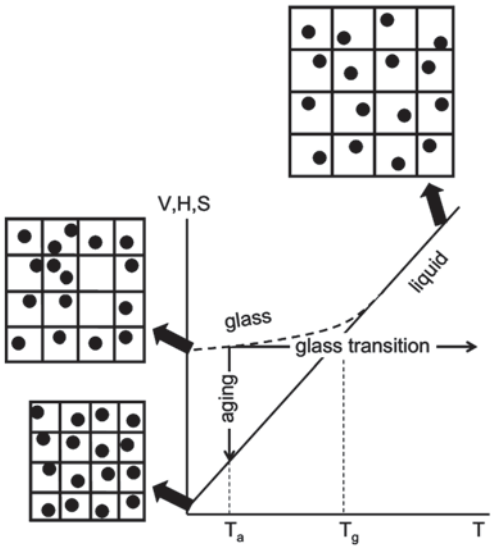

Fig. 3.20 Relaxation of the nonequilibrium glassy structure can occur under rising temperature conditions as the glass transition or at constant temperature as aging

The kinetics of physical aging is of great practical importance because it determines for how long a glassy material can remain useful at temperature of operation. The stability of a glass increases with increasing the difference between the temperatures of the glass transition and operation. For example, regular household glassware made of silicate glass is used about 500 °C below its glass transition temperature. This makes it stable for all designed practical purposes.

However, even in the case of silicate glasses used far below T_g, the signs of aging are detectable on the scale of decades [60–62]. An intriguing example [60, 62] includes data on aging of glass thermometers used by the renowned physicist James Prescott Joule. Joule regularly calibrated his thermometers and noticed that what he called the zero point was increasing systematically, shifting totally by 0.91 F over 23 years. The effect is explicable [60, 62] by the glass shrinkage due to physical aging.

The kinetics of physical aging is usually followed by measuring either volume of enthalpy of a glassy sample. The heat flow released during physical aging is too small to follow the process by regular DSC instruments in real time. The measurements are thus conducted discretely, i.e., in steps. The idea is that the enthalpy lost on aging can be recovered when heating an aged glassy sample through the glass transition temperature. As seen from Fig. 3.21, the sample held at aging temperature T_a will continue to lose its enthalpy until the glass reaches equilibrium, i.e., turns into supercooled liquid. As discussed earlier (Fig. 3.9), reheating of unaged glass results in the enthalpy overshoot. When glass ages, it assumes a denser and more ordered structure that results in a decrease of the molecular mobility and an increase of the relaxation time. For this reason, when aged glass crosses the equilibrium liquid line, it takes longer to restore the liquid structure than for unaged glass.

Thus, the more glass aged (points B and C in Fig. 3.21), the more it overshoots the liquid line. The inflection point on the enthalpy recovery line corresponds to the temperature, T_p, of the DSC peak that appears at the end of the glass transition step

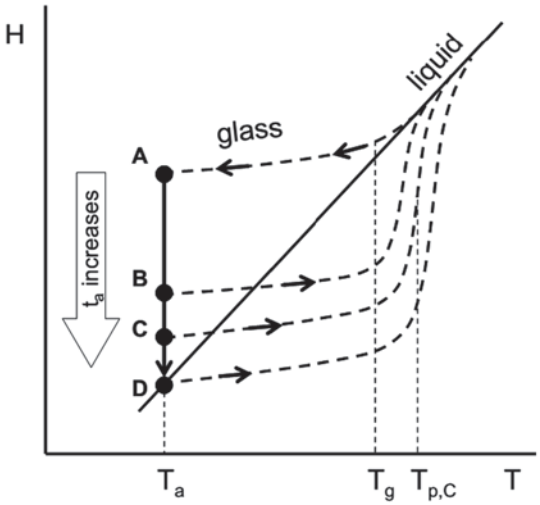

Fig. 3.21 As glass ages, its enthalpy lowers and its mobility slows down so that on reheating the enthalpy overshoot becomes larger and shifts to higher temperature. T_p denotes the position of the overshoot peak

measured on heating. The size of the peak is proportional to the enthalpy lost on aging. The effect is illustrated in Fig. 3.22 [63]. Both peak temperature and recovered enthalpy increase with aging time, t_a, until they reach ultimate values, which correspond to completely relaxed glass (point D in Fig. 3.21). The magnitude of the ultimate values depends on chosen T_a.

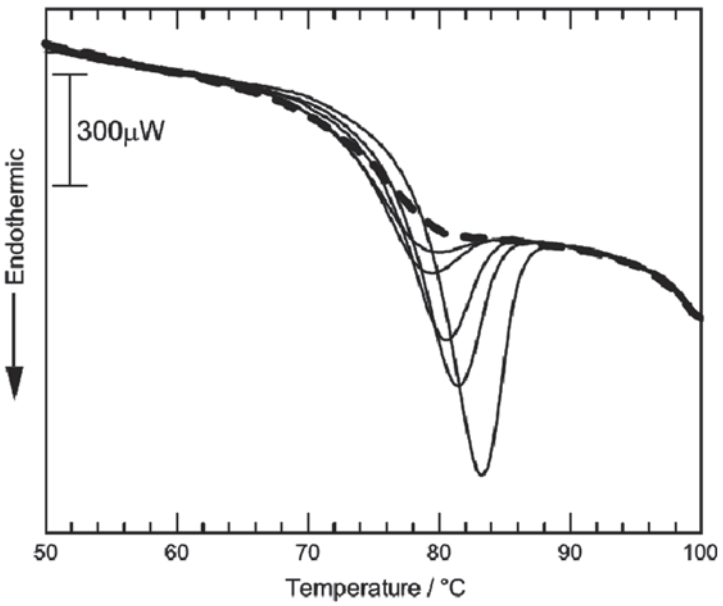

Fig. 3.22 DSC curves of poly(cyanobiphenyl ethylacrylate) heated at 5 °C min–1 after aging at 64 °C for 34, 64, 305, 725, and 3963 min (*solid lines* in order of increasing the peak size). The *dash line* represents the curve for unaged sample. (Reproduced from Tanaka and Yamamoto [63] with permission of Elsevier)

3.4.2 Isoconversional Treatment

The recovered enthalpy of aging, ΔH_a, can be estimated as the difference in the integrals of the DSC curves for aged and unaged samples [64]. The measurements are performed on the same sample, which is first relaxed for a few minutes at a temperature well above T_g, then cooled quickly at a controlled rate to a temperature well below T_g, and then heated back to the initial temperature at a given heating rate. This would produce a DSC trace for unaged glass. To obtain the trace for aged glass, the sample is exposed to the same temperature protocol, except that the cooling segment is interrupted by the aging segment, which maintains temperature T_a for a period t_a. After that the cooling segment continues, followed by the heating segment. The difference in the integrals of the respective DSC traces would yield ΔH_a related to a given aging time t_a. Another point on the kinetic curve ΔH_a versus t_a is produced by maintaining the whole cooling–heating protocol but changing the length of the aging segment. An example of ΔH_a versus t_a is shown in Fig. 3.23 for aging of maltitol (Mt) glass [65].

The aging temperatures are usually taken within 10 °C below the glass transition temperatures. It may take months to reach equilibrium at 10 °C below T_g and about a day at 5 °C below T_g. Equilibrium is easy to detect when converting the time to the logarithmic scale (Fig. 3.23). On this scale, aging progresses almost linearly with time. On approaching equilibrium, the line breaks and turns horizontal. For example, it takes Mt glass about 20 h to reach equilibrium at 6 °C below its T_g (Fig. 3.23). The time to equilibrium in seconds, t_∞, can be estimated by using an equation proposed by Struik: [59]

$$t_\infty \approx 100 \exp[0.77(T_g - T_a)]. \tag{3.26}$$

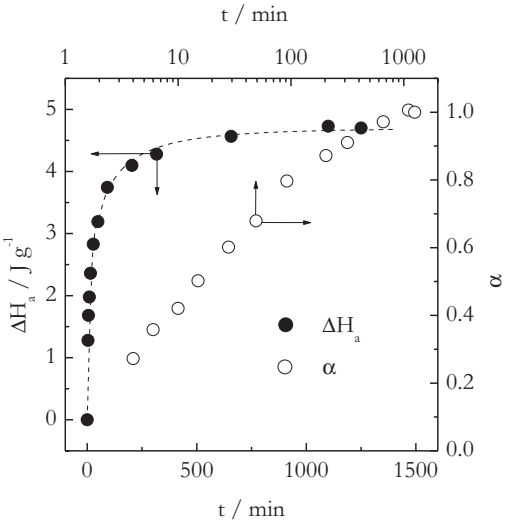

Fig. 3.23 Progress of maltitol aging at 40 °C. *Solid circles* represent recovered enthalpy of aging, *open circles* conversion. (Partially adapted from Chen and Vyazovkin [65] with permission of ACS)

The equation is not very accurate [66] because it was derived assuming that the temperature dependence of the relaxation time obeys the WLF equation [32]. However, below T_g, the relaxation processes tend to follow [33, 67] the Arrhenius equation that predicts much weaker temperature dependence. In addition, the rate of aging can differ substantially for different materials. For instance, the aging data [68] for polycarbonate and PS suggest that at similar $T_g - T$, the former reaches equilibrium almost ten times faster than the latter. Nonetheless, Eq. 3.26 can provide a reasonable estimate for the magnitude of the aging time, i.e., hours, days, and months.

To perform the isoconversional calculations, experimentally measured curves of the recovered enthalpy versus aging time need to be converted to the curves of the conversion versus time. For any given aging time, the extent of aging, i.e., the extent of conversion from the glass to supercooled liquid phase, is determined as:

$$\alpha = \frac{\Delta H_a(t)}{\Delta H_\infty}, \tag{3.27}$$

where $\Delta H(t)$ is the enthalpy measured at the aging time, t, and ΔH_∞ in the equilibrium (plateau) value. Since aging runs are conducted isothermally, the activation energy can be evaluated straightforwardly by Eq. 3.28

$$E_\alpha = R\frac{\mathrm{d}\ln t_\alpha}{\mathrm{d}T^{-1}}, \tag{3.28}$$

i.e., as the slope of a plot of the natural logarithm of the time, t_a, to reach a given extent of aging, α, against the reciprocal aging temperature. By repeating this procedure for a series of the conversions, one obtains a dependence of E_α on α.

The use of Eq. 3.28 requires determining the time to reach a given extent of conversion at different aging temperatures. Unfortunately, it is impossible to measure reliably small extents of conversion. The aging rate is the fastest in the initial moments so that the smallest values of conversion are experimentally detected after only a few minutes of aging. For instance, 4-min aging of Mt resulted in α being about 0.27 (Fig. 3.23). The values of t_α can be found by interpolating the discrete experimental dependence of α versus t by the Kohlrausch–Williams–Watts (KWW) equation [3, 4]

$$\alpha = 1 - \exp\left[-\left(\frac{t}{\tau_{ef}}\right)^\gamma\right]. \tag{3.29}$$

The equation has two fit parameters: τ_{ef}, which is the effective relaxation time, and γ, which is the stretch exponent. The KWW equation is generally found to describe accurately the relaxation kinetics of glasses, although it is commonly found that [69] the parameter γ varies systematically with temperature. Once the values of τ_{ef} and γ are estimated, Eq. 3.29 can be used to find t_α for any α.

The isoconversional plots of $\ln t_\alpha$ versus T^{-1} for aging of Mt glass are seen in Fig. 3.24. The most remarkable feature of these plots is that their slopes increase

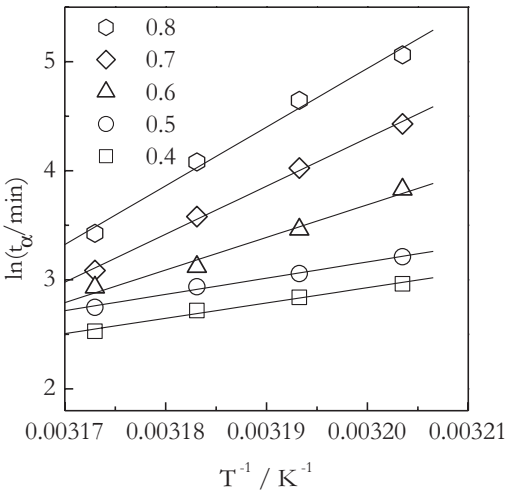

Fig. 3.24 Isoconversional plots obtained from the enthalpy recovery data for maltitol aged at temperatures 39, 40, 41, and 42 °C. (Reproduced from Chen and Vyazovkin [65] with permission of ACS)

markedly with increasing conversion. This means that the activation energy of aging increases throughout the aging process. A dependence of the isoconversional values of E_α on α is shown in Fig. 3.25. The data suggest that the later stages of aging demonstrate the activation energies whose values are similar to the activation energy of the glass transition process in Mt, i.e., 413±20 kJ mol^{-1}[70]. However, the most important is that the activation energy of the early stages of aging is several times smaller.

The kinetics of physical aging can also be followed by the heat capacity relaxation. Physical aging is known [71, 72] to be accompanied by a decrease in the excess heat capacity, C_P. The effect is measured by temperature-modulated (TM) DSC under quasi-isothermal conditions that are accomplished by overlaying a constant

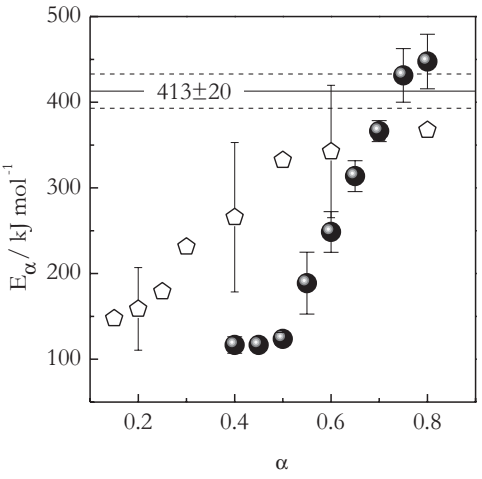

Fig. 3.25 Variation of the activation energy of aging of maltitol with the extent of conversion from glass to supercooled liquid. *Pentagons* and *spheres* represent respectively the values derived from the heat capacity and enthalpy relaxation data. (Reproduced from Chen and Vyazovkin [65] with permission of ACS)

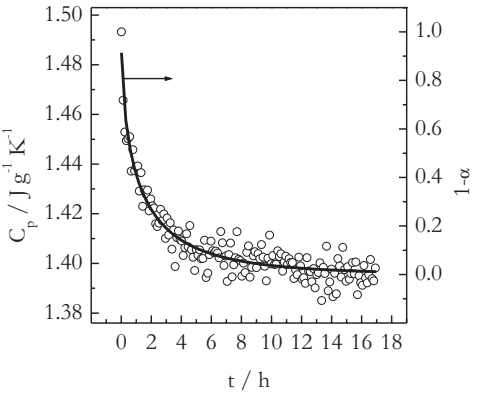

Fig. 3.26 Decrease in the excess heat capacity of maltitol at 39 °C. *Solid line* represents the KWW fit (Eq. 3.29). KWW Kohlrausch–Williams–Watts. (Adapted from Chen and Vyazovkin [70] with permission of Elsevier)

temperature with small amplitude temperature perturbations. The effect has been attributed [71] to the heat capacity contributions from faster modes of molecular motion that include the noncooperative β or Johari–Goldstein process and faster portions of the cooperative α-process. An advantage of the heat capacity relaxation measurements is that the measurements are conducted continuously and take less time than the discrete and laborious enthalpy relaxation measurements.

The loss of the excess heat capacity for Mt glass is presented in Fig. 3.26. The C_P versus t data are converted to the α versus t curves as follows:

$$\alpha = \frac{C_{P,\mathrm{i}} - C_P(t)}{C_{P,\mathrm{i}} - C_{P,\mathrm{f}}}, \tag{3.30}$$

where $C_{P,\,\mathrm{i}}$, $C_{P,\,\mathrm{f}}$, and $C_P(t)$ are respectively the initial (nonaged), final (plateau), and current values of the heat capacity. The resulting α versus t curves obtained at several aging temperatures can be treated by an isoconversional method in the same fashion as the enthalpy relaxation curves. The E_α versus α dependence evaluated from the heat capacity relaxation data is quite similar to that determined from the enthalpy relaxation measurements (Fig. 3.25). In both cases, the E_α values for the early stages of aging are about three times smaller than the activation energy for the glass transition.

Isoconversional analysis of the aging kinetics indicates that the early stages of the process are dominated by a faster process having smaller activation energy and the later stages by a slower process of larger activation energy. Because at conversions close to unity, the E_α value approaches the activation energy of the glass transition, it is logical to conclude that the slower process of larger activation energy is the cooperative α-relaxation. Then the faster process of lower activation energy is likely to be associated with relaxations of low cooperativity. As discussed earlier (Fig. 3.12), these may include the nonequilibrium mode of α-, α'-, and β-relaxations. They have progressively smaller activation energies, each of which being smaller than the typical values found for the α-relaxation. Mt is known [73] to demonstrate the nonequilibrium α-mode. Although the activation energy has not been reported

for this process, the slope of the respective Arrhenius plot is significantly larger than that for the β-relaxation. For the latter, the activation energies have been reported to be 62 [73], 57 [74], and 71 [35] kJ mol^{-1}. On the other hand, extending the aging temperatures of Mt below 30 °C brings the activation energies of the initial stages of aging down to 60–80 kJ mol^{-1}[65].

All in all, it appears that the activation energy of the early stages of aging is much closer to the activation energy of the β- than α-relaxation. Also, the values get even closer when aging is performed at lower temperatures. This is in agreement with the results of Nemilov [60, 61] and Nemilov and Johari [62] for silicate glasses, of Cangialosi et al. [75] for polycarbonate, and of Hu and Yue [76] for hyperquenched GeO_2 that demonstrate that at temperatures markedly below T_g, the overall aging kinetics is controlled by processes whose activation energy is approaching the values characteristic of the β-relaxation process.

Considering the spatial heterogeneity of glass (Fig. 3.11), the initial stages of aging should occur predominantly via collapse (densification) of low-density mobility islands. This process would be driven by faster relaxation processes of lower cooperativity and lower activation energy. As aging glass becomes denser and more homogenous, the molecular mobility becomes more cooperative that causes the energy barrier to increase continuously toward the value characteristic of cooperative α-relaxation. This simple phenomenological picture explains well an increase in the effective activation energy revealed by an isoconversional analysis. In conclusion, we should note that the observed increase in the effective activation energy is not unique to physical aging of Mt. The effect has been reported [77, 78] for metallic glasses, although was not correlated with the α- or β-relaxation processes in the respective glasses.

3.4.3 Activation Energies of β-Relaxation from DSC

As discussed in the previous section, the activation energy of the early stages of aging approaches the activation energy of the β-relaxation, E_β, when the aging temperature is decreased significantly below T_g. In that regard, it is of interest to consider an original method proposed by Bershtein and Egorov [79] for estimating E_β from the pre-glass transition annealing peaks. The peaks of this kind were originally reported by Illers [80], who observed that reheating of PVC annealed significantly below T_g gives rise to small and broad endothermic DSC peak that may occur well before the glass transition step. Similar observation was made later by Chen [81, 82] for several metallic glasses and by Bershtein et al. [83, 84] for several polymers. Chen interpreted the effect as the partial enthalpy relaxation (during annealing) and recovery (during reheating) that occurs at the expense of the faster part of a broad relaxation spectrum of the glassy state. However, Bershtein et al. [83, 84] linked the effect to the β-relaxation process that is typically detected by mechanical [85] and dielectric [86] spectroscopy.

Chen as well as Bershtein et al. proposed that a shift in the annealing peak temperature, T_p, with the heating rate, β, can be used to determine the activation energy of the underlying process as follows:

$$E = -R\frac{\mathrm{d}\ln\beta}{\mathrm{d}T_p^{-1}}. \tag{3.31}$$

The E values estimated from the annealing peaks were found [81–84] being several times smaller than the respective activation energies for the glass transition (i.e., α-relaxation) event. The ratio of the respective activation energies was consistent with that reported [85, 86] for the β- and α-relaxations in polymers.

The annealing peaks observed below T_g result from the same reason as the regular aging peaks at the end of the glass transition step (Fig. 3.22). It is nothing else but endothermic recovery of the enthalpy lost on aging. The only difference is that when a glass is aged well below T_g (typically around $0.8T_g$), the recovery takes place before the glass transition step begins. However, as aging temperature is increased, the position of the annealing peak shifts to higher temperature so that it can appear at the beginning of the glass transition step, or in its middle, or ultimately at its end as regular aging peak (Fig. 3.27).

As long as the recovery occurs below the beginning of the glass transition step, the molecular mobility in the respective temperature region is likely to be dominated by the local noncooperative process, including the β-relaxation (Fig. 3.12). It thus seems reasonable to expect that a fair estimate of the E_β value can be obtained by analyzing the annealing peak data. We have tested this method of estimating E_β on a variety of polymeric (PS and its nanocomposite [30], PVP [87], poly(methyl methacrylate) (PMMA) [35], PET [35]), and small molecule organic (ursodeoxycholic acid [87], IM [41], glucose (Gl) [35], Mt [35]) glasses. For most of these glasses, the E_β values are known from traditional studies based on dielectric or me-

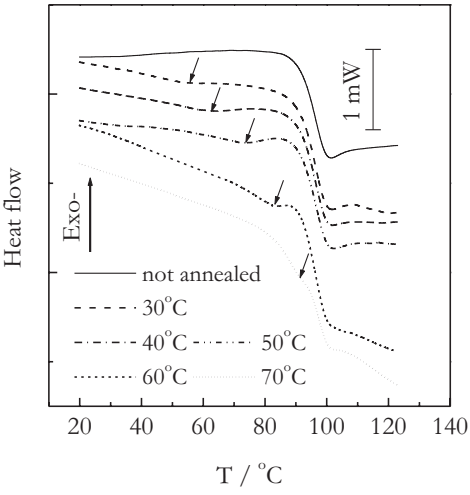

Fig. 3.27 DSC curves obtained on heating of polystyrene at 10 °C min^{-1} without annealing and after annealing for 30 min at different temperatures. *Arrows* point at the location of annealing peaks. (Adapted from Vyazovkin and Dranca [30] with permission of ACS)

chanical spectroscopy and, thus, can be directly compared with the values derived from the annealing peaks. An additional test is possible by comparing the activation energies estimated from the annealing peaks against the empirical correlation:

$$E_\beta = (24 \pm 3) R T_g \tag{3.32}$$

reported by Kudlik et al. [88]. This correlation holds very well for a great number of the E_β values for both polymers and small-molecule glasses [89].

The annealing peaks are produced by annealing a glass at about $0.8T_g$. The peaks are especially easy to produce in rapidly cooled glasses, which can be obtained by fast cooling directly in DSC or by quenching separately in liquid nitrogen. Faster cooling freezes a glass further from equilibrium that secures faster initial rate of aging. For rapidly cooled glasses, it usually takes about half an hour of aging to produce a well-detectable annealing peak. Once the aging period is finished, the glass needs to be cooled quickly well below the aging temperature to stop aging and immediately after that reheated at a relatively fast heating rate.

In DSC, the annealing peak manifests itself as a very broad and shallow endotherm, which starts to evolve above the annealing temperature (Fig. 3.27). The peaks are readily detected when comparing DSC traces for annealed and not annealed samples. The peaks obtained at any given annealing temperature would shift to higher temperature with increasing the heating rate. This permits estimating the activation energy from the slope of the plot $\ln\beta$ versus T_p^{-1} (Eq. 3.31). A series of such plots corresponding to different annealing temperatures is seen in Fig. 3.28.

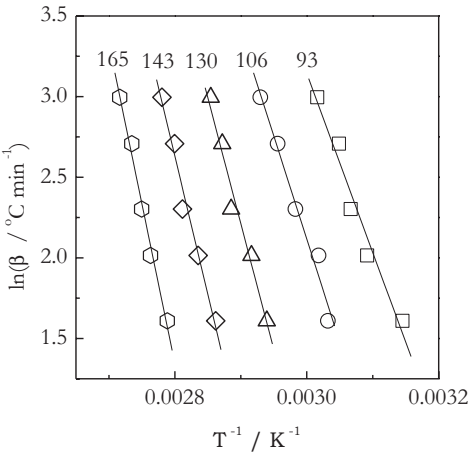

Fig. 3.28 Evaluating activation energies (Eq. 3.31) from the annealing peaks for polystyrene aged at different temperatures: 30 °C (*squares*), 40 °C (*circles*), 50 °C (*triangles*), 60 °C (*diamonds*), and 70 °C (*hexagons*). Numbers by the lines are the activation energies in kJ mol^{-1}. (Adapted from Vyazovkin and Dranca [30] with permission of ACS)

The slope of the plots as well as the activation energy decreases systematically with decreasing the annealing temperature.

For reasons explained earlier, the use of the lowest feasible annealing temperature yields better estimates for the activation energy of the β-relaxation. Following this principle, we have found [35] that considering their respective confidence intervals, all E_β values estimated from the annealing peaks are consistent with the correlation (Eq. 3.32). Furthermore, the obtained estimates of E_β appear to compare quite well against the literature values (Fig. 3.29). Our estimates typically involve ~10–20% of uncertainty. It is seen that most of the estimates deviate by less than 20% from the literature values, especially if one disregards a few extreme literature values, which may be outliers.

It is obvious that the activation energies derived from the annealing peaks correlate fairly well with the activation energies of the β-relaxation. Nevertheless, the respective assignment must be made with care. Note that annealing is conducted around $0.8T_g$, i.e., in the temperature region where one typically finds the absorption peaks due to the β-relaxation when using traditional methods of dielectric and mechanical spectroscopy [90]. However, the recovery process gives rise to the annealing peaks, whose peak temperatures are found about 20–30 °C above the annealing temperature. In this temperature range, the β-relaxation is not necessarily dominant so that the activation energy estimated from the annealing peaks may have a sizeable contribution from higher temperature and higher activation energy relaxation processes (see Fig. 3.12).

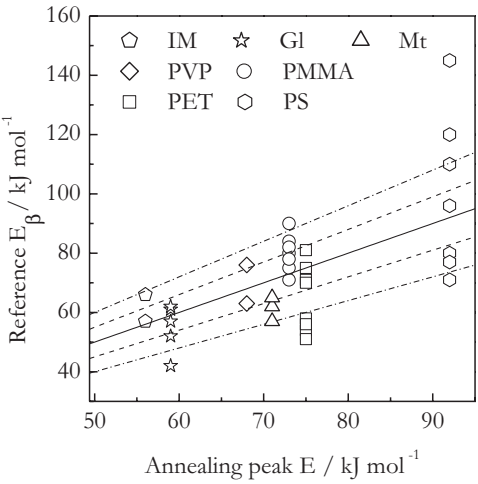

Fig. 3.29 Correlation of the E_β estimates from the annealing peaks with the literature values. *Solid line* represents exact equality; *dash* and *dash-dot lines* represent 10 and 20% deviations, respectively. *IM* indomethacin, *GI* glucose, *Mt* maltitol, *PVP* poly(vinylpyrrolidone), *PMMA* poly(methyl methacrylate), *PET* poly(ethylene terephthalate), *PS* polystyrene. (Reproduced from Vyazovkin and Dranca [35] with permission of Elsevier)

3.5 Nucleation

...matter cannot long do without the shaping, constructive force, and the force cannot do without the constructible material

J. C. Friedrich von Schiller, Letters upon the Æsthetic Education of Man

This section provides some basic introduction into the kinetics of nucleation because nucleation is the most common mechanism of the phase transition. The nucleation mechanism rests on a simple assumption that the formation of a new phase starts from the formation of a very small embryo of this phase. This mechanism is applicable to a variety of phase transitions, including the transitions discussed further in this chapter. Most common example is crystallization of melts on cooling. From the thermodynamic standpoint (Fig. 3.1), the melt should crystallize spontaneously as soon as temperature drops below the equilibrium melting temperature, T_m, because then the Gibbs free energy of the crystal is lower than that of the liquid phase (i.e., melt). The difference in the respective Gibbs energies is a negative value called the volume Gibbs energy, ΔG_V. In reality, crystallization occurs only when the melt reaches significant supercooling. Crystallization is delayed because the creation of the crystalline phase nucleus faces a free energy barrier associated with the surface free energy, ΔG_S. This value is the difference in the Gibbs energy of the surface and the bulk of the nucleus. The Gibbs energy of the surface is always larger by the value of the surface energy (surface tension), σ. That is why the value of ΔG_S is positive. The total free energy of nucleation is:

$$\Delta G = \Delta G_S + \Delta G_V. \tag{3.33}$$

It is clear from Eq. 3.33 that the spontaneous formation of a new phase nucleus can start only at temperature when ΔG_V is negative enough to outweigh ΔG_S.

If one assumes that the nucleus has a spherical shape of the radius, r, then the terms ΔG_S and ΔG_V can be determined respectively as the surface area of the sphere times the surface energy σ, and as the volume of the sphere times the volume energy per unit volume, ΔG_V:

$$\Delta G = 4\pi r^2 \sigma + \frac{4}{3}\pi r^3 \Delta G_V. \tag{3.34}$$

Figure 3.30 displays a dependence of ΔG_S and ΔG_V on the nucleus radius. The sum of these two terms (i.e., ΔG) passes through a maximum that represents the free energy barrier to nucleation, ΔG^*. The nucleus radius, r^*, that corresponds to ΔG^* is the critical size of a stable nucleus. A nucleus of a larger size would grow spontaneously forming a new phase. The size of the critical nucleus is found from the condition of ΔG maximum, i.e., by setting to zero the first derivative of ΔG with respect to r. This yields Eq. 3.35:

$$r^* = \frac{-2\sigma}{\Delta G_V}. \tag{3.35}$$

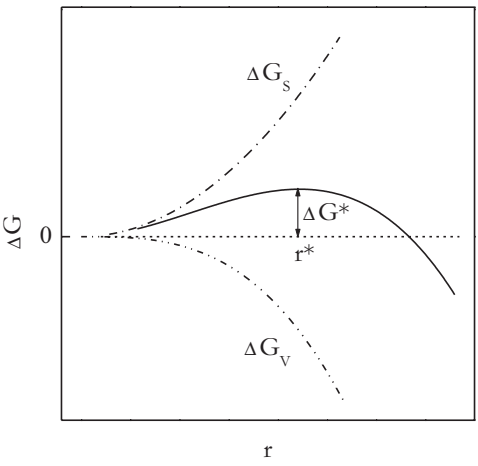

Fig. 3.30 Free energy of nucleation as a function of nucleus radius. (Adapted from Vyazovkin [91] with permission of Elsevier)

Inserting this value into Eq. 3.34 allows one to determine the height of free energy barrier as:

$$\Delta G^* = \frac{16\pi\sigma^3}{3(\Delta G_V)^2}. \tag{3.36}$$

The ΔG^* can be linked to supercooling through the temperature dependence of ΔG_V:

$$\Delta G_V = \Delta H_V - T\Delta S_V. \tag{3.37}$$

Assuming that ΔH_V and ΔS_V do not depend much on temperature, ΔS_V in Eq. 3.37 can be replaced with its value at equilibrium (i.e., when $T = T_m$ and $\Delta G_V = 0$):

$$\Delta G_V = \Delta H_V - T\frac{\Delta H_V}{T_m} = \frac{-\Delta H_f \Delta T}{T_m}, \tag{3.38}$$

where $\Delta T = T_m - T$ is the supercooling and $\Delta H_f = -\Delta H_V$ is the enthalpy of fusion per unit volume. Substitution of Eq. 3.38 into Eq. 3.36 gives:

$$\Delta G^* = \frac{16\pi\sigma^3 T_m^2}{3(\Delta H_f)^2(\Delta T)^2}, \tag{3.39}$$

where ΔH is the heat of fusion per unit volume. Similarly, substitution of Eq. 3.38 into 3.35 reveals a dependence of the critical nucleus size on supercooling:

$$r^* = \frac{2\sigma T_m}{\Delta H_f \Delta T}. \tag{3.40}$$

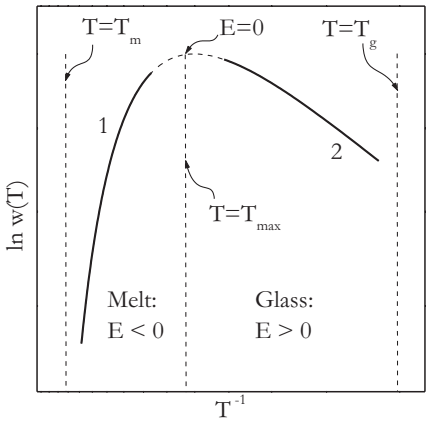

Fig. 3.31 Arrhenius plot for nucleation in temperature range T_g–T_m (1 melt nucleation, 2 glass nucleation). (Adapted from Vyazovkin [91] with permission of Elsevier)

The nucleation rate constant is commonly expressed in the Arrhenius form:

$$w(T) = w_0 \exp\left(\frac{-\Delta G^*}{RT}\right), \tag{3.41}$$

where w_0 is the preexponential factor. However, the temperature dependence of the nucleation constant is more complex than that of the regular rate constant (Eq. 1.2) because ΔG^* depends strongly on ΔT, whose magnitude changes with temperature. This causes the Arrhenius plots of $\ln w(T)$ versus T^{-1} to be nonlinear (Fig. 3.31) [91]. Also, as supercooling decreases with decreasing temperature, both critical nucleus size (Eq. 3.40) and energy barrier (Eq. 3.39) decrease so that the nucleation rate constant increases. Therefore, it demonstrates a negative (or anti-Arrhenian) temperature dependence. Figure 3.31 shows an Arrhenius plot for the nucleation rate. The plot has a positive slope that corresponds to the negative temperature dependence. When the melt crystallization data are fitted to the Arrhenius equation, the fit yields a negative value of the effective activation energy. Also, the slope varies strongly with the temperature, reaching infinity at $T = T_m$ (Eq. 3.39).

Just below the melting point, the nucleation rate quickly increases with decreasing temperature (Fig. 3.32). However, the nucleation rate does not increase indefinitely. It passes through a distinct maximum at a certain temperature, T_{max}. Below this temperature, the nucleation rate starts to decrease with decreasing temperature. This happens because the molecular mobility decreases with temperature. The melt becomes increasingly more viscous, creating an energy barrier, E_D, to diffusion of molecules across the phase boundary. Introduction of the respective energy term into Eq. 3.41 gives rise to the Turnbull and Fisher equation [92]:

$$w(T) = w_0 \exp\left(\frac{-\Delta G^*}{RT}\right)\exp\left(\frac{-E_D}{RT}\right), \tag{3.42}$$

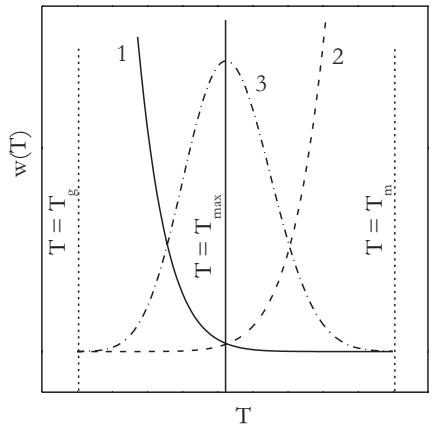

Fig. 3.32 Temperature dependence of nucleation rate (1 $\exp(-\Delta G^*/RT)$, 2 $\exp(-E_D/RT)$, 3 product of 1 and 2). (Adapted from Vyazovkin [91] with permission of Elsevier)

where E_D is the activation energy of the diffusion process. Unlike the ΔG^* term, the E_D term represents a typical Arrhenius temperature dependence (Fig. 3.32). The product of these two terms (Eq. 3.42) yields a temperature dependence that demonstrates a maximum in the nucleation rate. Below T_{max}, the process becomes controlled by diffusion that results in a dramatic decrease of the nucleation rate.

If for a particular compound the maximum nucleation rate is not very large, the respective melt can be readily turned into the glass phase on cooling. Glasses can crystallize on heating. Once the temperature rises above the glass transition temperature, the glass relaxes turning into the metastable supercooled liquid. As temperature continues to rise, the molecular mobility increases, promoting nucleation and crystallization of the supercooled liquid. The glass crystallization on heating is frequently called "cold crystallization." Cold crystallization normally occurs below T_{max}. In this temperature range, the nucleation rate increases with increasing temperature because the rate is limited by diffusion. The corresponding Arrhenius plot (Fig. 3.31) has the regular negative slope that represents a positive (or Arrhenian) temperature dependence. Fitting glass crystallization data to the Arrhenius equation yields a positive value of the effective activation energy. Note that the slope of the Arrhenius plot decreases with increasing temperature.

To better understand the temperature dependence of the effective activation energy for the process of nucleation in the melt and glass crystallization, we can use Eq. 3.42 to derive a theoretical expression for E versus T. The effective activation energy is generally defined as the logarithmic derivative of the rate constant with respect to the reciprocal temperature:

$$E = -R\frac{\mathrm{d}\ln w(T)}{\mathrm{d}T^{-1}}. \tag{3.43}$$

Assuming that the temperature dependence of ΔG^* is determined only by ΔT (see Eq. 3.39), Eq. 3.42 can be rewritten as:

$$w(T) = w_0 \exp\left[\frac{-A}{RT(\Delta T)^2}\right] \exp\left(\frac{-E_D}{RT}\right), \tag{3.44}$$

where A is constant that includes all the parameters from the right-hand side of Eq. 3.39 but ΔT. With regard to Eq. 3.43, the effective activation energy is:

$$E = E_D - A\left[\frac{2T}{(\Delta T)^3} - \frac{1}{(\Delta T)^2}\right]. \tag{3.45}$$

The temperature dependence of E that results from Eq. 3.45 is shown in Fig. 3.33. The equation suggests that when crystallization occurs on cooling from the melt at small supercoolings, E should demonstrate large negative values ($E \to -\infty$, when $\Delta T \to 0$). On the other hand, when crystallization occurs on heating from the glass phase, E should demonstrate positive value whose magnitude for early stages of crystallization should be comparable to the E_D value. When one decreases the temperature of the melt crystallization or increases the temperature of the glass crystallization, the effective activation energy respectively increases or decreases toward zero.

The above analysis can be extended to predict the dependencies of the isoconversional activation energies on conversion. Expressing the rate of the nucleation-driven crystallization by the basic rate equation

$$\frac{d\alpha}{dt} = w(T) f(\alpha), \tag{3.46}$$

the isoconversional activation energy can be estimated as usual (see Eq. 1.13):

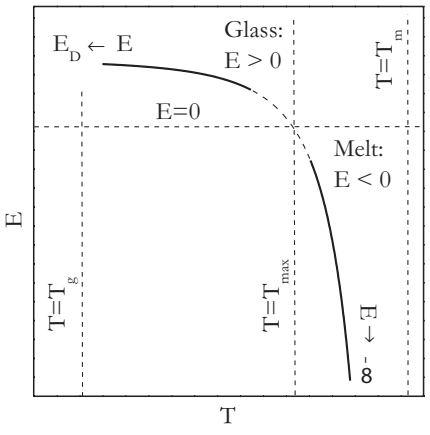

Fig. 3.33 Theoretical dependencies of the activation energy for the melt and glass crystallization predicted by Eq. 3.45

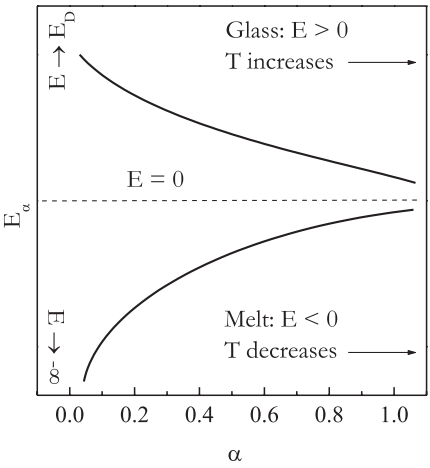

Fig. 3.34 Theoretically predicted dependencies of E_α on α for melt and glass crystallization. (Adapted from Vyazovkin [91] with permission of Elsevier)

$$E_\alpha = -R\left[\frac{\partial \ln(\mathrm{d}\alpha/\mathrm{d}t)}{\partial T^{-1}}\right]_\alpha . \tag{3.47}$$

By virtue of the isoconversional principle (Eq. 1.12), the right-hand side of Eq. 3.47 is equal to that of Eq. 3.45. It means that E_α has the same form as E in Eq. 3.45. Since an increase in α is equivalent to a decrease in T for the melt crystallization and to increase in T for the glass crystallization, the E_α versus α dependencies take the forms displayed in Fig. 3.34. Having the opposite signs, the E_α values for the melt and glass crystallization tend toward zero as crystallization progresses from $\alpha = 0$ to 1.

To conclude this section, two short comments need to be made about limitations of the above derivations. First, the derivations have been performed for a spherical, i.e., three-dimensional type of nucleus. Changing the assumption about the nucleus shape to a two-dimensional type, such as a disk, would introduce important changes into some of the equations [93]. For instance, ΔG^* would be inversely proportional to ΔG_V, not to $(\Delta G_V)^2$ as in the case of the three-dimensional type of nucleus (Eq. 3.36). Consecutively, $(\Delta T)^2$ in Eq. 3.44 would change to ΔT. Second, the derivations have been made under the assumption of homogeneous nucleation, i.e., when a nucleus is formed inside the melt phase. However, the nuclei can form on the substrate (e.g., solid impurity, container wall, etc.), i.e., heterogeneously. The free energy barrier of heterogeneous nucleation is substantially smaller than that of homogeneous nucleation. For example, when a spherical nucleus is formed homogeneously, the free energy barrier of its formation is proportional to the surface free energy of the entire surface of the sphere. However, when the nucleus is formed at the substrate, it assumes the shape of a spherical cup, which at the same radius has a smaller surface area than the whole sphere. As a result, the free energy barrier to heterogeneous nucleation, G^*_{het}, is always smaller than that for the homogeneous one, by some geometrical factor, $f(\Theta) < 1$:

$$\Delta G^*_{het} = \Delta G^* f(\Theta). \tag{3.48}$$

The magnitude of $f(\Theta)$ is determined by the contact angle, Θ, between the substrate and forming phase. For a spherical nucleus on a flat substrate, the geometrical factor is defined by the following equation: [3, 4, 93].

$$f(\Theta) = \frac{(2+\sin\Theta)(1-\cos\Theta)^2}{4}. \tag{3.49}$$

A detailed discussion of the geometrical factors for different type of nuclei and substrates is provided by Mandelkern [93].

3.6 Crystallization of Polymers

the crystal has only one manifestation of life, crystallisation, which afterwards has its fully adequate and exhaustive expression in the rigid form, the corpse of that momentary life.
Arthur Schopenhauer, The World as Will and Idea

3.6.1 Background

As any first-order transition, crystallization is accompanied by a significant enthalpy change that makes DSC a method of choice for measuring the overall rates of polymer crystallization [93, 94]. The overall kinetics of isothermal conversion from the amorphous (liquid or solid) to crystalline phase is commonly described in terms of the equation:

$$\alpha = 1 - \exp\left[-k(T)t^{\mathrm{m}}\right] \tag{3.50}$$

which is frequently called the Avrami equation [95–97]. In Eq. 3.50, t is the time, α is the extent of conversion from the amorphous to crystalline phase, m is the Avrami exponent that is associated with the crystallization mechanism, and $k(T)$ is the overall (macroscopic) rate constant. The latter is usually replaced with $k'(T) = [k(T)]^{1/\mathrm{m}}$ to keep the product in the brackets dimensionless. There are several techniques that allow Eq. 3.50 to be applied to nonisothermal conditions [93, 94].

It should be stressed that the rate constant in Eq. 3.50 does not have the Arrhenius temperature dependence. As long as the temperature range is sufficiently wide, the Arrhenius plots reveal substantial nonlinearity as seen in Fig. 3.35 that presents the $k'(T)$ values reported [98] for the melt and glass crystallization of poly(trimethylene terephthalate). It is easy to recognize that the presented plot is similar to the one (Fig. 3.31) derived theoretically from the Turnbull and Fisher equation (3.42). Needless to say that the use of such plots for estimating the activation energy would yield the value that varies with temperature in accord with Eq. 3.45 (Fig. 3.33).

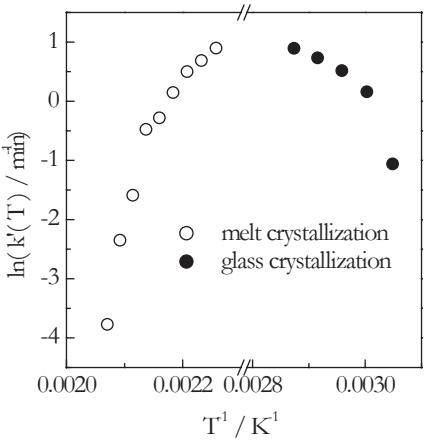

Fig. 3.35 Arrhenius plot for crystallization of poly(trimethylene terephthalate) from melt and crystalline phases. (The Avrami rate constants are taken from Hong et al. [98])

Speaking of estimating the activation energies for polymer crystallization, a special comment needs to be made about the widespread application of the Kissinger method [99, 100] to the melt crystallization data, i.e., data obtained on cooling. The method allows for a quick and simple evaluation of the activation energy by the following equation:

$$E = -R\frac{\mathrm{d}\ln(\beta / T_\mathrm{p}^2)}{\mathrm{d}T_\mathrm{p}^{-1}}, \tag{3.51}$$

where β is the heating rate, and T_p is the temperature of DSC (or differential thermal analysis, DTA) peak. Unfortunately, the application is so common that it is claimed sometimes that the method was developed for crystallization and that β in its equation is the cooling rate. None of that is true. As a matter of fact, neither of the two papers [99, 100] that introduce the method even contains the words "cooling" or "crystallization." Furthermore, it has been demonstrated [101] that the use of cooling rates in Eq. 3.51 is a mathematically invalid operation that results in evaluation of erroneous values of the activation energy. As far as the application of the method to the glass crystallization data (i.e., data obtained on heating), the limitation is that the method produces a single value of the activation energy for the whole temperature range whereas the value is likely to be temperature dependent.

Although the Avrami equation generally fits the polymer crystallization data quite well, one should remember that the model was developed having in mind crystallization of metals. Therefore, it does not account for any specifics of crystallization of long, flexible, and entangled polymer chains. For example, in Eq. 3.50, α is supposed to represent the absolute extent of crystallinity that changes from 0 (entirely amorphous phase) to 1 (fully crystalline phase). The metals readily attain fully crystalline state. However, crystallization of polymers results in the extents of crystallinity that are significantly smaller than 1, which is a direct consequence of the polymer chain dynamics. Thus, the application of the Avrami equation to poly-

mers requires an empirical adjustment, when the actual maximum extent of crystallinity is taken as $\alpha = 1$. In addition to the rate constant, the Avrami analysis yields the Avrami exponent, which according to the theory can take some specific values from ½ to 4. Note that even in this case, the values of m do not allow for singular mechanistic interpretation [93, 94]. It is also not uncommon when the m values vary markedly with temperature. All in all, the Avrami analysis is rather "a convenient representation of experimental data" [102] than a way of obtaining physical insights in the polymer crystallization kinetics.

A widely accepted kinetic theory of polymer crystallization was developed by Hoffman and Lauritzen [103, 104]. The theory makes use of the Turnbull–Fisher model (Eq. 3.42) and adjusts it to the chain folding mechanism that drives crystallization of polymers. The basic equation of the theory describes the temperature dependence of the growth rate of polymer spherulites as follows:

$$\Lambda = \Lambda_0 \exp\left(\frac{-U^*}{R(T - T_\infty)}\right)\exp\left(\frac{-K_g}{T\Delta T f}\right), \tag{3.52}$$

where Λ_0 is the preexponential factor, U^* is the activation energy of the segmental jump, $\Delta T = T_m - T$ is the supercooling, $f = 2T/(T_m + T)$ is the correction factor, and T_∞ is a hypothetical temperature where motion associated with viscous flow ceases that is usually taken 30 K below the glass transition temperature, T_g. The kinetic parameter K_g has the following form:

$$K_g = \frac{nb\sigma\sigma_e T_m}{\Delta h_f k_B}, \tag{3.53}$$

where b is the surface nucleus thickness, σ is the lateral surface free energy, σ_e is the fold surface free energy, T_m is the equilibrium melting temperature, Δh_f is the heat of fusion per unit volume of crystal, k_B is the Boltzmann constant, and n takes the value 4 for crystallization regime I and III, and 2 for regime II. The dependence of the growth rate on temperature passes through a maximum (Fig. 3.36) in similar fashion as the rate of nucleation (Fig. 3.32).

The parameter U^* is typically assumed to have the universal value 6.3 kJ mol^{-1} (i.e., 1.5 kcal mol^{-1}) [103]. This assumption in combination with little algebra affords Eq. 3.52 to be transformed to Eq. 3.54:

$$\ln\Lambda + \frac{U^*}{R(T - T_\infty)} = \ln\Lambda_0 - \frac{K_g}{T\Delta T f}. \tag{3.54}$$

Then K_g can be determined from the linear plot of the left-hand side of Eq. 3.54 against $(T\Delta T f)^{-1}$. The equation is known [103] to describe adequately the growth kinetics in a range of supercoolings as wide as 40–100 °C. This means that at least potentially both melt and glass crystallization kinetics can be described by a single set of the constant parameters U^* and K_g.

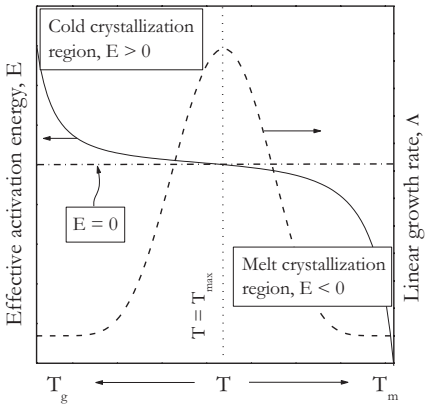

Fig. 3.36 Schematic presentation of the temperature dependencies for the growth rate (*dash line*) from Eq. 3.52 and the effective activation energy (*solid line*) from Eq. 3.60. (Adapted from Vyazovkin and Dranca [108] with permission of Wiley)

Equations 3.54 and 3.52 rely on the spherulite growth rate that is measured directly by using microscopy. This rate cannot be measured by DSC. The technique measures the heat flow of crystallization that is proportional to the overall growth rate. On the other hand, the heat flow is linked to the growth rate as follows: [105]

$$\Phi = \Delta h S \Lambda, \tag{3.55}$$

where Δh is the volumetric heat of crystallization and S is the total area of the growth surface. The problem here is the unknown value of S. Toda et al. [105] have demonstrated that it can be eliminated when determining the logarithmic derivative of the heat flow:

$$\frac{\mathrm{d}\ln\Phi}{\mathrm{d}T} = \frac{\mathrm{d}\ln\Lambda}{\mathrm{d}T}. \tag{3.56}$$

Equation 3.56 is remarkable because it establishes the equivalence of the temperature coefficients of the heat flow and the growth rate. Toda et al. [105, 106] have confirmed this equivalence experimentally for several polymers by applying TM DSC and microscopy to measure respectively the left- and right-hand sides of Eq. 3.56.

Equation 3.56 can easily be transformed into Eq. 3.57:

$$-R\frac{\mathrm{d}\ln\Phi}{\mathrm{d}T^{-1}} = -R\frac{\mathrm{d}\ln\Lambda}{\mathrm{d}T^{-1}}. \tag{3.57}$$

In DSC, the overall crystallization rate is determined as the ratio of the heat flow to the total heat of crystallization, ΔH, i.e.,

$$\frac{\mathrm{d}\alpha}{\mathrm{d}t} = \frac{\Phi}{\Delta H}. \tag{3.58}$$

Then, if in Eq. 3.57, the derivate of Φ is taken at a constant extent of conversion, it would yield an isoconversional value of the activation energy:

$$E_\alpha = -R\frac{\mathrm{d}\ln\Lambda}{\mathrm{d}T^{-1}}. \tag{3.59}$$

Substituting Λ from Eq. 3.52 into Eq. 3.59 and taking its respective derivative allows us to derive [107] a practically important equation:

$$E_\alpha = U^* \frac{T^2}{(T-T_\infty)^2} + K_g R \frac{T_m^2 - T^2 - T_m T}{(T_m - T)^2 T}. \tag{3.60}$$

In this equation, the left-hand side represents an experimental temperature dependence of the effective activation energy derived by an isoconversional method. The right-hand side, however, is a theoretical dependence whose parameters U^* and K_g can be determined by fitting this dependence to the experimental one. Therefore, isoconversional analysis of the overall rate of DSC data can be used to extract the parameters of the Hoffman–Lauritzen theory that otherwise would have to be evaluated from the microscopy data on linear growth of the spherulites.

Analysis of the right-hand side of Eq. 3.60 suggests that the second term is negative in the temperature range between $\sim 0.618T_m$ and T_m. The absolute value of this term quickly increases as temperature approaches T_m. This means that the effective activation energy of the melt crystallization should have very large negative values at small supercoolings as well as at low extents of conversions when the measurements are done on continuous cooling. As temperature of the melt crystallization decreases further away from T_m, the effective activation energy should increase toward zero. The first term, on the other hand, is always positive. Its value increases as temperature approaches T_∞. Therefore, as the temperature of the glass crystallization increases, the effective activation energy should decrease toward zero. The overall temperature dependence of the effective activation energy is shown in Fig. 3.36 [108].

3.6.2 Isoconversional Treatment

The first step in isoconversional analysis of the polymer crystallization data is identifying an appropriate isoconversional method. The major point of concern is the treatment of the melt crystallization data, i.e., the data obtained on cooling. It has been emphasized in Sect. 2.1.2 (Figs. 2.6, 2.10) that the rigid integral methods should not be used for treating the data obtained on cooling. Adequate isoconversional methods include the flexible integral methods or the differential method of Friedman.

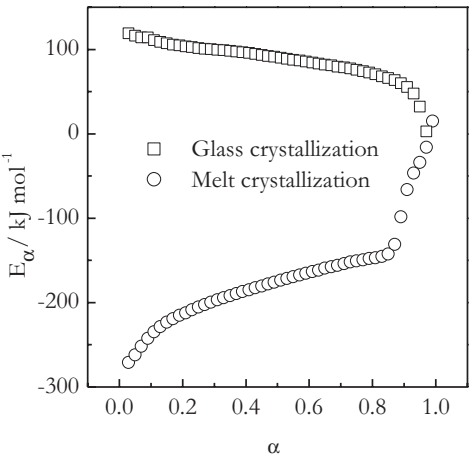

Fig. 3.37 Isoconversional values of the effective activation energy for glass and melt crystallization of poly(ethylene terephthalate). (Adapted from Vyazovkin et al. [107, 108] with permission of Wiley)

Once an appropriate method is selected, it can be applied to a set of DSC curves collected at several heating or cooling rates. As a result, one obtains a dependence of the effective activation energy on the extent of conversion from the amorphous to crystalline state. Example of such dependencies for crystallization of PET is shown in Fig. 3.37. In agreement with the earlier discussion (Fig. 3.36), the activation energies for the melt crystallization are negative and for the glass crystallization positive. It is also seen that in both cases the E values tend to zero as crystallization progresses from $\alpha=0$ to 1. Again, this is consistent with the temperature-dependent trends for E presented in Fig. 3.36. Recall that an increase in α represents an increase in temperature for the glass crystallization and a decrease in temperature for the melt crystallization.

In order to be able to parameterize the obtained isoconversional activation energies in terms of the Hoffman–Lauritzen theory, one needs to switch from a dependence of E_α versus α to a dependence of E_α versus T. Since any given value α is reached at different temperatures, depending on the heating (or cooling) rate (Fig. 1.8), the respective set of temperatures is replaced with a single mean value. Then, by replacing each value of α with the mean temperature related to it (Fig. 3.38), one obtains a dependence of E_α versus T.

The E_α versus T dependence for the melt crystallization of PET is shown in Fig. 3.39. As follows from Fig. 3.36, the E_α values are expected to be negative at temperatures below T_{max} that is experimentally found for PET in the region 170–190 °C [109]. A remarkable feature of the dependence is a break point at ~475 K (i.e., ~202 °C) that signals a change in the crystallization mechanism. For isothermal PET crystallization, Lu and Hay [110] and Rahman and Nandi [111] have reported a change in the crystallization mechanism revealed as a break point in the Hoffman–Lauritzen plot (Eq. 3.54) at the respective temperatures 217 and 236 °C. Also, Okamoto et al. [112] have observed a change in the crystallization regime at 202 °C.

Because of the change in the crystallization mechanism, the higher temperature ($T>475$ K) and lower temperature ($T<475$ K) portions of the E_α versus T dependence should be analyzed separately. It means that Eq. 3.60 should be fitted individ-

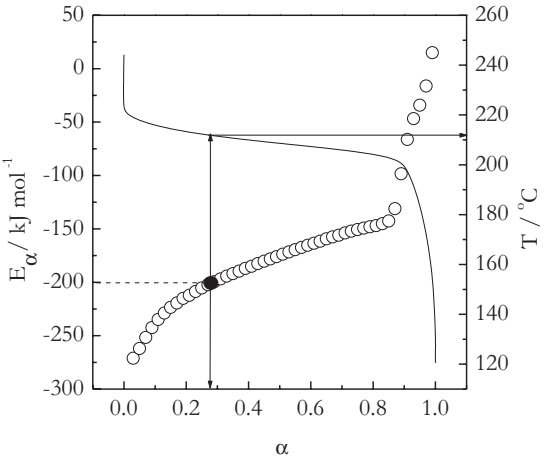

Fig. 3.38 Converting dependence of E_α versus α (*circles*) to dependence of E_α versus T. *Solid line* represents a dependence of α on the mean temperature. $E_\alpha = -200$ kJ mol^{-1} corresponds to $\alpha = 0.28$, which, in turn, corresponds to the mean temperature 212 °C. (Adapted from Vyazovkin and Sbirrazzuoli [107] with permission of Wiley)

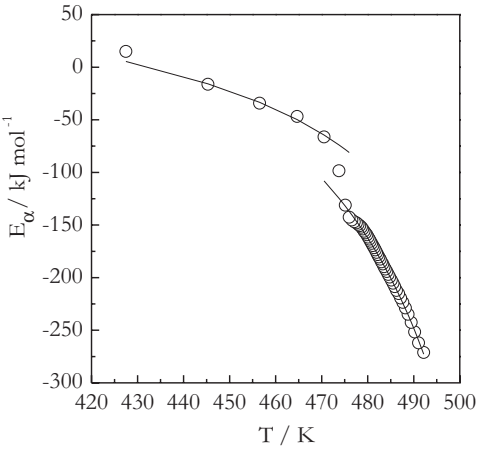

Fig. 3.39 Dependence of the effective activation energy on the mean temperature. *Solid lines* represent fits of Eq. 3.60. (Adapted from Vyazovkin and Sbirrazzuoli [107] with permission of Wiley)

ually to the two portions of the experimental E_α versus T dependence. The computation requires the values of T_g and T_m which are 342 and 553 K, respectively [113].

The fits result in the K_g and U^* values shown in Table 3.2 that also collects the values reported in the literature [110, 111, 114–118] for isothermal crystallization of PET. There is obviously a considerable spread in the literature values. However, the values obtained from fitting Eq. 3.60 to the experimental E_α versus T dependence appear to be reasonably consistent with the reported values, although seem to be on the low side. At least partially, this is because Eq. 3.60 treats both K_g and U^* as variables whereas most of the calculations in Table 3.2 have been done by setting U^* in Eq. 3.54 to the constant value 6.3 kJ mol^{-1} and fitting K_g. Although 6.3 kJ mol^{-1} is used widely as "the universal value," Hoffman et al. [103] have found that for a set of polymers studied, the best-fit values of U^* vary between 4 and 17 kJ mol^{-1}. In addition, they have noted that increasing the value of U^* results in evaluating a

Table 3.2 Hoffman–Lauritzen parameters for crystallization of PET

$K_g \times 10^{-5}$ (K^2)		U^* (kJ mol^{-1})	Ref.
Regime I/III	Regime II		
5.0	2.5	6.3	[110]
8.7	6.1	6.3	[111]
12.80[a]		12.75	[114]
	2.8	6.3	[115]
	3.0	6.3	[116]
3.7[b]		6.3	[117]
	2.3	6.3	[118]
3.2	1.9	4.3/2.3	Equation 3.60

[a] *Identified as* regime III
[b] *Regime is not identified*

larger value of K_g. Therefore, fitting both K_g and U^* seems like a better approach that should result in more reliable estimates of these values.

The use of Eq. 3.60 yields the K_g values 3.2 and 1.9×10^5 K^2 for respectively higher and lower temperature portions of E_α versus T dependence. It is noteworthy that the higher temperature portion gives the K_g value that is 1.7 times larger than the value related to the lower temperature portion. The ratio is very close to the theoretical ratio 2 that represents a change in the crystallization mechanism from regime I to regime II [103]. This is an important clue regarding the mechanism of crystallization.

It was mentioned earlier that the Hoffman–Lauritzen equation holds for supercoolings as large as 100 °C that makes it potentially possible to fit both melt and glass crystallization kinetics with one set of the K_g and U^* parameters. Figure 3.40 presents the E_α versus T dependencies for crystallization of PET glass and melt. The

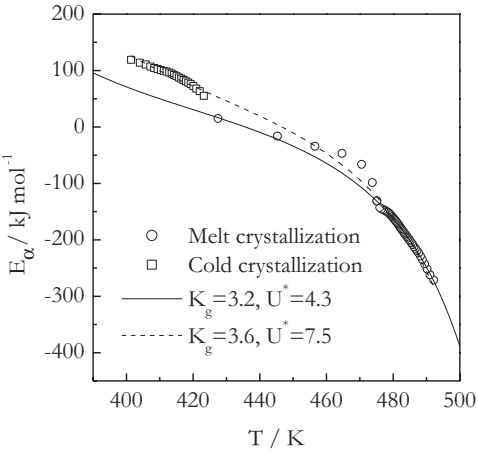

Fig. 3.40 Experimental E_α versus T data for melt (*circles*) and glass (*squares*) crystallization of PET. *Solid line* represents a fit for the melt data. *Dashed line* has been obtained by fitting combined (*melt and glass*) crystallization data. (Reproduced from Vyazovkin and Dranca [108] with permission of Wiley)

E_α versus T dependence for the glass crystallization is obtained from the E_α versus α data (Fig. 3.37) in the same manner as explained earlier for the melt crystallization data. It is seen that the higher temperature portion of the E_α versus T data for the melt crystallization appears to follow the same trend as the E_α versus T data for the glass crystallization.

Fitting Eq. 3.60 to the combined dataset yields the following parameters: $K_g = 3.6 \times 10^5$ K^2 and $U^* = 7.5$ kJ mol^{-1}. Both values have increased relative to their counterparts values obtained from the melt data (Table 3.2). The value of K_g has increased by a little over 10%. Its ratio to the regime II $K_g = 1.9 \times 10^5$ K^2 has become even closer to 2. The U^* value has increased significantly by over 70%. Note that the obtained value of U^* has moved much closer to the universal value 6.3 kJ mol^{-1}. It seems logical to expect that adding the cold crystallization data may improve the accuracy of the U^* value. The cold crystallization kinetics is limited primarily by diffusion so that cold crystallization data contain mostly information about this process and, thus, should afford its better description in the form of a more accurate value of U^*. More importantly, this and other examples [108, 119, 120] clearly demonstrate that both melt and glass crystallization kinetics can be fitted successfully with a single set of the Hoffman–Lauritzen parameters.

3.7 Melting of Polymers

the damsel took the lute, and tuned its strings, and played upon it in a manner that would melt iron

The story of Nur-Ed-Din and Enis-El-Jelis, One Thousand and One Nights

3.7.1 Background

A most common approach to the process of melting is based on thermodynamics. It suggests that melting occurs nearly instantaneously at an equilibrium temperature that remains constant throughout the crystal-to-melt conversion because the heat supplied to the crystal phase is converted to the entropy of the liquid phase. However, it has long been known that melting occurs at a finite rate, whose magnitude increases with the superheating, i.e., the difference between the actual and equilibrium temperature. This feature of the melting process is reminiscent of nucleation, whose rate is exponentially proportional to the supercooling (Sect. 3.5). The exponential dependence of the rate on the superheating has been demonstrated by Toda et al. [121] for melting of several polymers, including PET and poly(ε-caprolactone) (PCL). This prompted Toda et al. [121] to propose a model of nucleation-driven kinetics of polymer melting. The aforementioned exponential dependence has been reported in several other publications [122–126].

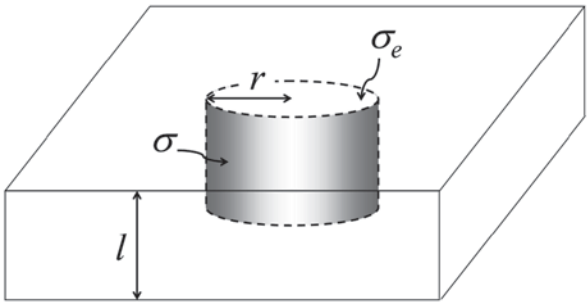

Fig. 3.41 Schematic depiction of a cylindrical nucleus of the radius r formed inside a lamellar crystal of the thickness l. σ and σ_e represent the free energy of the lateral and the fold surface, respectively

The melt nucleation model is derived as follows [127]. Similar to Eq. 3.33, the free energy barrier to the formation of a melt nucleus consists of the surface and volume components:

$$\Delta G = \Delta G_S S + \Delta G_V V, \tag{3.61}$$

where ΔG_S and ΔG_V are the free energy per unit area and unit volume, respectively, and S and V are the nucleus area and volume. The melt nucleus is assumed to have the shape of a cylinder and form inside a lamellar crystal whose thickness is l (Fig. 3.41). The assumption of the cylindrical shape is quite common for crystalline polymers because they crystallize by chain folding so that a crystalline nucleus presents itself as several chain folds of about the same height. Under this assumption, Eq. 3.61 can be written as:

$$\Delta G = 2\pi rl\sigma - 2\pi r^2\sigma_e + \pi r^2 l\Delta G_V, \tag{3.62}$$

where the first and second terms represent respectively the lateral (side) and folding (top and bottom) surface free energy of a cylinder. The second term is negative because during melting, the folding surface disappears, merging with the surrounding melt. The third term represents the volume free energy. Its value depends on temperature as follows:

$$\Delta G_V = \Delta H_f \frac{T_m^0 - T}{T_m^0}. \tag{3.63}$$

Equation 3.63 is obtained the same way as Eq. 3.38, the only difference being that for melting $\Delta H_V = \Delta H_f$. When lamellar crystal is sufficiently thin (l is very small), it can melt at temperature T_m below reaching the equilibrium melting temperature T_m^0. The temperature difference is determined by the Gibbs–Thomson equation: [128]

$$T_m^0 - T_m = \frac{2\sigma_e T_m^0}{l\Delta H_f}. \tag{3.64}$$

It follows from Eq. 3.64 that

$$2\sigma_e = l\Delta H_f \frac{T_m^0 - T_m}{T_m^0}. \tag{3.65}$$

Substitution of the right-hand sides of Eqs. 3.63 and 3.65 into Eq. 3.62 followed by some rearrangements yields:

$$\Delta G = 2\pi rl\sigma - \pi r^2 l\Delta H_f \frac{T - T_m}{T_m^0}. \tag{3.66}$$

Taking the derivative of ΔG with respect to r and setting it to zero allows one to determine the critical radius of the nucleus:

$$r^* = \frac{\sigma T_m^0}{\Delta H_f \Delta T}, \tag{3.67}$$

where $\Delta T = T - T_m$ is superheating with respect to the nonequilibrium melting temperature, T_m. Substitution of r^* into Eq. 3.66 gives rise to the magnitude of the nucleation barrier to the polymer crystal melting:

$$\Delta G^* = \frac{\pi l\sigma^2 T_m^0}{\Delta H_f \Delta T}. \tag{3.68}$$

Then ΔG^* can be substituted into Eq. 3.41 for the nucleation rate constant. Assuming that the temperature dependence of ΔG^* is determined by ΔT alone, the nucleation rate constant can be written as:

$$w(T) = w_0 \exp\left(\frac{-\Delta G^*}{RT}\right) = w_0 \exp\left(\frac{-A}{RT\Delta T}\right), \tag{3.69}$$

where A is a constant that includes all parameters from ΔG^* (Eq. 3.68) but ΔT.

According to Toda et al. [121], the overall rate of polymer melting can be described by the following equation:

$$\frac{d\alpha}{dt} = -w(T)\alpha, \tag{3.70}$$

where α is the crystalline fraction that changes from 1 to 0 as crystals melt. By replacing α with $1-\alpha$, Eq. 3.70 can be easily rewritten for the extent of conversion from crystal to melt that:

$$\frac{d\alpha}{dt} = w(T)(1-\alpha). \tag{3.71}$$

This is a well-familiar form of a first-order rate equation. Equation 3.71 can now be used to derive an equation for the isoconversional activation energy. As usual, it is done by taking the logarithmic derivative of the rate (Eq. 3.71) at a constant extent of conversion. This leads to Eq. 3.72: [129]

$$E_\alpha = -R\left[\frac{\partial \ln\left(\mathrm{d}\alpha / \mathrm{d}t\right)}{\partial T^{-1}}\right]_\alpha = A\left[\frac{1}{\Delta T} + \frac{2T}{(\Delta T)^2}\right]. \tag{3.72}$$

Note that because the derivative is taken at a constant extent of conversion, the obtained result is independent of the type of the reaction model used in Eq. 3.71.

In Eq. 3.72, E_α is the temperature-dependent activation energy estimated by an isoconversional method. The right-hand side of this equation represents a theoretical E versus T dependence determined by a single parameter A. By its meaning, A is always positive and so is the expression in the brackets. At very early stages of meting, when temperature is just above the nonequilibrium melting temperature (T_m), ΔT is close to zero so that E_α can take on extremely large values. However, the E_α values would decrease as ΔT continues to increase throughout the melting process. Overall, the nucleation model predicts that the effective activation energy of melting should exhibit a decreasing dependence on temperature. Also, fitting the theoretical E versus T dependence to the experimental one should afford estimating the parameter A and possibly the lateral surface free energy, if other parameters composing A are known.

3.7.2 Isoconversional Treatment

DSC is an efficient way of measuring the polymer melting kinetics. However, a straightforward application of an isoconversional method to polymer melting data presents a certain challenge. The problem is that the DSC melting peaks shift very little when changing the heating rate. For example, a tenfold increase in the heating rate shifts the DSC melting peak for PET by less than 3 °C (Fig. 3.42).

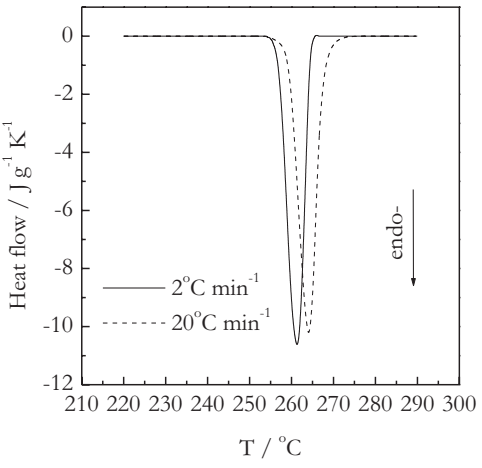

Fig. 3.42 DSC curves of PET melting at the heating rates 2 and 20 °C min^{-1}. Heat flow is normalized to the sample mass and heating rate. *PET* poly (ethylene terephthalate). (Adapted from Vyazovkin et al. [129] with permission of Wiley)

If one spreads this interval evenly between, say, five heating rates ranging from 2 to 20 °C min^{-1}, the shift in DSC peaks related to two successive heating rates would be about ~0.7 °C. For an isoconversional method to work successfully, the temperatures related to the same conversion, T_α, must increase systematically with increasing β for each value of α. This condition is hard to fulfill at the smallest and largest values of α because the shifts in T_α are so small that they become comparable to the T_α variation associated with the selection of the DSC peaks baseline.

Nonetheless, the baseline selection and adjustment does not affect practically the DSC peak temperature. This brings about the idea [129] of adapting the Kissinger method [99, 100] for estimating the experimental dependence of E versus T. The Kissinger method (Eq. 3.51) estimates the effective activation energy from the shift of the DSC peak temperature (T_p) with the heating rate. It should be noted that the method is not exactly isoconversional, i.e., the conversion related to the peak temperature may not be the same value at different heating rates [130]. Experimental data need to fulfill the isoconversional condition because this is the condition under which the theoretical E versus T dependence is derived (Eq. 3.72). The condition is easy to check by determining the conversion at T_p from the actual DSC peaks. For example, the isoconversional condition appears to be fulfilled quite satisfactorily for melting of PET and PCL because the respective conversions do not show any systematic dependence on the heating rate giving rise to the value 0.59 ± 0.02 [129] and 0.61 ± 0.03 [131]. Thus, the use of the Kissinger method for estimating the experimental E versus T dependence would be justified.

The Kissinger plots for melting of PET and PCL are presented in Fig. 3.43. It is immediately clear that the plots are nonlinear. Since at any given temperature the slope of this plot is the effective activation energy, it can be concluded that the effective activation energy of the melting process is temperature dependent. Fur-

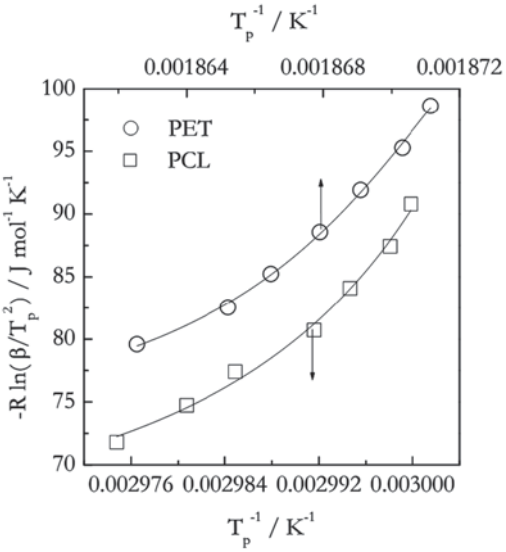

Fig. 3.43 The Kissinger plots for melting of PET and PCL. The *solid lines* represent interpolation of the experimental points. *PET* poly(ethylene terephthalate), *PCL* poly(ε-caprolactone). (Adapted from Vyazovkin et al. [129, 131] with permission of Wiley)

thermore, the effective activation energy decreases with increasing temperature as predicted by Eq. 3.72. This certainly lends support to the nucleation model because the Kissinger plot is obtained directly from the experimental data without making any assumption about nucleation.

In order to convert the Kissinger plot to the experimental E versus T dependence, one needs to differentiate the plot numerically and then replace the reciprocal temperature with temperature. To get around the problems of dealing with noisy numerical derivative of experimental data, the Kissinger plot can be replaced with some interpolating function. Differentiation of the latter would result in smooth numerical derivative.

The E versus T dependencies derived from the Kissinger plots for melting of PET and PCL are shown in Fig. 3.44. A striking feature of these dependencies is the enormous values of the effective activation energy. Lippits et al. [132] have reported similarly large values for melting of ultrahigh molecular weight polyethylene. This fact has been rationalized [132] by hypothesizing that detachment of polymer chain from the crystalline surface occurs in highly cooperative manner, i.e., by simultaneously breaking multiple bonds. However, the nucleation model suggests (Eq. 3.72) that the absolute value of E cannot be interpreted directly as the energy barrier height. Furthermore, interpretation of the large magnitude of the activation energy does not require invoking the hypothesis of cooperativity. Instead, the nucleation model provides a straightforward explanation that the E value is necessarily large because in Eq. 3.72 the ΔT is very small.

Fitting of the theoretical E versus T dependence (Eq. 3.72) to the experimental one requires estimating the nonequilibrium melting temperature because it is a part

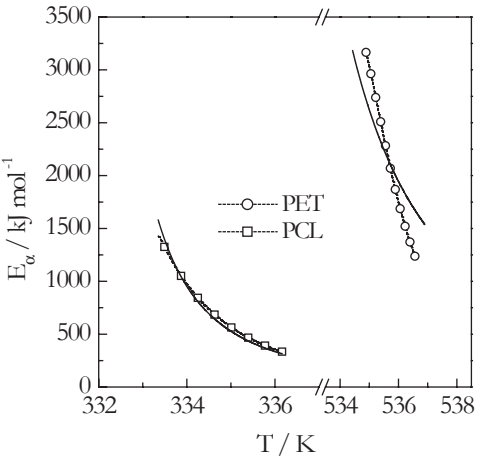

Fig. 3.44 Temperature dependence of the effective activation energy for melting of PET and PCL. Points connected by *dash line* represent the experimental dependence derived from the Kissinger plot. The *solid lines* are fits of Eq. 3.72. *PET* poly(ethylene terephthalate), *PCL* poly(ε-caprolactone). (Adapted from Vyazovkin et al. [129, 131] with permission of Wiley)

of the ΔT value. An estimate of this value is obtained from individual DSC peaks as an extrapolated onset temperature, $T_{m,\beta}$. The $T_{m,\beta}$ value depends on the heating rate, β. A heating rate-independent value is found by extrapolation of the $T_{m,\beta}$ values to $\beta = 0$, using an equation proposed by Illers: [133]

$$T_{m,\beta} = T_m + a\beta^{0.5}. \tag{3.73}$$

The intercept of the linear plot of $T_{m,\beta}$ against $\beta^{0.5}$ yields the value of T_m that can be used in fitting of Eq. 3.72 to the experimental E versus T dependence.

The fits of Eq. 3.72 to the experimental E versus T dependencies derived from the Kissinger plots for melting of PET and PCL are seen in Fig. 3.44. The fits are quite satisfactory, considering that Eq. 3.72 has only one adjustable parameter. The estimated values of the parameter A are 92 ± 4 (PET) and 11.9 ± 0.2 (PCL) kJ K mol^{-1}. The value can be used to estimate the interfacial free energy, σ. It should be noted that ΔG^* in Eq. 3.68 is in joules, whereas A is estimated (Eq. 3.72) from the values of E which are in joules per mole. With regard to this, A takes the following form:

$$A = \frac{N_A \pi l \sigma^2 T_m^0}{\Delta H_f}, \tag{3.74}$$

where N_A is the Avogadro number, 6×10^{23} mol^{-1}. Solving Eq. 3.74 for σ yields:

$$\sigma = \sqrt{\frac{A \Delta H_f}{N_A \pi l T_m^0}}. \tag{3.75}$$

For polymers, the values of T^0_m and ΔH_f are available from various literature sources, e.g., from Wunderlich [113]. For PET, $T^0_m = 553$ K and $\Delta H_f = 2.1 \times 10^8$ J m^{-3}. For PCL, according to the literature data collected by Sasaki [126], $T^0_m = 342.2$ K and $\Delta H_f = 1.9 \times 10^8$ J m^{-3}. The lamellar thickness, l, can be estimated at T_m by the Gibbs–Thomson equation (3.64) from the literature values [107, 126] of the fold surface free energy σ_e. For both polymers, l is about 15 nm [129, 131]. By inserting the above values in Eq. 3.75, one estimates the σ values to be 1.1×10^{-3} J m^{-2} (PET) and 5.1×10^{-4} J m^{-2} (PCL). Unexpectedly, both of these values are about an order of magnitude smaller than the values estimated from crystallization data: 1.2×10^{-2} J m^{-2} for PET [107] and 8.2×10^{-3} J m^{-2} for PCL [126]. A similar observation has been made in the original paper [121] by Toda et al., who found from their melting data that the Thomas–Staveley ratio [134] is about an order of magnitude smaller than is typically found from crystallization data on a variety of polymers. When applying the nucleation model to melting of PCL, Sasaki [126] has also found the σ value to be an order of magnitude smaller than that determined from crystallization data. It appears that the analysis of the polymer melting kinetics in terms of the nucleation model yields consistently the values of the lateral surface free energy which is about an order of magnitude smaller than that derived from crystallization kinetics.

The observed difference can be rationalized by considering the difference in the nature of the nucleation during crystallization and melting. If no foreign phase is present, crystallization occurs by homogenous nucleation throughout the whole melt phase. Melting, on the contrary, is a surface process [135–137]. The nuclei of the melt phase are formed at the interface, i.e., heterogeneously. The difference in the nature of homogeneous and heterogeneous nucleation entails significant energetic differences. As discussed earlier (Sect. 3.5, Eq. 3.48), the free energy barrier to heterogeneous nucleation, G^*_{het} is always smaller than that for the homogeneous one by some geometrical factor, $f(\Theta)$. For a cylindrical nucleus on a flat substrate, the geometrical factor is as follows: [93, 138]

$$f(\Theta) = \frac{(\Theta - \frac{1}{2}\sin 2\Theta)}{\pi}. \tag{3.76}$$

Note that the value of A (Eq. 3.74) corresponds to the free energy of homogenous nucleation. Thus, a small estimate of the A value unavoidably results in an unusually small value of σ (Eq. 3.75). On the other hand, if A is to be derived from the free energy of heterogeneous nucleation, the right-hand side of Eq. 3.74 would have to be multiplied by $f(\Theta)$. Then, a small value of A determined experimentally can be explained naturally by a small value of $f(\Theta)$ without invoking any changes in σ. According to Eq. 3.75, an order of magnitude decrease in σ would result from a two orders of magnitude decrease in A. This would be equivalent to $f(\Theta)$ being around 0.01. The respective contact angle estimated by Eq. 3.76 would be roughly 20°. It should be remarked that when liquid is in contact with solid of the same kind, the contact angle can be as small as a few degrees [139]. Overall, it appears that the polymer melting kinetics is consistent with the nucleation model, although it can be improved further by treating the process as heterogeneous nucleation.

3.8 Solid–Solid Transitions

The nature of the universe loves nothing so much as to change the things that are and to make new things like them. For everything that exists is in a manner the seed of that which will be

Marcus Aurelius, Meditations

3.8.1 Background

The solid–solid transitions are quite common in ionic [6, 7] and molecular [8] crystalline compounds. They represent transitions between different crystalline forms (polymorphs) of the same compound. For example, on heating above ~125 °C, ammonium nitrate crystal is known to change its crystalline structure from tetragonal to cubic lattice (Fig. 3.45) [140]. If in the cubic lattice, all three sides are perpen-

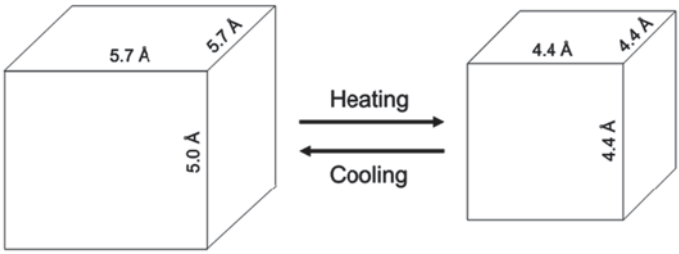

Fig. 3.45 Schematic depiction of the lattice rearrangement during the tetragonal to cubic solid–solid phase transition in ammonium nitrate. Side lengths are taken from crystallographic data [140]

dicular to each other and of the same size, in the tetragonal lattice, all sides are perpendicular but only two of them remain of equal size. Although the molecular composition of the solid compound remains unchanged during the transition, the distances between the atoms change. While may seem subtle, these changes are very important as they affect numerous physical properties of a crystalline solid.

The solid–solid phase transitions are more diverse and complex than the transitions involving the fluid media. If a liquid or gas exists in one disordered form, crystals are found in 230 space groups that represent different spatial configurations of a crystal. In terms of the rotational symmetry, crystals fall in seven different types: triclinic, monoclinic, orthorhombic, rhombohedral, tetragonal, hexagonal, and cubic [18]. This is the order in which the symmetry increases. On heating, the solid–solid transitions typically occur in the direction of increasing the symmetry.

In accord with Ehrenfest's classification, the solid–solid transitions can be designated [6–8] as being first and second order. However, the existence of second-order solid–solid transitions is a subject of significant controversy [141]. It appears that the condition for second-order transitions to proceed without changes in the enthalpy (or other first-order derivatives of the Gibbs energy) is a too stringent idealization. For example, the condition is practically satisfied by the so-called lambda transitions [6, 7] that demonstrate a discontinuity in the heat capacity (i.e., second-order derivative of the Gibbs energy) and tend to have very small enthalpy, which, however, may be not good enough to claim the value being exactly zero.

From the thermodynamic standpoint, first-order solid–solid state transitions occur at temperature, T_0, which is the intersection point of the G versus T curves for two solid phases (Fig. 3.46). The crystalline phases are commonly identified by roman numerals in order of their appearance on cooling from the melt state. That is, the highest temperature phase would be identified as phase I. As in the case of other first-order transitions (Fig. 3.1), heating across the equilibrium temperature means an abrupt increase in the slope of the G trace. Therefore, both enthalpy and entropy increase in accord with respective Eqs. 3.2 and 3.1. This means that the solid–solid phase transition is endothermic on heating and exothermic on cooling. The volume also undergoes a significant change during the transition, but it can increase as well as decrease.

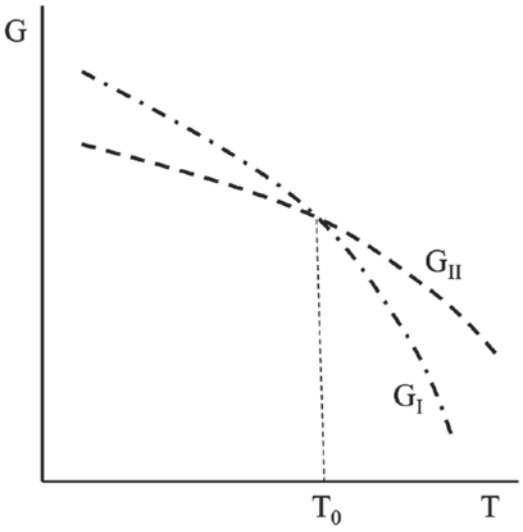

Fig. 3.46 Temperature dependence of the Gibbs energy for high temperature phase I (*dash-dot line*) and low temperature phase II (*dash line*). T_0 is the equilibrium temperature of transition between the phases

Note that the increase in entropy does not contradict to the aforementioned increase in the symmetry that also takes place on heating. The notion of the symmetry is related to the spatial arrangement of the molecules, atoms, or ions inside a crystal, whereas the entropy refers to the vibrational motion of these species around their positions in the crystalline lattice. As temperature rises, the crystalline lattice has to change to provide the medium that can accommodate increasing amplitude of the vibrations. Initially, it is accomplished by expanding and ultimately by rearranging the lattice. Apparently, a more symmetrical lattice provides the medium that affords more degrees of freedom for degenerate vibrations, therefore, putting fewer constraints on the vibrational motion.

By its meaning, the transition temperature, T_0, is the temperature at which two crystalline phases can coexist in equilibrium. It should be remarked that due to the nature of the solid–solid transitions, this temperature is difficult to pinpoint precisely. The solid–solid transitions, at least those of first order, occur by the nucleation mechanism. This means that the rate of transition is zero at T_0, but increases as temperature deviates from T_0. In other words, the transition on heating involves superheating and transition on cooling involves supercooling. As a result, there is a significant gap between the temperatures, at which the transition on heating and on cooling becomes detectable. An example of the temperature hysteresis in the solid-state transition on heating and cooling is seen in Fig. 3.47. For the transition between the phases I (cubic) and II (tetragonal) in ammonium nitrate, the gap is about 15 °C. That is, the equilibrium transition temperature in this case can be found anywhere between 113 and 128 °C.

The situation with establishing the equilibrium temperature for the solid–solid transition obviously is quite different from that for the solid–liquid transition. As discussed earlier, the transition from a crystalline solid to liquid (i.e., melt) can

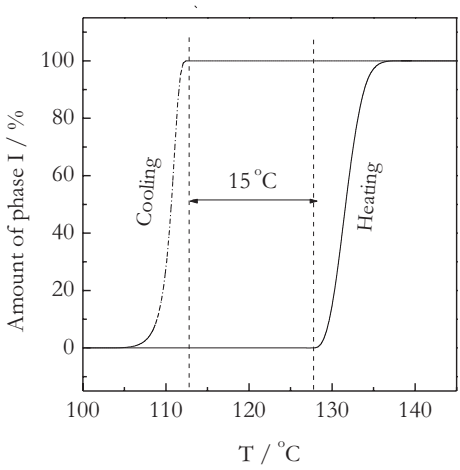

Fig. 3.47 Hysteresis in transition between phase I and II of ammonium nitrate measured on heating (*solid line*) and cooling (*dash-dot line*) at 20 °C min^{-1}

occur via nucleation (Sect. 3.7) in the same manner as the reverse transition from melt to crystal, i.e., crystallization (Sect. 3.6). However, the superheating during melting is normally negligibly small. Melting starts from the surface, and because the surface possesses higher molecular mobility, the surface layer melts before temperature reaches the bulk melting temperature. In a sense, the crystal surface is pre-nucleated so that the melt layer grows very rapidly when temperature reaches the equilibrium temperature of melting, T_m. This is the only reason why T_m provides an accurate estimate for the temperature at which a crystal can coexist in equilibrium with its melt.

The kinetics of the solid–solid transitions is generally consistent with the Turnbull–Fisher nucleation model [92]. The temperature dependence of the transition rate has a rather complex form shown in Fig. 3.48. One can obtain this dependence

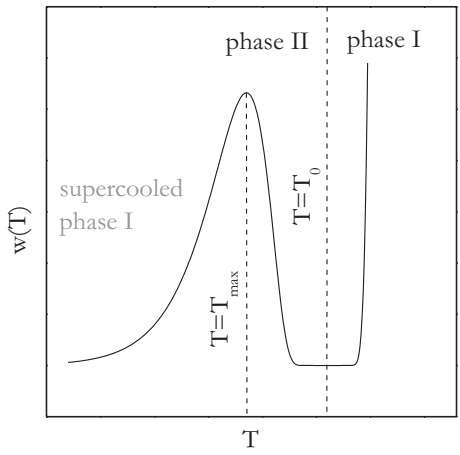

Fig. 3.48 Nucleation rate dependence derived from the Turnbull–Fisher equation (Eq. 3.44)

directly from Eq. 3.44 by varying temperature around T_0. At this temperature, the high temperature phase I is at equilibrium with the low temperature phase II. In the vicinity of T_0, the rate of the solid–solid transition is close to zero. Heating a solid above T_0 accelerates the transition from the phase II to the phase I. The temperature dependence of the rate is positive above T_0. If fitted to the Arrhenius equation, it would yield positive activation energy. When cooled below T_0, the phase I transforms to the phase II. The rate of the transition increases with decreasing temperature. Below T_0, the temperature dependence of the rate is negative. Fitting it to the Arrhenius equation would result in negative activation energy.

An interesting feature of the temperature dependence of the solid–solid transition rate is the existence of the rate maximum (Fig. 3.48) that can be found at larger supercoolings. The maximum is due to the same reason as the one observed for the rate of crystallization (Fig. 3.36). It is the deceleration of the molecular mobility (diffusion) with decreasing temperature. If the transition from the phase I to the phase II is fast, the maximum may be impossible to detect experimentally, unless one uses very fast rates of cooling. On the other hand, some of the transitions from the high- to low-temperature phase are very slow. In this circumstance, cooling of the phase I may not result in the formation of the phase II. In terms of the G versus T diagram (Fig. 3.46), the phase I continues to follow the G_I trace below T_0. When temperature drops below T_{max}, the phase I freezes kinetically in the supercooled metastable state. While metastable, the supercooled phase can exist in this state indefinitely. Recall De Beers' slogan "a diamond is forever," although at ambient temperature and pressure, diamond is a metastable crystalline form of carbon and it is bound thermodynamically to transform to graphite.

On heating, the supercooled phase I transforms to the phase II. This process normally occurs below T_{max} (Fig. 3.48). In that region, the temperature dependence of the phase transition rate is positive. When fitted to the Arrhenius equation, it would yield positive activation energy. Note that this process would be exothermic because as seen from Fig. 3.46 G_I trace has a larger slope than G_{II} so that the enthalpy for the phase I is larger than for the phase II. For a similar reason, the process would be accompanied by a decrease in entropy.

Villafuerte-Castrejon and West [142] provide a good example of the kinetics of the solid–solid phase transition between β and γ forms of Li_2ZnSiO_4 measured in all three regions (Fig. 3.49). The high-temperature γ form is at equilibrium with the low-temperature β form at around 880 °C. Heating the compound above this temperature causes the transition from the β to γ form. The rate constant, k, increases with temperature. The slope of the Arrhenius plot of log k versus T^{-1} is negative that corresponds to positive value of E. On cooling below 880 °C, the γ form converts to the β form. The rate constant increases with decreasing temperature that is consistent with the E value being negative. Finally, the γ form can be prepared in a metastable state by quick cooling below T_{max}, which is ~800 °C. Heating the metastable γ form initiates its conversion to the β form, which is the stable form below 880 °C. The respective Arrhenius plot for this transition gives rise to positive E.

Since the Turnbull–Fisher model (Eq. 3.44) is capable of correctly predicting the temperature dependence of the solid–solid transition rate, it can also be used to

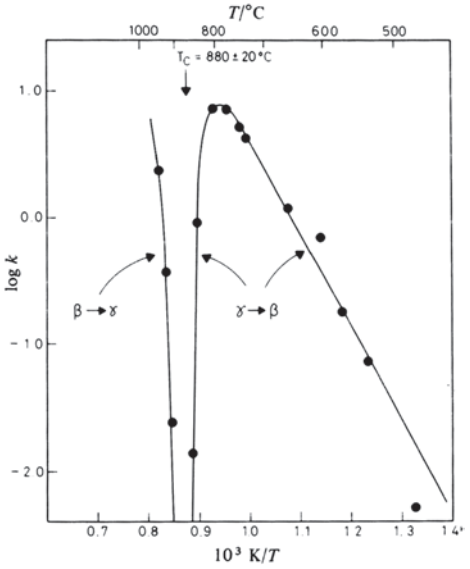

Fig. 3.49 Arrhenius plot for the kinetics of the phase transition between the β and γ forms of Li_2ZnSiO_4. T_c is the equilibrium transition temperature. (Reproduced from Villafuerte-Castrejon and West [142] with permission of RSC)

predict the temperature dependence of the effective activation energy. The equation that can be used for this purpose is Eq. 3.45. Variation of temperature around T_0 produces the E versus T dependence displayed in Fig. 3.50. It is seen that the dependence has a discontinuity at T_0. On heating above T_0, the activation energy for the transition from the phase II to I decreases from $+\infty$ down to the activation energy of diffusion E_D. On cooling below T_0, the activation energy for the transition from the phase I to II increases from $-\infty$ toward 0. If the phase I can be supercooled below T_{max}, its heating would result in the transition from the phase I to II. For this process, the activation energy would decrease from E_D toward 0.

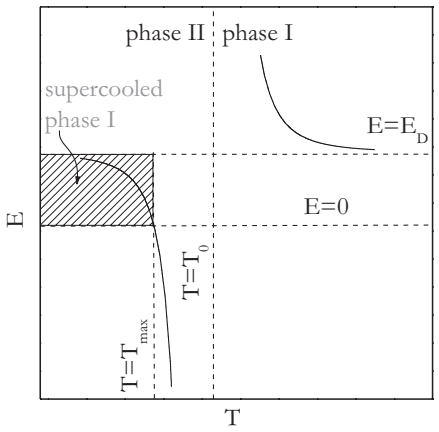

Fig. 3.50 Theoretical E versus T dependence derived from Eq. 3.45

In conclusion, we should mention that the aforementioned nucleation analysis is identical to that considered earlier for the solid–liquid (melting) and liquid–solid (crystallization) phase transitions. Since first-order transitions are accompanied by a change in volume, the molar volumes of the solid and liquid phase are generally different. Because of the mismatch of the volumes, the formation of a new phase nucleus would have to overcome an energy barrier associated with elastic strain energy. When one of the phases is liquid, the strain energy can be neglected. However, if both phases are solid, a more accurate representation of nucleation needs to account for the strain energy term as a part of the free energy barrier of the process [143].

3.8.2 Isoconversional Treatment

The kinetics of the solid–solid phase transitions is conveniently measured by DSC. Generally, one can produce a set of data at several heating rates for the transition from the low- to high-temperature phase and a set of data at several cooling rates for the reverse transition. Obtaining the high-temperature phase in the supercooled metastable state may be difficult for many substances. However, if obtained, a dataset should be generated at multiple heating rates to be able to study the kinetics of the transition from the metastable high-temperature phase into the stable low-temperature phase. The datasets are then treated by an isoconversional method. It should be emphasized that not every isoconversional method is applicable to the data obtained on cooling. The methods suitable to this task have been discussed in Sect. 2.1.2.

The application of an isoconversional method to the datasets obtained on heating and cooling results in the E_α versus α dependencies such as those shown in Fig. 3.51 for the transition between the form I (cubic) and II (tetragonal) of ammonium nitrate. The dependencies are in agreement with the E versus T dependence

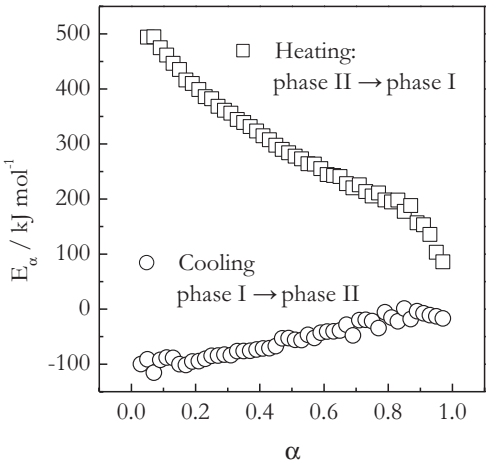

Fig. 3.51 Isoconversional activation energies estimated for the phase transition between tetragonal (*phase II*) and cubic (*phase I*) forms of ammonium nitrate

predicted by the Turnbull–Fisher model (Fig. 3.50). The transition from the form II to the form I demonstrates positive values of E_α that decrease with increasing α, which is expected because the measurements are done on heating so that α increases monotonously with increasing T. Similarly, for the transition from the form I to the form II that is measured on cooling, E_α is expected to be negative and to increase with increasing α (i.e., with decreasing T) toward 0.

The obtained E_α dependencies (Fig. 3.51) are converted to the E_α versus T dependencies by replacing each value of α with the mean temperature related to it. The resulting dependencies (Fig. 3.52) look quite similar to the theoretical ones derived from the Turnbull–Fisher model (Fig. 3.50). We can now try to fit the theoretical E_α versus T dependence (Eq. 3.45) to the experimental one. For simplicity, we assume that the E_D and A parameters of Eq. 3.45 remain the same for the forward (heating) and reverse (cooling) transition. The value of T_0 can also be used as a fit parameter. This would permit estimating the position of the equilibrium transition temperature, which, as explained earlier, is hard to measure experimentally. The resulting fit suggests that T_0 is ~396 K (~123 °C). This places the equilibrium transition temperature much closer to the onset of the transition measured on heating (128 °C) than to the one measured on cooling (113 °C; Fig. 3.47). Also, the fit yields an estimate for the activation energy of diffusion, $E_D = 63 \pm 2$ kJ mol^{-1}. This value falls in the range of the activation energies measured [144] by nuclear magnetic resonance (NMR) for translational diffusion of ammonium ion in the phases I and II of ammonium nitrate.

The solid–solid transitions are a new application area of isoconversional methods. Their full potential in this area is yet to be discovered.

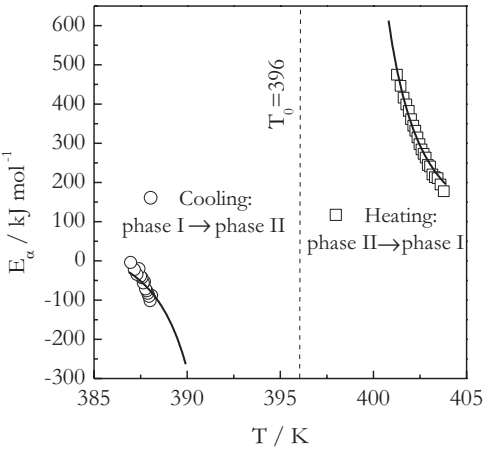

Fig. 3.52 Fitting E versus T data (*points*) to Eq. 3.45 (*solid lines*)

3.9 Mixing and Demixing

...he took the materials, of which he made a compound, mixing them all and boiling them a good while until it seemed to him they had come to perfection

Miguel de Cervantes Saavedra, Don Quixote

3.9.1 Background

So far we have discussed the phase transitions in single-component systems. If a system contains more than one component, it can exist as a single mixed phase and as several demixed phases. A transition between mixed and demixed phases is the phase transition specific to multicomponent systems. The mixed and demixed phases can coexist at equilibrium at certain temperature and pressure. A simple example is equilibrium between a solid solute and liquid solvent. If a small amount of sodium chloride (solute) is put in a large volume of water (solvent), it will disappear forming a solution, which is a single mixed phase (solution) containing sodium and chloride ions and water molecules. However, if we keep increasing the amount of sodium chloride, at some point the solution will saturate so that an excess of solid sodium chloride will coexist in equilibrium with its aqueous solution as two immiscible phases.

The transition between the mixed and demixed phases can be stimulated by changing temperature. Normally, the solubility of a solid solute increases with temperature as follows: [18]

$$\ln x = \frac{-\Delta H_{\mathrm{f}}}{RT}\left(\frac{1}{T} - \frac{1}{T_{\mathrm{m}}}\right), \tag{3.77}$$

where x, ΔH_{f}, and T_{m} are respectively the mole fraction, enthalpy of fusion, and melting temperature of the solid. This means that upon heating above certain equilibrium temperature, T_0, the two phases would merge into one. Conversely, the single-phase solution can be separated in two phases by dropping its temperature below T_0 that would force the solid solute out of solution or, in other words, would cause crystallization of the solute. Equation 3.77 gives rise to the phase diagram shown in Fig. 3.53. The solid line represents temperatures at which the solutions of different concentration can coexist at equilibrium with the solute. A solution prepared at higher temperature obviously has higher equilibrium concentration. A solution of the concentration x_1 prepared at T_1, i.e., above the respective equilibrium temperature, is a single-phase system. Dropping its temperature to T_2 would cause the solution to separate in two phases that eventually would come to equilibrium. The concentration of the solution would drop from x_1 to x_2, and the excess of the solute (i.e., $x_1 - x_2$) would fall out of solution to form the solid phase.

Something similar happens when mixing two partially miscible liquids, i.e., liquids that have limited solubility in each other. The respective phase diagram for liq-

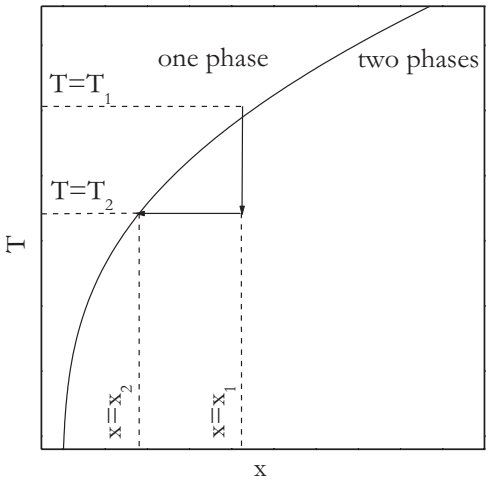

Fig. 3.53 Phase diagram for a solid–liquid system. The *solid line* represents the temperature at which solid and liquid can coexist at equilibrium

uid B dissolved in liquid A is seen in Fig. 3.54. The solid line bell curve tracks the temperatures at which a solution forms two phases of different concentration that can coexist in equilibrium. The ascending wing of the curve reflects an increase in the solubility of B as a function of temperature. The trend is similar to that seen in Fig. 3.53. The trend continues until reaching the critical temperature, T_c, above which both liquids become infinitely soluble in each other. The descending wing of the curve corresponds to the solubility of A in B. When the fraction of B becomes larger than that of A, B turns from solute to solvent. Thus, this wing represents an increase in the solubility of A as a function of temperature. If a solution of the concentration x_{B1} prepared at the temperature T_1, which is above the respective equilibrium temperature, it will exist as a single-phase system. Decreasing the solution temperature to the tem-

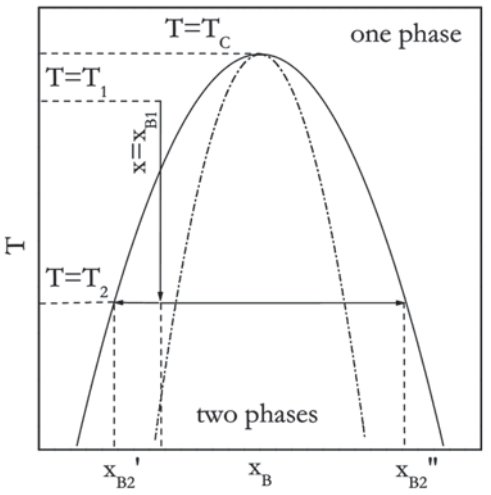

Fig. 3.54 Phase diagram for a liquid–liquid system. The *solid line* represents the temperature at which two liquid phases of different composition can coexist at equilibrium. The *dash-dot line* is the spinodal line

perature T_2 below the equilibrium temperature would make the solution to separate in two phases that over time would come to equilibrium. The two phases would be the B-poor and B-rich phases, whose respective concentrations of B are x_{B2}' and x_{B2}''.

The two considered systems (Figs. 3.53 and 3.54) are the systems that demonstrate the normal temperature dependence of the solubility, i.e., an increase with increasing temperature. In the case of the liquid–liquid mixtures, such systems are called upper critical solution temperature systems. Some systems however have the inverse temperature dependence of the solubility. Their respective phase diagrams are similar to those shown in Figs. 3.53 and 3.54 but inverted. The liquid–liquid systems of the inverse solubility are called the lower critical solution temperature systems.

The solid–liquid and liquid–liquid systems have one feature in common. When their temperature is changed from the one-phase to two-phase region, they become metastable. All metastable systems relax toward equilibrium via the process of nucleation. Nevertheless, if temperature of the liquid–liquid system is brought beyond the spinodal line (Fig. 3.54), it would become unstable. Unstable systems relax to equilibrium by another process called spinodal decomposition [3, 4]. The difference between nucleation and spinodal decomposition boils down to how concentration (density) fluctuations occur in these systems. Nucleation requires the fluctuation to be of a significant size, i.e., a nucleus must include a significant number of molecules to become stable. However, such fluctuations are very small in spatial extent because they occupy a very small fraction of the overall macroscopic volume. The fluctuation is accompanied by a large energy barrier, which decreases as temperature departs from its equilibrium value. When the energy barrier becomes negligible, the formation of a new phase becomes possible via spinodal decomposition. It is characterized by very small but multiple fluctuations of the concentration that occupy a large fraction of the macroscopic volume, i.e., they are large in spatial extent. Further discussion is limited only to nucleation because this is the mechanism that controls the new phase formation at smaller and slower departures from equilibrium.

In a solution, the driving force of the new phase formation is the supersaturation caused by a change in temperature. The supersaturation is defined as the ratio of the nonequilibrium to equilibrium concentration, x_0:

$$S = \frac{x}{x_0}. \tag{3.78}$$

If a solution of the concentration x is cooled from T_1 to T_2 (Fig. 3.53 and 3.54), i.e., from a temperature inside the one-phase region to a temperature inside the two-phase region, the supersaturation increases because the x_0 value becomes smaller. The larger the supersaturation, the faster the rate of the new phase nucleation. This is expressed by the following equation: [145]

$$w(T) = w_0 \exp\left(\frac{-16\pi\sigma^3 N_A^2 V^2}{3R^3T^3(\ln S)^2}\right)\exp\left(\frac{-E_D}{RT}\right), \tag{3.79}$$

where V is the molecular volume and N_A is the Avogadro number. The equation is arrived at from Eq. 3.35 for the critical radius of a spherical nucleus. The equation is combined with the Gibbs–Thomson relationship for size-dependent solubility to give:

$$-\Delta G_V = \frac{2\sigma}{r} = \frac{RT \ln S}{N_A V}. \tag{3.80}$$

Substitution of the right-hand side of Eq. 3.80 into Eq. 3.36 for the height of the free energy barrier yields:

$$\Delta G^* = \frac{16\pi\sigma^3}{3(\Delta G_V)^2} = \frac{16\pi\sigma^3 N_A^2 V^2}{3R^2T^2(\ln S)^2}. \tag{3.81}$$

Then Eq. 3.79 is obtained by plugging ΔG^* from Eq. 3.81 into the Turnbull–Fisher equation (3.42). Equation 3.79 can be rewritten in a simpler form

$$w(T) = w_0 \exp\left(\frac{-A}{T^3(\ln S)^2}\right)\exp\left(\frac{-E_D}{RT}\right), \tag{3.82}$$

where the constant A includes all parameters that are either independent or weakly dependent on temperature.

As derived [145], Eq. 3.79 (and, thus, 3.82) does not include directly the supercooling, i.e., $\Delta T = T_0 - T$. It can be introduced by explicitly accounting for the temperature dependence of the supersaturation. The temperature dependence of the solubility can be expressed in many forms [145]. One of them is given by Eq. 3.75 that can be rewritten as:

$$\ln x = Z + \frac{B}{T}. \tag{3.83}$$

If temperature drops from T_0 to T, the supersaturation becomes:

$$\ln S = B\left(\frac{T_0 - T}{T_0 T}\right) = \frac{-B\Delta T}{T_0 T}. \tag{3.84}$$

Then the supercooling is introduced in Eq. 3.82 by replacing ln$S$ with the right-hand side of Eq. 3.84. Now we can evaluate the temperature-dependent activation energy as usual (Eq. 3.43):

$$E = -R\frac{\mathrm{d}\ln w(T)}{\mathrm{d}T^{-1}} = E_D + \frac{AT_0^2}{B^2}\left[\frac{1}{(\Delta T)^2} - \frac{2T}{(\Delta T)^3}\right]. \tag{3.85}$$

This equation holds for a system that forms a new phase on cooling, i.e., ΔT is the supercooling. If the new phase is formed on heating, as in systems with the inverse solubility, ΔT would become the superheating, i.e., $T - T_0$. Then Eq. 3.85 would change to:

$$E = E_D + \frac{AT_0^2}{B^2}\left[\frac{1}{(\Delta T)^2} + \frac{2T}{(\Delta T)^3}\right]. \tag{3.86}$$

As mentioned earlier, Eq. 3.83 is not the only form of the temperature dependence of the solubility. A change of the form of this dependence would result in changing the final equation for the temperature-dependent activation energy. For instance, the use of an alternative form: [145]

$$\ln x = Z' + B'T \tag{3.87}$$

yields the following equation for the supersaturation:

$$\ln S = B'(T_0 - T) = B'\Delta T. \tag{3.88}$$

Replacing the supersaturation in Eq. 3.82 with the right-hand side of Eq. 3.88 followed by taking the derivative (Eq. 3.85) gives rise to the temperature-dependent activation energy of the following form:

$$E = E_D + \frac{A}{B'^2}\left[\frac{3}{(\Delta T)^2 T^2} - \frac{2}{(\Delta T)^3 T}\right]. \tag{3.89}$$

Again, ΔT in this equation is the supercooling and it holds for systems that form a new phase on cooling. For systems that form a new phase on heating, ΔT would be the superheating, and the second term in the brackets would change its sign.

Equations 3.85 and 3.86 can be used to predict the behavior of the experimental activation energy (Fig. 3.55). It is easy to demonstrate that the expression in the

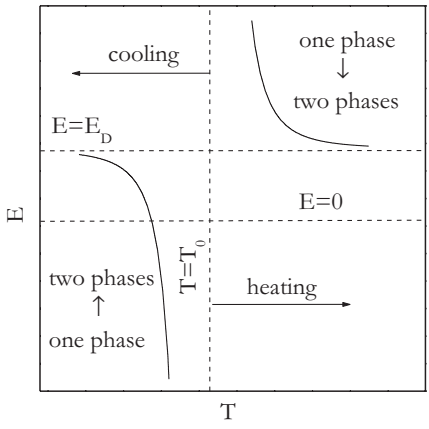

Fig. 3.55 Temperature dependence of the activation energy for the processes of the new phase formation on heating and on cooling

brackets of Eq. 3.85 tends to $-\infty$ as temperature approaches T_0 and to 0 as it departs further below T_0. It means that the effective activation energy experimentally determined on cooling should have large negative values that increase toward E_D with decreasing temperature. On the other hand, the expression in the brackets of Eq. 3.86 tends to $+\infty$ when temperature approaches T_0 and to 0 as it increases above T_0. Therefore, the activation energy estimated on heating should have large positive values at lower temperature and should decrease toward E_D as temperature rises. Similar trends can be demonstrated for Eq. 3.89.

It is noteworthy that at larger supercoolings, the system hypothetically can be brought to the state when the activation energy of the new phase formation becomes positive. In principle, this could be accomplished by cooling the system fast enough to outrun nucleation. The heating of the supercooled system then would result in the formation of a new phase, and the activation energy of this process would be positive. Something of that nature happens during the anomalous gelation discussed in Sect. 3.10.2

3.9.2 Isoconversional Treatment

The phase transitions between mixed and demixed state are usually accompanied by a significant change in the enthalpy that are detectable by DSC. As already stated, normally the solubility increases with temperature. The systems with the normal solubility absorb heat during mixing. That is, demixing in such systems is an exothermic process that takes place on cooling. The inverse solubility is not very common. It typically results from some specific interaction between solute and solvent. For example, some compounds demonstrate the inverse solubility in water because they turn into hydrated form stabilized by hydrogen bonding. The respective mixing is exothermic. While stable at lower temperature, hydrogen bonds between a solute and water break on heating and the solute molecules become dehydrated. If interaction between the dehydrated molecules is sufficiently strong, they associate with each other forming an individual phase on heating. The process is endothermic.

An example of the low critical solution temperature system is a mixture of triethylamine and water. It mixes releasing a significant amount of heat [146] and has the critical temperature of ~18 °C [147]. On heating above this temperature, the system undergoes endothermic demixing (Fig. 3.56). The application of an isoconversional method to a set of DSC curves obtained at different heating rates gives rise to the E_α dependence shown in Fig. 3.56. Since α increases monotonically with T, the decreasing shape of this dependence is consistent with that predicted by Eq. 3.86.

The actual temperature dependence of the isoconversional activation energy is obtained from the E_α versus α by replacing the values of α with the mean temperatures related to them. The resulting dependence is shown in Fig. 3.57. It is seen that the theoretical E versus T dependence established by Eq. 3.86 provides a fairly good fit to the experimental dependence. It is noteworthy that the E_D value resulted from

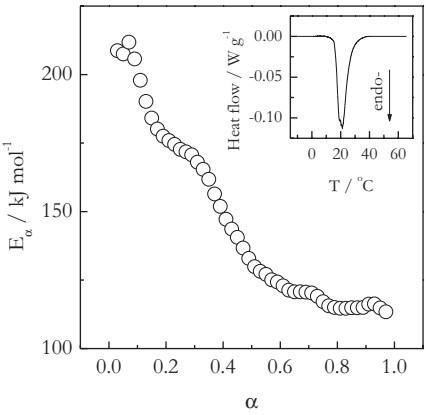

Fig. 3.56 Conversion dependence of the effective activation energy for demixing of an aqueous solution of triethylamine that takes place on heating. The inset shows a typical DSC curve of the process measured at heating rate 1 °C min^{-1}

the fit appears rather high, 117±3 kJ mol^{-1}. The activation energy of diffusion in liquids is about the same value as those of viscous flow [148]. For small spherical molecules, the latter value is about one third of the vaporization enthalpy [149], i.e., a few tens of kilojoules per mole. The obtained value is more characteristic of large molecules [148]. However, triethylamine in water exists as relatively big hydrated molecule, $(C_2H_5)_3 \cdot 2H_2O$ [150], the diffusion of which is likely to involve the breakage and restoration of hydrogen bonds that can create a significant energy barrier. Note that a solution of triethylamine in water has viscosity that is about four times larger than that of water [150]. It should also be noted that the activation energies of viscous flow in aqueous solutions of some amino acids have been reported [151] to be around a 100 kJ mol^{-1}.

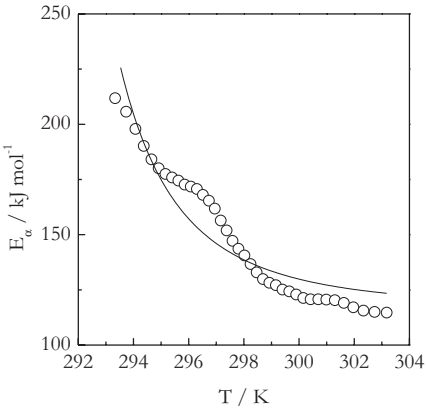

Fig. 3.57 Temperature dependence of the effective activation energy derived from E_α versus α dependence (Fig. 3.56). The *solid line* is a theoretical fit by means of Eq. 3.86

3.10 Gelation and Gel Melting

The soft overcomes the hard;
the gentle overcomes the rigid.
Everyone knows this is true,
but few can put it into practice

Lao Tzu, Tao Te Ching: 78

3.10.1 Background

Solutions may undergo a very special type of a phase transition called gelation. The latter is typically encountered in polymer solutions [13] but may occur also in sols of clays, soaps, aggregated globular proteins, etc. [152]. The initial liquid state is usually termed as sol to emphasize that a gel can form in various kinds of suspensions as well as in a true homogenous solution. The transition from sol to gel is best defined in mechanical terms. It is a transition from a flowing liquid (i.e., a sol) to a soft solid (i.e., a gel) that cannot flow. In order to be able to flow, the molecules of the solute and solvent should be able to move past each other freely. This is what happens when a polymer is dissolved in a good solvent, i.e., a solvent, in which an interaction between the solute and solvent is significantly stronger than between the solute and solute. In a poorer solvent, the solute–solvent interaction is not much stronger than the solute–solute one. Since the power of a solvent (i.e., the solubility) depends on temperature, the strength of the solute–solvent and solute–solute interactions can invert when changing temperature. As the solvent power decreases, the polymer molecules may form cross-links, losing their ability to move past each other and, thus, to flow.

A gel is a network of cross-linked solute molecules that entrap a solvent. Depending on the cross-link strength, gels can be either thermo-reversible or thermo-irreversible. Strong cross-links are formed by means of covalent bonding. In a solvent, a covalently cross-linked polymer network can swell, forming a gel, but it cannot dissolve because the solvent cannot break the covalent cross-links. In this chapter, we focus only on thermo-reversible gels. In such gels, the cross-links are formed by means of weak bonds (e.g., hydrogen or van der Waals bonds). The best known example of thermo-reversible (or physical) gelation is the thermal behavior of an aqueous solution of gelatin. Gelatin readily forms a solution in hot water. When cooled, the solution turns into a gel. Heating of the resulting gel causes its melting that gives rise to the initial solution.

Thermo-reversible gelation can been explained in terms of the phase diagrams [13, 153], which are similar to those for demixing transition in solutions (Sect. 3.9, Fig. 3.54). In the simplest case such as that of the gelatin–water system, there are only two phases: sol and gel (Fig. 3.58). The one- and two-phase regions separated by the binodal line that links the gelation temperature, T_{gel}, to the equilibrium concentrations of the polymer-rich (i.e., gel) and polymer-poor (i.e., solution) phases. The phase separation in gels is sometimes called syneresis [13, 153]. The process is quite different from demixing of two liquids that leads to the formation

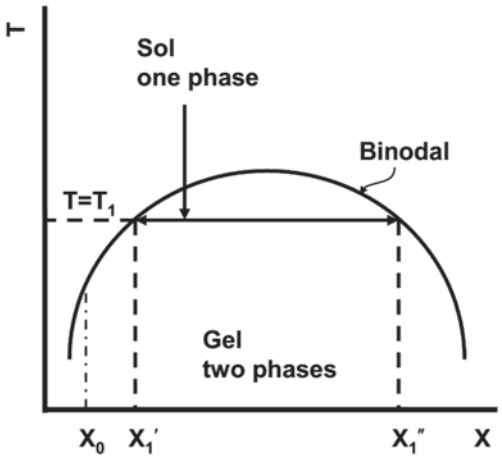

Fig. 3.58 Phase diagram for a gelling system that can exist in two states: *one-phase sol* and *two-phase gel*. Gel is not formed below the critical concentration x_0

of two homogenous macroscopic phases. In gel, the phase-separated state is microscopically heterogeneous. That is, the solvent-rich phase forms microdroplets inside the polymer-rich phase. The process of approaching equilibrium in the two-phase gels is extremely slow so that for all practical purposes such gels are fundamentally nonequilibrium systems similar to glasses. For this reason, the gel state and structure depend significantly on the thermal history of its formation. This feature of gels reveals itself vividly in the gel melting kinetics discussed in Sect. 3.10.3.

Gels cannot form when the concentration of a solution is below some critical value, x_0 (Fig. 3.58). If a solution has lower concentration, cooling it below the equilibrium temperature results in demixing of the solution without gelation.

Some gelling systems may demonstrate a more complex phase behavior (Fig. 3.59). An example is a solution of atactic PS in carbon disulfide [154]. Below

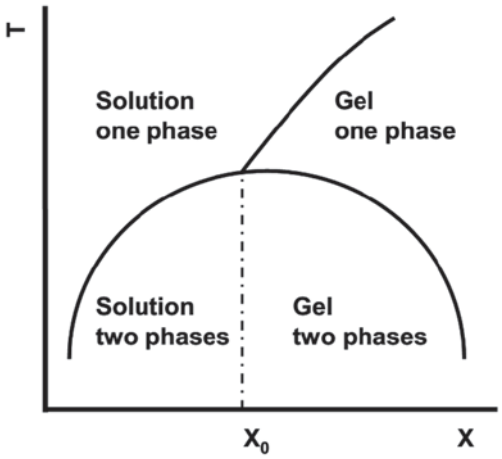

Fig. 3.59 Phase diagram for a gelling system that can form an equilibrium one-phase gel

a certain critical concentration, x_0, cooling of the one-phase solution results in the formation of a two-phase solution. However, increasing the solution concentration, while staying above the binodal line, results in the formation of a one-phase gel. This is microscopically homogeneous and equilibrium state. Cooling one-phase gel below the binodal line initiates phase separation of the gel. The clear one-phase gel turns into the turbid two-phase gel.

The described phase diagrams represent the behavior observed in solutions with the upper critical solution temperature. In these systems, the solubility increases with increasing temperature. Gelation of such solutions occurs on cooling. Gelation may also occur in solutions with lower critical temperature. Such solutions gel on heating because an increase in temperature decreases the solubility. There are a few rare examples of systems that gel on heating such as aqueous solutions of polymethacrylic acid [155] and cellulose derivatives [156, 157]. The respective phase diagrams for such systems are similar to those for regular systems (Fig. 3.58) but inverted. The gels formed on heating melt on cooling. Analogous to the process of demixing (Sect. 3.9), gelation on cooling is exothermic, whereas on heating endothermic.

The kinetics of physical gelation has been found [158] to be strikingly similar to that of polymer crystallization [93, 94]. The similarity is not surprising considering that the formation of the gel network junctions has been identified with the formation of microcrystallites in a wide variety of polymers [13, 159], including gelatin [158, 160]. For example, in gelatin gels, the microcrystallites are believed [13, 161, 162] to form via partial restoration of the triple helix structure characteristic of collagen that occurs via cooperative hydrogen bonding of gelatin coils. The rate of reversion from gelatin coil to collagen helix has long been known [163] to have the negative temperature dependence and to follow the nucleation-type kinetics, in which the nucleus is an embryo of the triple helix structure whose stability is determined by a critical length.

As in the case of crystallization, the rate of physical gelation initially increases as temperature drops further below T_{gel} but then passes through a maximum and finally drops to zero. A schematic diagram of this temperature dependence is seen in Fig. 3.60 [164]. At the high temperature end, gelation stops upon reaching equi-

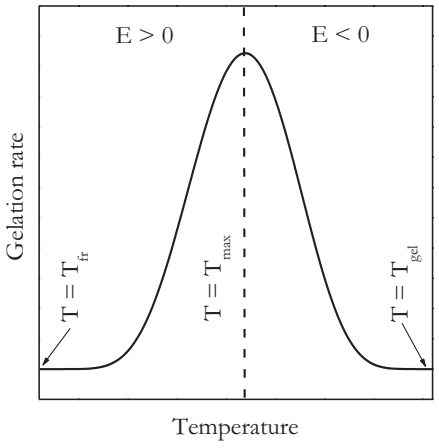

Fig. 3.60 The gelation rate passes through a maximum found between the temperatures of gelation (T_{gel}) and freezing (T_{fr}). The activation energy changes its sign when temperature traverses T_{max}. (Adapted from Guigo et al. [164] with permission of RSC)

librium at T_{gel}. At the low temperature side, it ceases on gel freezing at T_{fr}. The temperature rate dependence is obviously akin to that presented in Figs. 3.32 and 3.36 to illustrate respectively the nucleation rate in accord with the Turnbull–Fisher model and crystallization rate in accord with the Hoffman–Lauritzen model. The temperature dependence of the rate is negative above T_{max} and positive below it. Consecutively, the effective Arrhenius activation energy should be negative when estimated in the temperature range T_{max}–T_{gel} and positive when evaluated in the range T_{fr}–T_{max}. An actual example [165] of the Arrhenius plot for gelation of a gelatin solution at several temperatures is presented in Fig. 3.61. The maximum of the gelation rate is found in the range 14–19 °C. The activation energy is estimated to be −130 kJ mol^{-1} above T_{max} and 55 kJ mol^{-1} below it.

All in all, empirical evidence suggests that the kinetics of physical gelation can be parameterized in terms of some nucleation model. However, there are no nucleation models designed specifically for the process of physical gelation. In this situation, one can use the Turnbull–Fisher (Eq. 3.44) and Hoffman–Lauritzen (Eq. 3.52) models as empirical tools for exploring the kinetics of physical gelation as demonstrated in a number of publications [158, 164, 166–169].

3.10.2 Isoconversional Treatment of Gelation

Aqueous solutions of gelatin provide a well-known example of physical gelation that takes place on cooling. Gelatin is denatured (i.e., randomly coiled) form of collagen, whose native state is a triple helix made of three polypeptide chains cross-linked

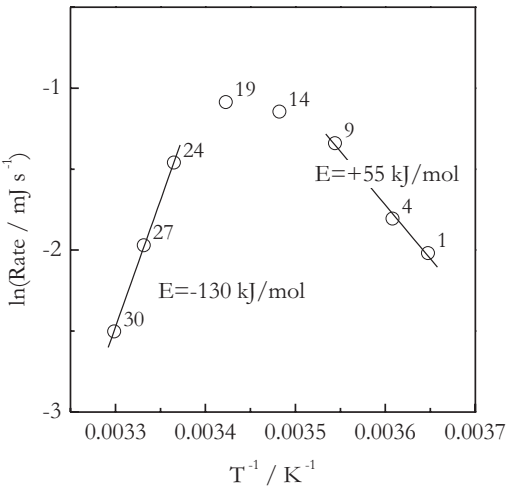

Fig. 3.61 Arrhenius plot of the initial rate of the heat release for gelation of a gelatin solution measured at eight different temperatures. The numbers by the points are the temperatures in °C. The activation energy is negative in the temperature range 24–30 °C and positive in the temperature range 1–9 °C. (Reproduced from Chen and Vyazovkin [165] with permission of Wiley)

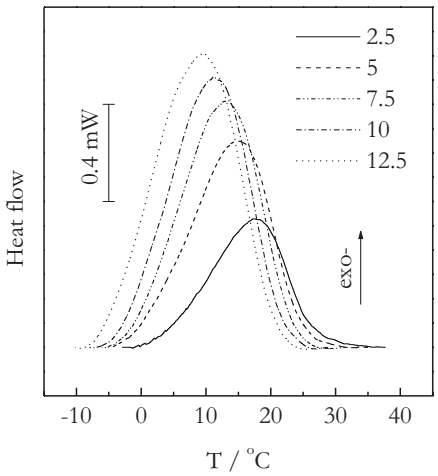

Fig. 3.62 DSC curves for gelation of 17 wt.% solution of gelatin in water. The numbers by the line types are cooling rates in °C min^{-1}. (Reproduced from Chen and Vyazovkin [165] with permission of Wiley)

by multiple hydrogen bonds. Gelatin dissolves readily in hot water. Decreasing the temperature of an aqueous gelatin solution increases the stability of the hydrogen bond cross-links that allow the polypeptide chains to restore a helical structure. This process takes place in dilute gelatin solutions [163, 170, 171]. In concentrated solutions, cross-linking becomes predominantly intermolecular, so that instead of forming separate helices, the polypeptide chains form an infinite network (i.e., a gel), in which partially restored helices serve as cross-link centers (i.e., network junctions).

The formation of hydrogen bonds during gelation of a gelatin solution produces sufficient amount of heat to follow the process by DSC (Fig. 3.62) [165]. On cooling, gelation becomes detectable below 40 °C. The gelation temperature depends on the concentration of the solution as seen from the phase diagrams (Figs. 3.58, 3.59). According to rheological measurements by Michon et al. [172], a decrease in the concentration of a gelatin solution from 20 to 1 wt.% causes a drop in T_{gel} from 33 to 26 °C. Just as in the case of crystallization, the DSC peaks shift to lower temperature with increasing the cooling rate (Fig. 3.62).

The application of an isoconversional method to DSC data on gelation of a gelatin solution is illustrated in Fig. 3.63. The obtained E_α on α dependencies demonstrate negative values of the effective activation energy. The E_α values tend to increase with the extent of the sol to gel conversion that is explicable by the departure from the equilibrium temperature (i.e., T_{gel}). In accord with either Turnbull–Fisher (Eq. 3.45) or Hoffman–Lauritzen (Eq. 3.60) equation, the effective activation energy turns to $-\infty$ at the equilibrium temperature but increases toward zero as temperature departs from the critical value. A similar type of dependencies (i.e., negative E_α increasing with α) is found for crystallization of polymer melts measured on continuous cooling, i.e., when an increase in the extent of the melt to crystal conversion reflects the departure from the melting point. An example of such behavior is seen in Fig. 3.37.

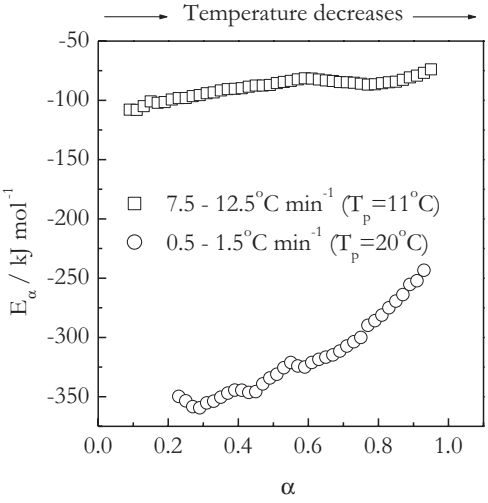

Fig. 3.63 The E_α dependencies obtained by applying an advanced isoconversional method to DSC data on gelation of 17 wt.% solution of gelatin in water. *Squares* and *circles* denote respectively different intervals of cooling rates. The intervals differ in the mean value of the DSC peak temperature, T_p, shown in parentheses. (Adapted from Chen and Vyazovkin [165] with permission of Wiley)

The effect of temperature on the E_α is even more evident when the E_α dependencies are evaluated from the data collected in different ranges of the cooling rates. As already noted with increasing the cooling rate, the DSC peaks shift to lower temperatures (Fig. 3.62). For the range of faster cooling rates (7.5, 10, and 12.5 °C min^{-1}), the average DSC peak temperature is ~11 °C so that the average value of E_α is about −90 kJ mol^{-1}. However, at slower cooling rates (0.5, 1.0, and 1.5 °C min^{-1}), the average peak temperature is markedly higher (20 °C), i.e., closer to T_{gel} so that the average E_α estimated from the slower heating rates is around −300 kJ mol^{-1} [165]. Therefore, isoconversional analysis of the continuous cooling DSC data demonstrates that under these conditions the rate of sol–gel conversion has a negative temperature coefficient, whose absolute value becomes larger when the process is measured closer to T_{gel}.

As already suggested, the kinetics of physical gelation can be reasonably well described by the Turnbull–Fisher and Hoffman–Lauritzen models. This means that one generally should be able to fit the temperature dependencies of the isoconversional activation energy to Eqs. 3.45 and/or 3.60 by substituting T_{gel} for the equilibrium temperature. For example, Eq. 3.45 derived from the Turnbull–Fisher model would take the following form:

$$E = E_D - A\left[\frac{2T}{\left(T_{gel}-T\right)^3} - \frac{1}{\left(T_{gel}-T\right)^2}\right]. \tag{3.90}$$

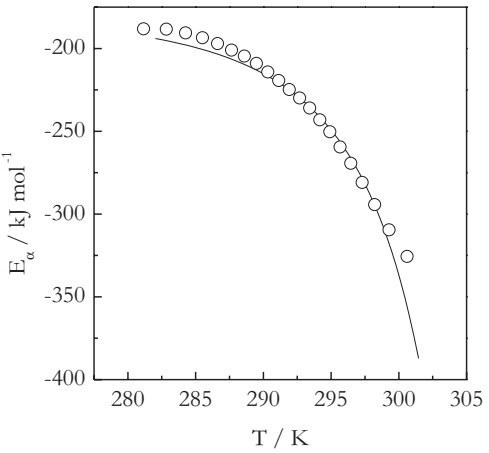

Fig. 3.64 Experimental E_α versus T dependence (*circles*) for gelation of 40 wt.% solution of gelatin in water. The *solid line* is a fit by Eq. 3.90

As seen from Fig. 3.64, this equation fits quite well the temperature dependence of the effective activation energy for gelation of 40 wt.% solution of gelatin [164]. The dependence has been derived from the E_α versus α dependence by replacing α with the average temperature corresponding to this conversion at different cooling rates. T_{gel} for this solution is ~317 K as estimated by extrapolating the gel melting data of Godard et al. [158].

Although the application of the Turnbull–Fisher and Hoffman–Lauritzen models to the process of gelation is rather empirical, it can still be used to extract meaningful information, especially for comparative purposes. One such example is the effect of the concentration on the kinetics of physical gelation of aqueous solutions of methylcellulose [169].

Aqueous solutions of methylcellulose gel on heating. The mechanism of the process has been examined in a number of studies, the results of which are briefly summarized by Kobayashi et al. [173]. Methylcellulose has the inverse solubility in water, i.e., it is soluble in cold but not in hot water. Dissolution occurs via hydration of methoxyl groups. When the solution temperature is increased, hydrogen bonds break, causing dehydration of hydrated methoxyl groups. The latter then undergo hydrophobic association forming a network, i.e., a gel.

Breakage of hydrogen bonds is accompanied by an endothermic effect that can be used to monitor gelation by using DSC. Typical DSC curves of gelation are shown in Fig. 3.65. An increase in the concentration of the methylcellulose solution causes some small shift of the process to lower temperatures. The heat of gelation per gram of methylcellulose is about −7 J g^{-1} for both 2 and 4% solutions that indicates that both samples have reached similar extent of cross-linking. For 8% solution, the heat of gelation is −5 J g^{-1}; that means, that the extent of cross-linking is about 30% smaller than in the two other samples. This is not surprising because the molecular mobility of the methylcellulose chains in the highly viscous 8% solution should be dramatically slowed down, therefore, limiting the process of cross-linking.

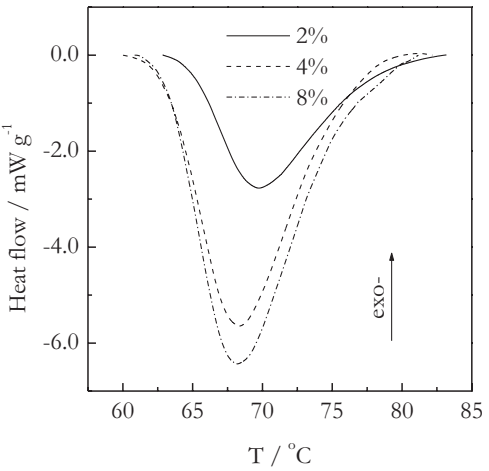

Fig. 3.65 DSC curves for heating of methylcellulose solutions of different concentration at 10 °C min^{-1}. (Reproduced from Chen et al. [169] with permission of Wiley)

The E_α versus T plots obtained from the E_α dependencies estimated by an isoconversional method are shown in Fig. 3.66. All three plots have a similar concave downward shape but shift to higher E_α values with increasing the concentration of the solutions. The initial decreasing portion of the E_α versus T dependence is consistent with that predicted by the Turnbull and Fisher model. Indeed, Eq. 3.90 suggests that just above T_{gel}, the E_α values should be large but decrease toward E_D as temperature continues to rise above T_{gel} (see Fig. 3.50 and related discussion). However, the final increasing portion cannot be rationalized within the aforementioned model.

An increase in E_α in the later stages of gelation (Fig. 3.66) is likely to be associated with changing conditions of diffusion. Cross-linking of polymer chains obstructs their mobility so that the formation of new cross-links may encounter continuously growing energy barrier to diffusion. This means that the constant activation energy

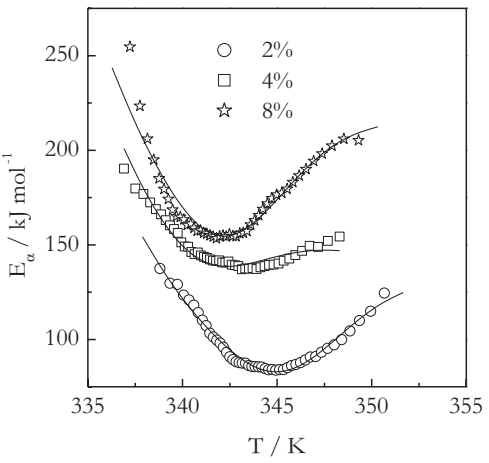

Fig. 3.66 Fits of Eq. 3.91 to experimental E_α versus T dependencies. (Reproduced from Chen et al. [169] with permission of Wiley)

in Eq. 3.90 needs to be replaced with the value that increases with increasing α. A similar approach is used to adequately describe the temperature dependence of viscosity in a system undergoing reactive polymerization [174]. A rather simple modification of Eq. 3.90:

$$E = \varepsilon\alpha^n - A\left[\frac{2T}{\left(T_{gel} - T\right)^3} - \frac{1}{\left(T_{gel} - T\right)^2}\right] \tag{3.91}$$

has proven [169] to be sufficient to account for the effect. Equation 3.91 includes three parameters. The parameter A represents a contribution of the nucleation process to the overall temperature dependence. This contribution manifests itself through a decreasing dependence of E on T. The increasing portion of the dependence corresponds to the diffusion contribution that is represented by the parameters ε and n. By its meaning, ε is the activation energy of diffusion at complete conversion, i.e., at $\alpha = 1$. The parameter n characterizes the strength of diffusion contribution: the smaller the n, the stronger the contribution, i.e., becomes operative earlier and contributes more.

Fitting Eq. 3.91 to the experimental dependencies (Fig. 3.66) requires knowledge of the T_{gel} values. They have been reported by Takahashi et al. [175] and are about 40, 38, and 36 °C for 2, 4, and 8% solutions, respectively. The resulting fits are statistically significant. The values of the adjustable parameters are given in Table 3.3. The diffusion parameters reflect an increasing contribution of diffusion to the overall temperature dependence with increasing concentration. When comparing the 2 and 8% solutions, an increase in the concentration results in larger ε (i.e., larger activation energy of diffusion at $\alpha = 1$) as well as in smaller n (i.e., larger strength of the contribution). The behavior of the 4% solution is a bit more complex. Compared to the 2% solution, it shows 10% smaller ε that would be consistent with a slightly smaller diffusional contribution. However, it also demonstrates 2.5 smaller n that suggests the overall diffusional contribution to be stronger and larger compared to the 2% solution.

On the other hand, the nucleation parameter A can be used to estimate of the free energy barrier to nucleation at any temperature as follows (see Eq. 3.44):

$$\Delta G^* = \frac{A}{\left(T_{gel} - T\right)^2}. \tag{3.92}$$

For comparison purposes, the ΔG^* values can be estimated at $T = 60$ °C, which is the threshold temperature above which gelation becomes detectable by DSC

Table 3.3 The results of fitting Eq. 3.91 to experimental E_α versus T dependencies

C (%)	A (K^2 kJ mol^{-1})	ε (kJ mol^{-1})	n	ΔG^*(60 °C; kJ mol^{-1})
2	3315.4	95.0	5	8.3
4	4879.8	85.2	2	10.1
8	6915.0	151.9	3	12.0

(Fig. 3.65). The resulting ΔG^* (Table 3.3) do not demonstrate any significant dependence on the concentration and are around 10 kJ mol^{-1}, which is comparable to the energy of a hydrogen bond [139]. Note that breaking a hydrogen bond between water and methoxyl group is likely to be a limiting step in nucleation of methylcellulose microcrystallites that serve as cross-link points in the gel. Overall, empirical application of the Turnbull–Fisher model suggests that the effect of the concentration on the kinetics of gelation of aqueous methylcellulose is due to a change in the conditions of diffusion but not the conditions of nucleation.

To conclude this section, we need to mention an interesting fact that the solutions that normally gel on cooling can be made to gel on heating [164, 176]. Anomalous gelation of this kind can be accomplished when the solution is cooled fast enough to outrun gelation. Then the solution can reach a supercooled state that can be turned into gel on heating. This situation is similar to cooling the melt fast enough to bypass crystallization so that it turns into a glass which can then crystallize on heating, i.e. undergo cold crystallization. It has been demonstrated [176] that in very diluted (~1 wt.%) solutions of gelatin, gelation can be suppressed when the solutions are cooled at 20 °C min^{-1}. However, the solutions of regular concentration that gel much faster require very fast cooling rates to bypass gelation. For example, suppressing gelation in a 40 wt.% solution of gelatin requires the solution to be cooled not slower than 500 °C s^{-1} [164]. Such fast cooling rates are accomplishable when using ultrafast DSC [177] on samples of very small (typically submicrogram) masses.

Figure 3.67 shows ultrafast DSC data obtained on heating of supercooled gelatin solution. The application of an isoconversional method to these data results in a

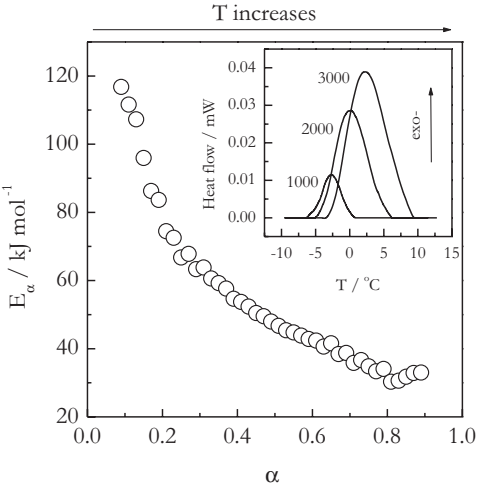

Fig. 3.67 Variation of the activation energy with conversion for gelation of 40 wt.% aqueous solution of gelatin on heating. The inset shows DSC curves obtained at the heating rates 1000, 2000, and 3000 °C s^{-1}. Prior to heating, the solution was cooled at 1000 °C s^{-1}. (Adapted from Guigo et al. [164] with permission of RSC)

decreasing dependence of effective activation energy on conversion (Fig. 3.67). It is noteworthy that the activation energies are positive and decrease toward zero as one would expect when gelation occurs below T_{max} (Fig. 3.60). Recall that it is exactly the type of dependence predicted by the Hoffman–Lauritzen model (see Fig. 3.36) for this temperature range. It is yet another example that illustrates the usefulness of the nucleation crystallization models as applied to the process of physical gelation.

3.10.3 Isoconversional Treatment of Gel Melting

As mentioned earlier, reaching equilibrium state in the two-phase gel region (Figs. 3.58 and 3.59) is generally very slow process. For example, Djabourov et al. [161] have found that 4.7 wt.% gelatin gel could not attain equilibrium at 10.5 °C for 42 days! It means that normally the two-phase gels are nonequilibrium systems, whose structure and properties depend on thermal history. This dependence manifests itself profoundly in the process of melting that can be readily studied by DSC.

The DSC peaks of gel melting can provide some quick clues about the gel network structure in terms of the total number of the network junctions points (i.e., the number of cross-links) and their size (i.e., the number of cross-links per junction). The total heat of melting is directly proportional to the number of cross-links, but it does not tell anything about the number of cross-links per junction. Indeed, the same amount of heat would be produced by melting of two gels prepared from the same amount of the same solution, if one of the gels has 100 junctions with 10 cross-links per junction and another 10 junctions with 100 cross-links per junction. However, these two gels would differ significantly in their thermal stability. The gel having more cross-links per junction has more stable junctions, breaking which would require more thermal energy. Thus, it would melt at higher temperature. Therefore, the gel meting temperature, taken from DSC as either peak or interpolated onset temperature, is representative of the size of network junctions. On the other hand, a change in thermal stability can also be expected to reveal itself in the value of the activation energy of gel melting [178].

The effect of the gel structure on the activation energy of aqueous gelatin gel melting has been explored in a kinetics study [178] that combined isoconversional method with extensive DSC measurements. Figure 3.68 demonstrates the effect of isothermal annealing time on DSC peaks of gel melting. The peaks obviously increase in size with increasing the annealing time. This is indicative of continuously increasing number of junctions. It is noteworthy that although the melting peak obtained after 2 h of annealing is about twice the size of the peak produced after 15 min, the peak temperature for these two peaks is nearly identical. That is, annealing appears to promote predominately the formation of new junctions rather than the growth of the existing ones. Since thermal stability of the gel is not affected significantly during annealing, it is reasonable to expect that the activation energies of gel melting would not be affected either.

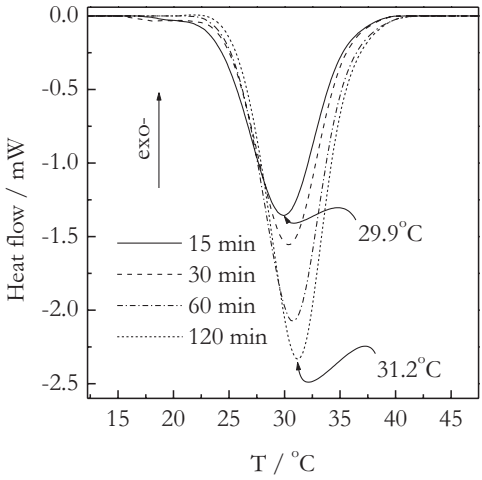

Fig. 3.68 Melting of 40 wt.% gels formed on annealing at 20 °C for periods of time from 15 to 120 min. Curved arrows mark the peak positions. Heating rate is 2.5 °C min^{-1}, sample mass 70.8 mg. (Reproduced from Dranca and Vyazovkin [178] with permission of Elsevier)

The isoconversional dependencies of the activation energy for the gelatin gel melting are seen in Fig. 3.69. As expected, the E_α dependencies evaluated for melting of the gels annealed for different periods are practically identical. For both systems, the effective activation energy decreases significantly (from ~170 to 95 kJ mol^{-1}) throughout the process of melting. Finding that E_α varies with α is typically a sign that the overall process includes multiple steps having different activation energies (see Sect. 1.2). It could be construed that the gel formed may consist of the network junctions having different stability (i.e., size) and, thus, a different energy barrier to melting. However, in such a case, the less stable junctions would disintegrate first followed by disintegration of the more stable ones so that the E_α value would rather have to increase with increasing α.

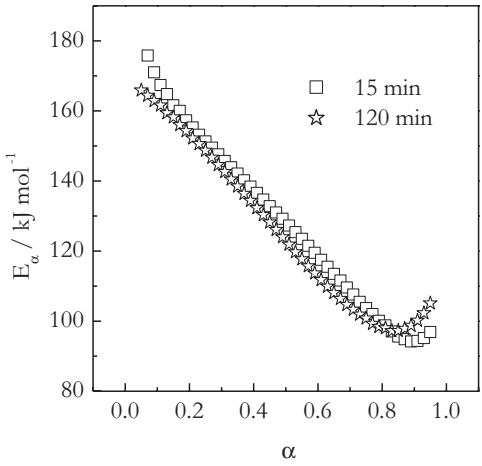

Fig. 3.69 E_α dependencies obtained for melting of 40 wt.% gels annealed at 20 °C for 15 and 120 min. (Reproduced from Dranca and Vyazovkin [178] with permission of Elsevier)

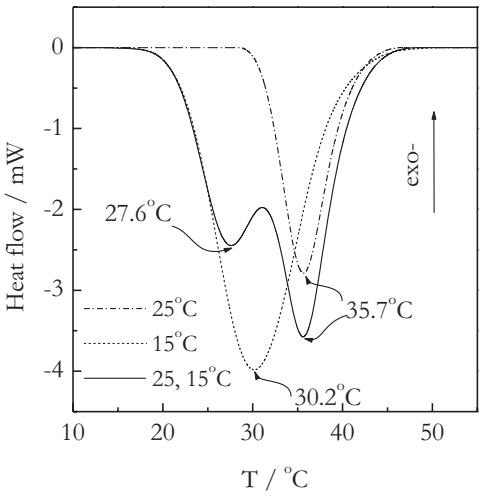

Fig. 3.70 Melting of 40 wt.% gel obtained in one- and two-step annealing at heating rate is 5 °C min^{-1}. Temperature of the annealing steps is shown by the curve types. Duration of each step is 30 min. *Curved arrows* mark the peak positions. (Adapted from Dranca and Vyazovkin [178] with permission of Elsevier)

On the other hand, the decrease observed in Fig. 3.69 is remarkably similar to that seen for the glass transition in various glasses (Sect. 3.3.2). In glasses, a large energy barrier for the initial stages of the process corresponds to strongly cooperative molecular motion under the conditions of constricted free volume. As the temperature rises, the free volume increases, relieving energetic constrains and causing the E_α values to decrease. Something similar is likely to occur in melting of gelatin gels. That is, disintegration of a typical network junction requires cooperative breaking of multiple hydrogen bonds that cross-link the polypeptide chains. Considering that typical range of hydrogen bond energies is 10–40 kJ mol^{-1} [139], the E_α values for the initial stages of melting (Fig. 3.69) can be interpreted as cooperative breaking of 5–15 bonds. After the initial large energy barrier is surmounted and multiple cross-links are broken, the polypeptide chains of the network junction gain new conformational degrees of freedom. The freed chain mobility destabilizes the network junction, therefore, lowering the energy barrier to melting.

Conversely, annealing temperature has a profound effect on thermal stability. DSC curves for melting of two gels annealed for the same period of time at two respectively different temperatures are shown in Fig. 3.70. The gel obtained at 15 °C demonstrates a larger heat of melting; that means, it has a larger number of junctions. However, the gel produced at 25 °C melts at about 5–6 °C higher temperature that suggests its network junctions contain more cross-links. The observed increase in thermal stability should entail an increase in the activation energy of gel melting. The respective E_α dependencies are presented in Fig. 3.71. Both dependencies are of the same shape as that observed in Fig. 3.69 that hints the similarity of the melting mechanisms. Nevertheless, the activation energies for melting of the gel annealed at 25 °C are consistently

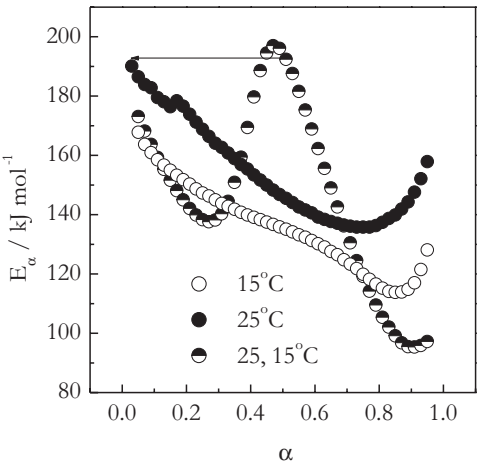

Fig. 3.71 E_α dependencies obtained for melting of 40 wt.% gels obtained in one and two 30-min annealing steps performed at temperatures shown by the point types. *Arrow* shows respectively comparable parts of two- and one-step annealing processes. (Reproduced from Dranca and Vyazovkin [178] with permission of Elsevier)

larger by 10–30 kJ mol^{-1} than those for the gel produced at 15 °C that indicates that the former gel has a few more hydrogen bonds per junction than the latter.

Another instructive experiment that illuminates the effect of the structure on gel melting involves two successive 30-min steps of annealing at 25 and 15 °C. A DSC curve for melting of the resulting gel is displayed in Fig. 3.70. The curve reveals two distinct melting peaks that apparently reflect the existence of two gel structures, which differ markedly in their thermal stabilities. The higher-temperature melting peak is found at the same temperature as the melting peak for the gel produced by single-step annealing at 25 °C. This is in agreement with the rheological measurements [179] that demonstrate that the structures formed at higher annealing temperatures are conserved during annealing at lower temperatures. In contrast, the lower temperature peak is detected at about 2–3 °C lower than the melting peak temperature for the gel produced by single-step annealing at 15 °C. That is, the gel produced on annealing at 15 °C in the two-step procedure is less thermally stable than the one formed in a single-step annealing at 15 °C. It means that the existence of the gel structures formed at 25 °C hinders the growth of the network junctions being formed at 15 °C. Apparently, the hindrance is due to the fact that in partially cross-linked gel, the conformational degrees of freedom of the polypeptide chains are largely restricted. Therefore, it is more difficult for new cross-links to form and for the network junctions to grow.

The E_α dependence determined for melting of the gel annealed consecutively at 25 and 15 °C is shown in Fig. 3.71. The dependence is easy to understand by comparison with the individual dependencies estimated for melting of the gels produced by the respective single-step annealings at 15 and 25 °C. The initial descending portion of the dependence is similar to the initial portion of the E_α dependence for melting of the gel annealed at 15 °C. For both dependencies, the E_α values at the lowest conversions are ~170 kJ mol^{-1} that suggests that the energy barriers to melting in both gels are similar. According to DSC (Fig. 3.70), melting of the gel structures formed on annealing at 15 °C contributes less to the total heat of

melting than melting of the gel structures formed on annealing at 25 °C. For this reason, a transition from melting of the lower temperature structures to melting of the higher temperature structures should occur at conversion less than 0.5. Indeed, the descending E_α dependence breaks down around $\alpha = 0.3$ and climbs sharply to $E_\alpha \approx 195$ kJ mol^{-1} at $\alpha \approx 0.5$. Since that point on the overall melting process becomes dominated by melting of the gel structures formed on annealing at 25 °C. Accordingly, the initial values of E_α for the second descending part are similar to the respective E_α values estimated for melting of the gel prepared at 25 °C. It is quite remarkable that the initial parts of both descending E_α dependencies reveal the existence of two differing energy barriers whose values agree with the values found for melting of the individual gels produced by annealing at 15 and 25 °C, respectively.

The gel structure becomes increasingly more complex when gels are prepared under the conditions of nonisothermal cooling. DSC melting data of gels prepared by continuous cooling at 1 °C min^{-1} are presented in Fig. 3.72. By comparison to isothermally prepared gels, these gels melt over a significantly wider temperature range. This indicates the existence of a wide distribution of the gel structures having differing thermal stabilities. On cooling, gelation initiates at ~40 °C, peaks at ~23.0 (40 wt.%) or 20.6 °C (20 wt.%), and finishes around 0 °C. Nonisothermal gelation can be thought of as a large number of short isothermal annealing steps conducted consecutively in the temperature range from 40 to 0 °C. Such annealing program should produce a large number of gel structures whose melting temperatures decrease with decreasing the annealing temperature in a manner similar to that shown in Fig. 3.70. The mass fractions of the structures should depend on the rate of cross-linking (Fig. 3.72). At the cooling rate 1 °C min^{-1}, the rate maxima occur around 20 ± 5 °C so that the structures formed in largest fractions should be expected to have thermal stability similar to that of the structures formed on isothermal annealing at 15, 20, and 25 °C. However, gelation continues at slower yet significant rate at temperature below 15 °C. This process should yield the gel structures whose

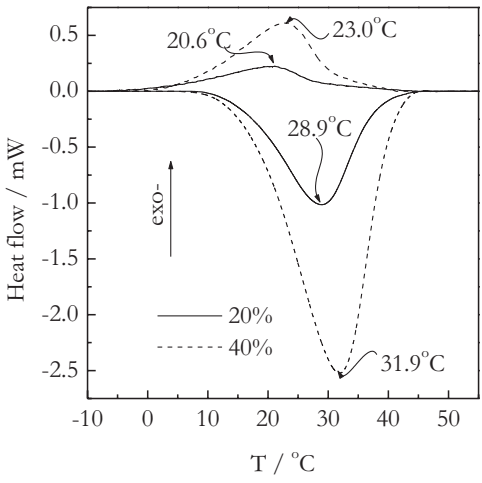

Fig. 3.72 Formation and melting of the gels obtained from 20 and 40 wt.% solutions. Exothermic gelation is measured on cooling at 1 °C min^{-1}, endothermic melting at 5 °C min^{-1}. (Reproduced from Dranca and Vyazovkin [178] with permission of Elsevier)

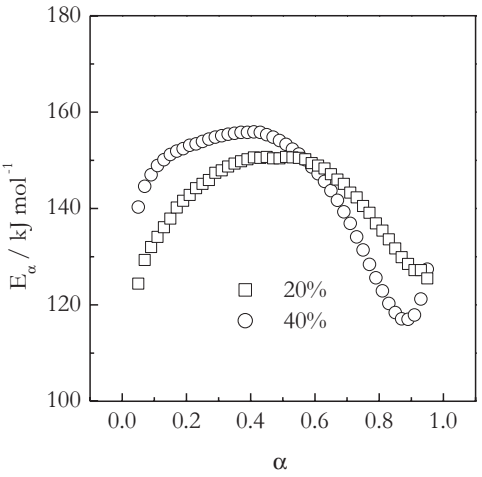

Fig. 3.73 E_α dependencies obtained for melting of 20 and 40 wt.% gels obtained on cooling of the respective solutions at 1 °C min^{-1}. (Reproduced from Dranca and Vyazovkin [178] with permission of Elsevier)

melting temperatures are lower than that of the gel prepared isothermally at 15 °C. These structures would have lower thermal stability and, thus, their melting should encounter a lower energy barrier.

The isoconversional activation energies evaluated for melting of nonisothermally prepared gels are displayed in Fig. 3.73. The resulting E_α dependencies differ noticeably from those found (Figs. 3.69 and 3.71) for melting of isothermally prepared gels. The initial part ($\alpha < 0.4$) of both dependencies is increasing. The initial E_α values are markedly smaller than the initial values estimated for melting of the isothermally prepared gels. This clearly suggests the existence of the gel structures whose disintegration encounters a lower energy barrier or, in other words, the presence of the structures, whose network junctions have fewer cross-links. While raising temperature, melting progresses by involving the structures of continuously increasing thermal stability that gives rise to the increasing E_α dependence. Note that the E_α values never rise to the values observed (Figs. 3.69 and 3.71) for the initial stages of melting of the gels prepared isothermally at 15 and 20 °C despite the aforementioned fact that the gel structures formed at 20 ± 5 °C should be present in the largest mass fraction. This is because melting of more thermally stable structures occurs in parallel with the continuing melting of less thermally stable structures so that the activation energy of the overall process is about the weight average of the activation energies of the individual parallel processes.

Once these most abundant structures become involved in melting, the E_α dependence becomes decreasing. Although there still are more thermally stable structures in the remaining gel, they are present in progressively smaller amounts so that the overall melting process is dominated by the later stages of melting of less thermally stable structures. As a result, the observed E_α dependence is similar to that estimated gels prepared by isothermal annealing at 15 and 20 °C.

In conclusion, we should mention that melting is not the only process that occurs on heating of gels. It should be remembered that as long as temperature is below the equilibrium value of T_{gel}, the solution formed by melting is capable of converting

to gel. The formation of gelation gels on heating has already been discussed [164, 176] (Sect. 3.10.2). It is also detectable during melting by using TM DSC that demonstrates [178] that about 40% of the melting heat is found in the reversing signal. That is, a substantial fraction of melted gel can form new gel structures that would have greater thermal stability than the structures melted. Perhaps, a small increase in E_α detectable at $\alpha > 0.8$ (Figs. 3.69, 3.71, and 3.73) is associated with melting of these newly formed structures of the highest thermal stability.

3.11 Helix–Coil Transition

Undoubtedly this, too, is a structure, growing and piling itself up in endless spiral lines

Victor Marie Hugo, Notre Dame de Paris

3.11.1 Background

In a solution, polymer chains normally assume the structure of a random coil. However, some polymers can assume an ordered helical structure [180]. The most notable examples of polymers forming helical structures include polypeptides, DNA, and RNA. The helical structure is stable within certain pressure and temperature limits and can be converted to the disordered coil structure by changing either of these parameters. The resulting helix–coil transition is a transition between the helical and coil phases. The transition has been commonly studied in proteins, which are composed of long-chain polypeptides.

In proteins, one recognizes the native and denatured states that respectively have the helical and coiled structure. From thermodynamic standpoint, the native and denatured states can coexist in equilibrium under certain temperature–pressure conditions as described by an elliptical phase diagram [181] shown in Fig. 3.74. At

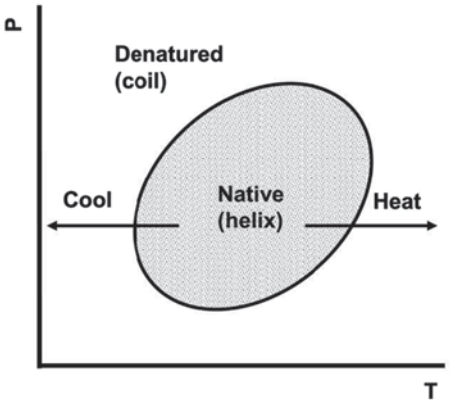

Fig. 3.74 Elliptical phase diagram of a protein. The *solid line* encompasses the area where a protein is stable in its native helical state. Outside this area a protein is stable in the denatured coiled state

a constant pressure, the helix–coil transition can be initiated by either cooling or heating. In the latter case, a protein is said to be thermally denatured. Heating of a protein causes breaking of hydrogen bonds that hold polypeptide chains in the helical conformation. As a result, the helices unfold, forming disordered coils. Since the polypeptide chains do not break but only change their conformation, the process is a phase transition somewhat similar to polymer melting. It is accompanied by significant absorption of heat that qualifies it as a first-order transition.

Unfolding of proteins is a very complex phenomenon that involves interplay of kinetic and thermodynamic factors. A largely simplified mechanism of the process was proposed by Lumry and Eyring [182].

$$\mathrm{N} \overset{K}{\Leftrightarrow} \mathrm{U} \overset{k}{\rightarrow} \mathrm{D}, \tag{3.93}$$

where N, U, and D stand respectively for the native, unfolded, and denatured states, K is the equilibrium constant of the reversible step, and k is the rate constant of the irreversible step. The model is found to be most suitable for denaturation under the conditions of high irreversibility [183]. A similar mechanism (Eq. 3.93) is used to describe the kinetics of various processes that include so-called pre-equilibria. Two most known examples are surface-catalyzed reactions that involve a reversible adsorption step (the Eley–Rideal mechanism) and enzyme-catalyzed reaction that involves a reversible formation of a bound state between the enzyme and its substrate (the Michaelis–Menten mechanism) [18]. The application of the Lumry–Eyring model to the kinetics of protein denaturation has been discussed at length in the literature [183, 184].

The rate equation for the Lumry–Eyring model is derived as follows. The rate of the formation of the denatured state is:

$$\frac{\mathrm{d}x_{\mathrm{D}}}{\mathrm{d}t} = kx_{\mathrm{U}}, \tag{3.94}$$

where x_{D} and x_{U} are respectively the mole fractions of the denatured and unfolded states. The unknown concentration of the unfolded state can be eliminated considering that the sum of all three fractions is unity, and the fraction of the native state x_{N} is related to that of the unfolded state via the equilibrium constant:

$$K = \frac{x_{\mathrm{U}}}{x_{\mathrm{N}}}. \tag{3.95}$$

Then

$$x_{\mathrm{U}} = 1 - x_{\mathrm{D}} - \frac{x_{\mathrm{U}}}{K}. \tag{3.96}$$

After some rearrangements, Eq. 3.96 converts to Eq. 3.97:

$$x_U = \frac{K}{K+1}(1 - x_D). \tag{3.97}$$

Considering that by its meaning x_D is the extent of conversion of the native to denatured state, we can replace it by customarily used α. Then substitution of Eq. 3.97 into 3.94 gives:

$$\frac{d\alpha}{dt} = \frac{kK}{K+1}(1-\alpha). \tag{3.98}$$

Equation 3.98 can now be used to derive the effective activation energy as follows:

$$E_{ef} = -R\left[\frac{\partial \ln(d\alpha / dt)}{\partial T^{-1}}\right]_\alpha = E + \frac{\Delta H^0}{K+1}, \tag{3.99}$$

where E is the activation of the irreversible step (U → D) and ΔH^0 is the enthalpy of the reversible step (N ⇔ U). The effective activation energy obviously depends on temperature because the equilibrium constant in Eq. 3.99 is temperature dependent. The general trend of this dependence is depicted in Fig. 3.75. It suggests that in the low temperature limit, i.e., just above equilibrium, the temperature dependence of the denaturation rate should demonstrate the effective activation energy close to the sum of the activation of the irreversible step and the enthalpy of the reversible step. Note that denaturation is an endothermic process, i.e., $\Delta H^0 > 0$. However, as the process temperature shifts further from the equilibrium value, the effective activation energy should asymptotically approach the activation energy of the irreversible step.

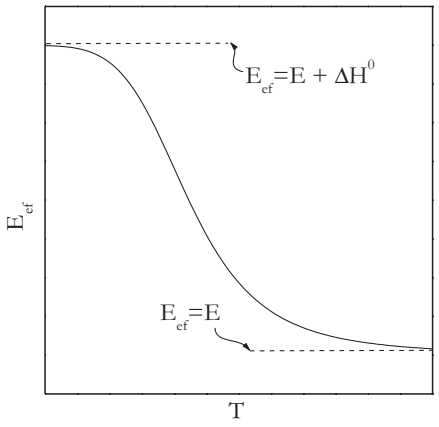

Fig. 3.75 Theoretical temperature dependence of the effective activation energy as derived from the Lumry–Eyring model (Eq. 3.99)

3.11.2 Isoconversional Treatment of Protein Denaturation

As an example of isoconversional treatment of the helix–coil transition, we consider the thermal denaturation of collagen [185]. The latter is a fibrous protein present in animal connective tissue. In its native form, collagen has a triple helical structure, whose individual strands are held together by hydrogen bonds. On heating, collagen undergoes thermal denaturation, during which the hydrogen bonds break, and the helices unfold, turning into coils. The process is accompanied by significant heat absorption that permits to monitor its kinetics by DSC.

The kinetics of the thermal denaturation of collagen and other proteins is most commonly treated as a single irreversible step N→D [186, 187], whose rate depends on temperature in accord with the Arrhenius equation. Such treatment of the collagen denaturation takes its origin in the pioneering work by Weir [188], who studied the rate of collagen shrinkage as a function of temperature. From the standpoint of the Lumry–Eyring model, the single-step treatment can be justified only in some special cases [183, 184]. For example, when denaturation occurs far from equilibrium temperature, the process can be treated as a single step describable by a constant activation energy of the irreversible step. Under other conditions, fitting the rate data to a single Arrhenius equation would yield effective activation energy whose value depends on the temperature region of measurements. The closer this region to equilibrium, the more this value would exceed the activation energy of the irreversible step and approach the sum of the activation energy of the irreversible step and the enthalpy of the reversible step.

The review papers [187, 189] report about two dozen values of the activation energy for the thermal denaturation of mammalian tissues. The range of the values is very wide (30–1300 kJ mol^{-1}). The extreme values can perhaps be explained by the strong compensation effect between the estimates of the preexponential factor and activation energy (see Sect. 2.2.2). However, a large fraction of such variation can be rationalized in terms of the temperature dependence of the effective activation energy (Eq. 3.99 and Fig. 3.75). In accord with the Lumry–Eyring model, the interval of E_{ef} variation can be as large as ΔH^0. Note that some of the literature values [190] of ΔH^0 for tissue denaturation exceed 400 kJ mol^{-1}. That is, for denaturation of exactly the same protein, the activation energy measured close to equilibrium can deviate from that measured far from equilibrium by as much as 400 kJ mol^{-1}.

Figure 3.76 displays DSC curves for the thermal denaturation of rehydrated (saturated with water) collagen. The presence of water stabilizes the denatured coiled form of collagen, which is an aqueous solution of gelatin. The process manifests itself in the form of well-defined nearly symmetrical DSC peaks. The endothermic heat of the process is around 60 J g^{-1} [191]. As expected for any kinetic process, the DSC peaks shift to higher temperature with increasing the heating rate.

The importance of the reversible step N ⇔ U in these regular DSC data is highlighted by TM DSC (Fig. 3.77). The latter demonstrates that a substantial fraction (~25 %) of the total heat flow signal arises from reversible process. This obviously lends support to the Lumry–Eyring mechanism (Eq. 3.93) and suggests that the measured kinetics is determined by both reversible and irreversible steps.

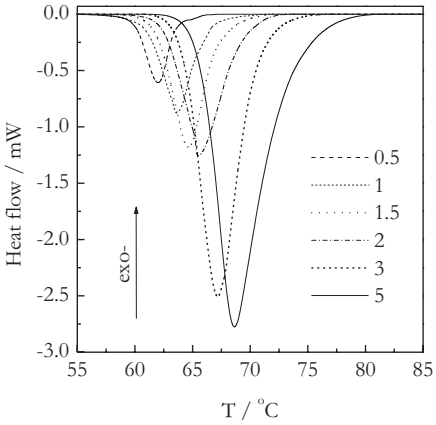

Fig. 3.76 DSC curves for the thermal denaturation of collagen in water measured at different heating rates. *Numbers by the lines* represent the heating rate in °C min^{-1}. (Reproduced from Vyazovkin et al. [185] with permission of Wiley)

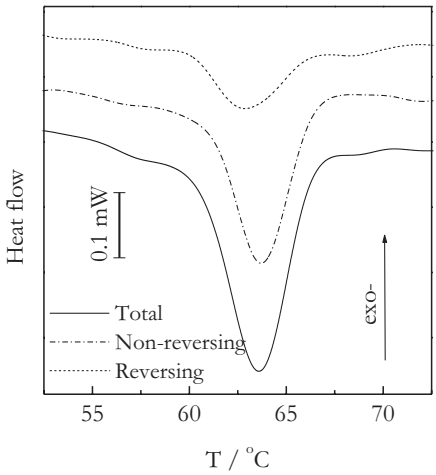

Fig. 3.77 Temperature-modulated DSC data for the thermal denaturation of collagen. The total, nonreversing, and reversing heat flow are respectively presented by *solid, dash,* and *dash-dot lines*. (Reproduced from Vyazovkin et al. [185] with permission of Wiley)

The application of an isoconversional method to the DSC data on thermal denaturation of collagen (Fig. 3.76) results in the E_α dependence seen in Fig. 3.78. Since the conversion increases with increasing temperature, the estimated dependence is consistent with the temperature dependence for the effective activation energy predicted by the Lumry–Eyring model. Undoubtedly, the model is suitable to explain the obtained isoconversional dependence of the effective activation energy. The question is whether it is suitable to extract accurate estimates of the intrinsic parameters from the E_α dependence.

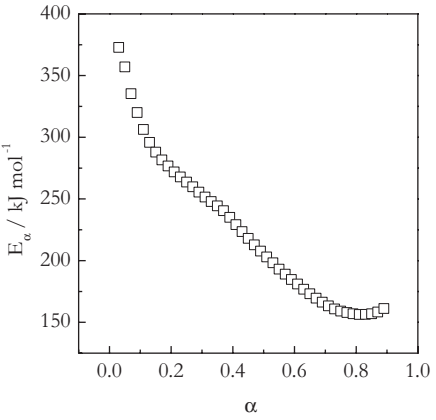

Fig. 3.78 Dependence of the effective activation energy on the extent of conversion determined by an isoconversional method. (Reproduced from Vyazovkin et al. [185] with permission of Wiley)

Clearly, E_α at $\alpha \to 1$ (Fig. 3.78) should provide an estimate for the activation energy of the irreversible step. In that region, the respective E_α values appear to approach asymptotically ~160 kJ mol^{-1}. Nevertheless, as stated earlier, most of the literature E values [187, 189] for the thermal denaturation of mammalian tissues are quite large. For example, a thermal denaturation study [192] of collagen in water in the temperature range 57–60 °C reports an activation energy 518 kJ mol^{-1}. This value is closer to the E_α at $\alpha \to 0$ (Fig. 3.78) that is associated with the lowest temperature range of the DSC data (Fig. 3.76).

E_α at $\alpha \to 0$ is approximately 370 kJ mol^{-1} that ideally should serve as an estimate for $E+\Delta H^0$. The difference between this value and 160 kJ mol^{-1}, which is an estimate for the activation energy of the irreversible step, is ~210 kJ mol^{-1}. This should give an estimate for ΔH^0. It is difficult to judge how accurate this estimate is because E_α at $\alpha \to 0$ does not demonstrate any tendency to plateau at 370 kJ mol^{-1}. Recall that the existence of the low-temperature plateau is predicted from the Lumry–Eyring model (Eq. 3.99 and Fig. 3.75). Therefore, the actual value of ΔH^0 can be larger than 210 kJ mol^{-1}. Nevertheless, this crude estimate fits fairly well within the range of the literature [190] ΔH^0 values: 190–430 kJ mol^{-1}.

The inceptive application [185] of an isoconversional method to denaturation of collagen has been followed by a series of isoconversional studies on several proteins. Several studies [193–196] have been conducted on thermal denaturation of collagen, including denaturation of dry [195] and fish [196] collagen as well as vitrified collagen gels [194]. All these studies demonstrated decreasing E_α dependencies similar to that shown in Fig. 3.78. None of these dependencies has shown a tendency to plateau at small values of α. On the other hand, decreasing E_α dependencies with a well-defined plateau at small α values has been reported [197, 198] for the thermal denaturation of the globular protein lysozyme. Also, a plateau in E_α followed by a decreasing dependence has been found [199] for thermal denaturation of keratin. On the other hand, for the thermal denaturation of bovine serum albumin, the isoconversional activation energy remains practically unchanged throughout the process [200].

References

1. Tammann G (1925) The states of aggregation. van Nostrand, New York
2. Lide DR (ed) (2002) CRC handbook of chemistry and physics, 83rd edn. CRC Press, Boca Raton
3. Debenedetti PG (1996) Metastable liquids. Concepts and principles. Princeton University Press, Princeton
4. Papon P, Leblond J, Meijer PHE (2002) The physics of phase transitions. Springer, Berlin
5. Ehrenfest P (1933) Phasenumwandlungen im ueblichen und erweiterten Sinn, classifiziert nach den entsprechenden Singularitaeten des thermodynamischen Potentiales. Proc Kon Akad Wetensch Amsterdam 36:153–157
6. Rao CNR, Rao KJ (1978) Phase transitions in solids. McGraw-Hill, New York
7. West AR (1992) Solid state chemistry and its applications. Wiley, Chichester
8. Bernstein J (2008) Polymorphism in molecular crystals. Oxford University Press, Oxford
9. Aasland S, McMillan PF (1994) Density driven liquid-liquid phase separation in the system Al_2O_3-Y_2O_3. Nature 369:633–636
10. Katayama Y, Mizutani T, Utsumi W, Shimomura O, Yamakata M, Funakoshi K (2000) A first-order liquid-liquid phase transition in phosphorus. Nature 403:170–173
11. Kurita R, Tanaka H (2004) Critical-like phenomena associated with liquid-liquid transition in a molecular liquid. Science 306:845–848
12. Kurita R, Tanaka H (2005) On the abundance and general nature of the liquid–liquid phase transition in molecular systems. J Phys Condens Matter 17:L293–L302
13. Guenet J-M (1992) Thermoreversible gelation of polymers and biopolymers. Academic, London
14. Collings PJ (2002) Liquid crystals. Nature's delicate phase of matter. Princeton University Press, Princeton
15. Langmuir I (1913) Chemical reactions at very low pressures. J Am Chem Soc 35:105–127
16. Langmuir I (1913) The vapor pressure of metallic tungsten. Phys Rev 2:329–342
17. Knudsen M (1909) Die Molekularströmung der Gase durch Offnungen und die Effusion. Ann Phys 333:999–1909
18. Atkins P, de Paula J (2010) Physical chemistry, 9th edn. W.H. Freeman, New York
19. Price DM, Hawkins M (1998) Calorimetry of two disperse dyes using thermogravimetry. Thermochim Acta 315:19–24
20. Chatterjee K, Dollimore D, Alexander K (2001) A new application for the Antoine equation in formulation development. Int J Pharm 213:31–44
21. Pieterse N, Focke WW (2003) Diffusion-controlled evaporation through a stagnant gas: estimating low vapour pressures from thermogravimetric data. Thermochim Acta 406:191–198
22. Seager SL, Geertson LR, Giddings JC (1963) Temperature dependence of gas and vapor diffusion coefficients. J Chem Eng Data 8:168–169
23. Vecchio S, Di Rocco R, Ferragina C (2008) Kinetic analysis of the oxidative decomposition in γ-zirconium and γ-titanium phosphate intercalation compounds. The case of 2,2'-bipyridyl and its copper complex formed in situ. Thermochim Acta 467:1–10
24. Vyazovkin S, Clawson JS, Wight CA (2001) Thermal dissociation kinetics of solid and liquid ammonium nitrate. Chem Mater 13:960–966
25. Cheng Y, Huang Y, Alexander K, Dollimore D (2001) A thermal analysis study of methyl salicylate. Thermochim Acta 367–368:23–28
26. Vyazovkin S, Chrissafis K, Di Lorenzo ML, Koga N, Pijolat M, Roduit B, Sbirrazzuoli N, Suñol JJ (2014) ICTAC kinetics committee recommendations for collecting experimental thermal analysis data for kinetic computations. Thermochim Acta 590:1–23
27. Prado JR, Vyazovkin S (2011) Activation energies of water vaporization from the bulk and from laponite, montmorillonite, and chitosan powders. Thermochim Acta 524:197–201
28. Ashcroft AS (1972) The measurement of enthalpies of sublimation by thermogravimetry. Thermochim Acta 2:512–514
29. Somorjai GA (1968) Mechanism of sublimation. Science 162:755–760

30. Vyazovkin S, Dranca I (2004) A DSC study of α- and β-relaxations in a PS-clay system. J Phys Chem B 108:11981–11987
31. Johari GP, Goldstein M (1970) Viscous liquids and glass transition. II. Secondary relaxation in glasses of rigid molecules. J Chem Phys 53:2372–2388
32. Williams ML, Landel RF, Ferry JD (1955) The temperature dependence of relaxation mechanisms in amorphous polymers and other glass-forming liquids. J Am Chem Soc 77:3701–3707
33. Di Marzio EA, Yang AJM (1997) Configurational entropy approach to the kinetics of glasses. J Res Natl Inst Stand Technol 102:135–157
34. Perez J, Cavaille JY (1995) Thermally stimulated creep: theoretical understanding of the compensation law. J Phys III 5:791–805
35. Vyazovkin S, Dranca I (2006) Activation energies derived from the pre-glass transition annealing peaks. Thermochim Acta 446:140–146
36. Faivre A, Niquet G, Maglione M, Fornazero J, Jal JF, David L (1999) Dynamics of sorbitol and maltitol over a wide time-temperature range. Eur Phys J B 10:277–286
37. Beiner M, Garwe F, Schroter K, Donth E (1994) Ageing effects on dynamic shear moduli at the onset of the dynamic glass transition in two poly(alkyl methacrylate)s. Polymer 35:4127–4132
38. Chen HS, Morito N (1985) Sub-Tg α′ relaxation in a PdCuSi glass; internal friction measurements. J Non-Cryst Solids 72:287–299
39. Colmenero J, Alegria A, Alberdi JM, del Val JJ, Ucar G (1987) New secondary relaxation in polymeric glasses: a possible common feature of the glassy state. Phys Rev B 35:3995–4000
40. Hodge IM (1994) Enthalpy relaxation and recovery in amorphous materials. J Non-Cryst Solids 169:211–266
41. Vyazovkin S, Dranca I (2005) Physical stability and relaxation of amorphous indomethacin. J Phys Chem B 109:18637–18644
42. Moynihan CT, Eastel AJ, Wilder J, Tucker J (1974) Dependence of the glass transition temperature of heating and cooling rate. J Phys Chem 78:2673–2677
43. Moynihan CT, Lee SK, Tatsumisago M, Minami M (1996) Estimation of activation energies for structural relaxation and viscous flow from DTA and DSC experiments. Thermochim Acta 280/281:153–162
44. Vyazovkin S, Sbirrazzuoli N, Dranca I (2006) Variation in activation energy of the glass transition for polymers of different dynamic fragility. Macromol Chem Phys 207:1126–1130
45. Adam G, Gibbs JH (1965) On the temperature dependence of cooperative relaxation properties in glass-forming liquids. J Chem Phys 43:139–146
46. Vyazovkin S, Sbirrazzuoli N, Dranca I (2004) Variation of the effective activation energy throughout the glass transition. Macromol Rapid Commun 25:1708–1713
47. Angell CA, Stell RC, Sichina W (1982) Viscosity-temperature function for sorbitol from combined viscosity and differential scanning calorimetry studies. J Phys Chem 86:1540–1542
48. Lacey D, Nestor G, Richardson MJ (1994) Structural recovery in isotropic and smectic glasses. Thermochim Acta 238:99–111
49. Hancock BC, Dalton CR, Pikal MJ, Shamblin SL (1998) A pragmatic test of a simple calorimetric method for determining the fragility of some amorphous pharmaceutical materials. Pharm Res 15:762–767
50. Badrinarayanan P, Zheng W, Simon SL (2008) Isoconversion analysis of the glass transition. Thermochim Acta 468:87–93
51. Angell CA (1991) Relaxation in liquids, polymers and plastic crystals—strong/fragile patterns and problems. J Non-Cryst Solids 131–133:13–31
52. Bohmer R, Angell CA (1993) Elastic and viscoelastic properties of amorphous selenium and identification of the phase transition between ring and chain structures. Phys Rev B 48:5857–5864
53. Bohmer R, Ngai KL, Angell CA, Plazek DJ (1993) Nonexponential relaxations in strong and fragile glass formers. J Chem Phys 99:4201–4209

54. Huang D, Colucci DM, McKenna GB (2002) Dynamic fragility in polymers: a comparison in isobaric and isochoric conditions. J Chem Phys 116:3925–3934
55. Beiner M, Huth H, Schroter K (2001) Crossover region of dynamic glass transition: general trends and individual aspects. J Non-Cryst Solids 279:126–135
56. Roland CM, Santangelo PG, Ngai KL (1999) The application of the energy landscape model to polymers. J Chem Phys 111:5593–5598
57. Nogales A, Denchev Z, Sics I, Ezquerra TA (2000) Influence of the crystalline structure in the segmental mobility of semicrystalline polymers: poly(ethylene naphthalene-2,6-dicarboxylate). Macromolecules 33:9367–9375
58. Bravard SP, Boyd RH (2003) Dielectric relaxation in amorphous poly(ethylene terephthalate) and poly(ethylene 2,6-naphthalene dicarboxylate) and their copolymers. Macromolecules 36:741–748
59. Struik LCE (1978) Physical aging in amorphous polymers and other materials. Elsevier, Amsterdam
60. Nemilov SV (2000) Physical ageing of silicate glasses at room temperature: general regularities as a basis for the theory and the possibility of a priori calculation of the ageing rate. Glass Phys Chem 26:511–530
61. Nemilov SV (2001) Physical ageing of silicate glasses at room temperature: the choice of quantitative characteristics of the process and the ranking of glasses by their tendency to ageing. Glass Phys Chem 27:214–227
62. Nemilov SV, Johari GP (2003) A mechanism for spontaneous relaxation of glass at room temperature. Philos Mag 21:3117–3132
63. Tanaka Y, Yamamoto T (2012) Enthalpy relaxation of comb-like polymer analysed by combining activation energy spectrum and TNM models. J Non-Cryst Solids 358:1687–1698
64. Petrie SEB (1972) Thermal behavior of annealed organic glasses. J Polym Sci Part A-2 10:1255–1272
65. Chen K, Vyazovkin S (2009) Isoconversional kinetics of glass aging. J Phys Chem B 113:4631–4635
66. Vyazovkin S, Dranca I (2007) Effect of physical aging on nucleation of amorphous indomethacin. J Phys Chem B 111:7283–7287
67. Donth E (2001) The glass transition: relaxation dynamics in liquids and disordered materials. Springer, Berlin
68. Rault J (2003) Ageing of glass: role of the Vogel-Fulcher-Tamman law. J Phys Condens Matter 15: S1193–S1213
69. McKenna GB, Simon SL (2002) The glass transition- its measurement and underlying physics. In: Cheng SZD (ed) Handbook of thermal analysis and calorimetry, vol 3. Elsevier, Amsterdam, pp 49–109
70. Vyazovkin S, Chen K (2007) Increase in effective activation energy during physical aging of a glass. Chem Phys Lett 448:203–207
71. Tombari E, Presto S, Salvetti G, Johari GP (2002) Spontaneous decrease in heat capacity of a glass. J Chem Phys 117:8436–8441
72. Fukao K, Sakamoto A, Kubota Y, Saruyama Y (2005) Aging phenomena in poly(methyl methacrylate) by dielectric spectroscopy and temperature modulated DSC. J Non-Cryst Solids 351:2678–2684
73. Faivre A, Niquet G, Maglione M, Fornazero J, Jal JF, David L (1999) Dynamics of sorbitol and maltitol over a wide time temperature range. Eur Phys J B 10:277–286
74. Carpentier L, Descamps M (2003) Dynamic decoupling and molecular complexity of glass-forming maltitol. J Phys Chem B 107:271–275
75. Cangialosi D, Wubbenhorst M, Schut H, van Veen A, Picken SJ (2004) Dynamics of polycarbonate far below the glass transition temperature: a positron annihilation lifetime study. Phys Rev B 69:134206-1–134206-9
76. Hu L, Yue YZ (2008) Secondary relaxation behavior in a strong glass. J Phys Chem B 112:9053

77. van den Beukel A (1986) Analysis of chemical short range ordering in amorphous Fe40Ni40B20. J Non-Cryst Solids 83:134–140
78. Koebrugge GW, Sietsma J, van den Beukel A (1992) Structural relaxation in amorphous Pd40Ni40P20. Acta Metall Mater 40:753–760
79. Bershtein VA, Egorov VM (1994) Differential scanning calorimetry of polymers: physics, chemistry, analysis, technology. Ellis Horwood Ltd, New York
80. Illers KH (1969) Einfluβ der thermischen Vorgeschichte auf die Eigenschaften von Polyvinylchlorid. Makromol Chem 127:1–33
81. Chen HS (1981) On mechanisms of structural relaxation in a Pd48Ni32P20 glass. J Non-Cryst Solids 46:289–305
82. Chen HS (1981) Kinetics of low temperature structural relaxation in two (Fe-Ni)-based metallic glasses. J Appl Phys 52:1868–1870
83. Bershtein VA, Egorov VM, Emelyanov YA, Stepanov VA (1983) The nature of β-relaxation in polymers. Polym Bull 9:98–105
84. Bershtein VA, Yegorov VM (1985) General mechanism of the β-transition in polymers. Polym Sci USSR 27:2743–2757
85. McCrum NG, Read BE, Williams G (1991) Anelastic and dielectric effects in polymeric solids. Dover, New York
86. Hedvig P (1977) Dielectric spectroscopy of polymers. Wiley, New York
87. Vyazovkin S, Dranca I (2006) Probing beta relaxation in pharmaceutically relevant glasses by using DSC. Pharm Res 23:422–428
88. Kudlik A, Benkhof S, Blochowicz T, Tschirwitz C, Rössler E (1999) The dielectric response of simple organic glass formers. J Mol Struct 479:201–218
89. Ngai KL, Capaccioli S (2004) Relation between the activation energy of the Johari-Goldstein β-relaxation and Tg of glass formers. Phys Rev E 69:031501-1–031501-5
90. Boyer RF (1976) Mechanical motions in amorphous and semi-crystalline polymers. Polymer 17:996–1008
91. Vyazovkin S (2008) Isoconversional kinetics. In: Brown ME, Gallagher PK (eds). The handbook of thermal analysis & calorimetry, vol 5: recent advances, techniques and applications. Elsevier, Amsterdam, pp 503–538
92. Turnbull D, Fisher JC (1949) Rate of nucleation in condensed systems. J Chem Phys 17:71–73
93. Mandelkern L (2004) Crystallization of polymers, vol 2. Cambridge University Press, Cambridge
94. Schultz JM (2001) Polymer crystallization. ACS & Oxford University Press, New York
95. Avrami M (1939) Kinetics of phase change. I General theory. J Chem Phys 7:1103–1112
96. Avrami M (1940) Kinetics of phase change. II Transformation time relations for random distribution of nuclei. J Chem Phys 8:212–224
97. Avrami M (1941) Granulation, phase change, and microstructure kinetics of phase change. III. J Chem Phys 9:177–184
98. Hong PD, Chung WT, Hsu CF (2002) Crystallization kinetics and morphology of poly(trimethylene terephthalate). Polymer 43:3335–3343
99. Kissinger HE (1956) Variation of peak temperature with heating rate in differential thermal analysis. J Res Natl Bur Stand 57:217–221
100. Kissinger HE (1957) Reaction kinetics in differential thermal analysis. Anal Chem 29:1702–1706
101. Vyazovkin S (2002) Is the Kissinger equation applicable to the processes that occur on cooling? Macromol Rapid Commun 23:771–775
102. Cheng SZD, Jin S (2002) Crystallization and melting of metastable crystalline polymers. In: Cheng SZD (ed) Handbook of thermal analysis and calorimetry, vol 3. Elsevier, Amsterdam, pp 167–195
103. Hoffman JD, Lauritzen JI Jr (1961) Crystallization of bulk polymers with chain folding: theory of growth of lamellar spherulites. J Res Natl Bur Stand 65A:297–336

104. Hoffman JD, Davis GT, Lauritzen JI Jr (1976) The rate of crystallization of linear polymers with chain folding In: Hannay NB (ed) Treatise on solid state chemistry, vol 3. Plenum, New York, pp 497–614
105. Toda A, Oda T, Hikosaka M, Saruyama Y (1997) A new method of analysing transformation kinetics with temperature modulated differential scanning calorimetry: application to polymer crystal growth. Polymer 38:231–233
106. Toda A, Arita T, Tomita C, Masamichi H (1999) Temperature-modulated DSC applied to the transformation kinetics of polymer crystallization. Polymer J 31:790–794
107. Vyazovkin S, Sbirrazzuoli N (2004) Isoconversional approach to evaluating the Hoffman-Lauritzen parameters (U* and Kg) from the overall rates of nonisothermal crystallization. Macromol Rapid Commun 25:733–738
108. Vyazovkin S, Dranca I (2006) Isoconversional analysis of combined melt and glass crystallization data. Macromol Chem Phys 207:20–25
109. Shultz JM, Fakirov S (1990) Solid state behavior of linear polyesters and polyamides. Prentice Hall, Engelwood Cliffs
110. Lu XF, Hay JN (2001) Isothermal crystallization kinetics and melting behaviour of poly(ethylene terephthalate). Polymer 42:9423–9431
111. Rahman MH, Nandi AK (2002) On the crystallization mechanism of poly(ethylene terepthalate) in its blends with poly(vinylidene fluoride). Polymer 43:6863–6870
112. Okamoto M, Shinoda Y, Kinami N, Okuyama T (1995) Nonisothermal crystallization of poly(ethylene terephthalate) and its blends in the injection-molding process. J Appl Polym Sci 57:1055–1061
113. Wunderlich B (2005) Thermal analysis of polymeric materials. Springer, Berlin
114. Phillips PJ, Tseng HT (1989) Influence of pressure on crystallization in poly(ethylene terephthalate). Macromolecules 22:1649–1655
115. Runt J, Miley DM, Zhang X, Gallagher KP, McFeaters K, Fishburn J (1992) Crystallization of poly(butylene terephthalate) and its blends with polyarylate. Macromolecules 25:1929–1934
116. Hwang CJ, Chen CC, Chen HL, Yang WCO (1997) Analysis of two-stage crystallization kinetics for poly(ethylene terephthalate)/ poly(ether imide) blends. Polymer 38:4097–4101
117. Chan TW, Isaev AI (1994) Quiescent polymer crystallization: modeling and measurements. Polym Eng Sci 34:461–471
118. Wu TM, Chang CC, Yu TL (2000) Crystallization of poly(ethylene terephthalate-co-isophthalate). J Polym Sci B Polym Phys 38:2515–2524
119. Bosq N, Guigo N, Zhuravlev E, Sbirrazzuoli N (2013) Nonisothermal crystallization of polytetrafluoroethylene in a wide range of cooling rates. J Phys Chem B 117:3407–3415
120. Bosq N, Guigo N, Persello J, Sbirrazzuoli N (2014) Melt and glass crystallization of PDMS and PDMS silica nanocomposites. Phys Chem Chem Phys 16:7830–7840
121. Toda A, Hikosaka M, Yamada K (2002) Superheating of the melting kinetics in polymer crystals: a possible nucleation mechanism. Polymer 43:1667–1679
122. Kovacs AJ, Gonthier A, Straupe C (1975) Isothermal growth, thickening, and melting of poly(ethylene oxide) crystals in the bulk. J Polym Sci Polym Symp 50:283–325
123. Minakov AA, Wurm A, Schick C (2007) Superheating in linear polymers studied by ultrafast nanocalorimetry. Eur Phys J E 23:43–53
124. Minakov AA, van Herwaarden AW, Wien W, Wurm A, Schick C (2007) Advanced nonadiabatic ultrafast nanocalorimetry and superheating phenomenon in linear polymers. Thermochim Acta 461:96–106
125. Toda A, Kojima I, Hikosaka M (2008) Melting kinetics of polymer crystals with an entropic barrier. Macromolecules 41:120–127
126. Sasaki T (2013) Melting of poly(ε-caprolactone) studied by step-heating calorimetry. J Therm Anal Calorim 111:717–724
127. Toda A Private communication
128. Cheng SZD (2008) Phase transitions in polymers. Elsevier, Amsterdam

129. Vyazovkin S, Yancey B, Walker K (2013) Nucleation driven kinetics of poly(ethylene terephthalate) melting. Macromol Chem Phys 214:2562–2566
130. Vyazovkin S, Burnham A K, Criado JM, Pérez-Maqueda LA, Popescu C, Sbirrazzuoli N (2011) ICTAC kinetics committee recommendations for performing kinetic computations on thermal analysis data. Thermochim Acta 520:1–19
131. Vyazovkin S, Yancey B, Walker K (2014) Polymer melting kinetics appears to be driven by heterogeneous nucleation. Macromol Chem Phys 215:205–209
132. Lippits DR, Rastogi S, Hohne GWH (2006) Melting kinetics in polymers. Phys Rev Lett 96:218303-1–218303-4
133. Illers KH (1974) Die Ermittlung des Schmelzpunktes von Kristallinen Polymeren mittels Warmeflusskalorimetrie (DSC). Eur Pol J 10:911–916
134. Thomas DG, Staveley LAK (1952) A study of the supercooling of drops of some molecular liquids. J Chem Soc 4569–4577
135. Wunderlich B (1980) Macromolecular physics, vol 3, Academic, New York
136. Maddox J (1987) Melting is merely skin-thick. Nature 330:599
137. Dash JG (1999) History of the search for continuous melting. Rev Mod Phys 71:1737–1743
138. Devoy C, Mandelkern L (1970) On the heterogeneous nucleation of long-chain molecules. J Chem Phys 52:3827–3830
139. Israelachvili J (1991) Intermolcular & surface forces, 2nd edn. Academic, Amsterdam
140. Hendricks SB, Posnjak E., Kracek FC (1932) Molecular rotation in the solid state. The variation of the crystal structure of ammonium nitrate with temperature. J Am Chem Soc 54:2766–2786
141. Mnyukh Yu (2009) Fundamentals of solid-state phase transitions, ferromagnetism and ferroelectricity, 2nd edn. Yuri Mnyukh, Farmington
142. Villafuerte-Castrejon ME, West AR (1981) Kinetics of polymorphic transitions in tetrahedral structures. Part 2. Temperature dependence of the transition $\beta \leftrightarrow \gamma$ Li2ZnSiO4. J Chem Soc Faraday Trans I 77:2297–2307
143. Balluffi RW, Allen SM, Carter WC (2005) Kinetics of materials. Wiley, Hoboken
144. Riggin MT, Knispel RR, Pintar MM (1972) Cation diffusion study in NH4NO3 by proton spin relaxation. J Chem Phys 56:2911–2918
145. Mullin JW (2002) Crystallization, 4th edn. Butterworth, Oxford
146. Campbell AN, Kartzmark EM (1969) Heats of mixing and dielectric constants of some partially miscible liquid pairs. Can J Chem 47:619–623
147. Kohler F, Rice OK (1957) Coexistence curve of the triethylamine-water system. J Chem Phys 26:1614–1618
148. Vyazovkin S, Sbirrazzuoli N (2000) Effect of viscosity on the kinetics of initial cure stages. Macromol Chem Phys 201:199–203
149. Glasstone S, Laidler K, Eyring H (1941) The theory of rate processes. McGraw-Hill, New York
150. Kartzmark EM (1967) System triethylamine-water: the equilibrium diagram and some physical properties. Can J Chem 45:1089–1091
151. Lark BS, Patyar P, Banipal TS (2007) Temperature effect on the viscosity and heat capacity behaviour of some amino acids in water and aqueous magnesium chloride solutions. J Chem Thermodyn 39:344–360
152. Flory PJ (1974) Introductory lecture. Faraday Discuss Chem Soc 57:229–241
153. de Gennes (1985) Scaling concepts in polymer physics. Cornell University Press, Ithaca
154. Tan HM, Moet A, Hiltner A, Baer E (1983) Thermoreversible gelation of atactic polystyrene solutions. Macrmolecules 16:28–34
155. Eliassaf J, Silberberg A (1962) The gelation of aqueous solutions of polymethacrylic acid. Polymer 3:555–564
156. Heymann E (1935) Studies on sol-gel transformations. I. The inverse sol-gel transformation of methylcellulose in water. Trans Faraday Soc 31:846–864
157. Doolittle AK (1946) Mechanism of solvent section. Influence of molecular size and shape on temperature dependence of solvent ability. Ind Chem Eng 38:535–540

158. Godard P, Biebuyck JJ, Daumerie M, Naveau H, Mercier JP (1978) Crystallization and melting of aqueous gelatin. J Polym Sci Polym Phys Ed 16:1817–1828
159. Domszy RC, Alamo R, Edwards CO, Mandelkern L (1986) Thermoreversible gelation and crystallization of homopolymers and copolymers. Macromolecules 19:310–325
160. Boedtker H, Doty P (1954) A study of gelatin molecules, aggregates and gels. J Phys Chem 58:968–983
161. Djabourov M, Leblond J, Papon P (1988) Gelation of aqueous gelatin solutions. I. Structural investigation. J Phys France 49:319–332
162. Guo L, Colby RH, Lusignan CP, Whitesides TH (2003) Kinetics of triple helix formation in semidilute gelatin solutions. Macromolecules 36:9999–10008
163. Flory PJ, Weaver ES (1960) Helix ↔ coil transition in dilute aqueous collagen solutions. J Am Chem Soc 82:4518–4525
164. Guigo N, Sbirrazzuoli N, Vyazovkin S (2012) Atypical gelation in gelatin solutions probed by ultra fast calorimetry. Soft Matter 8:7116–7121
165. Chen K, Vyazovkin S (2009) Temperature dependence of sol-gel conversion kinetics in gelatin-water system. Macromol Biosci 9:383–392
166. Ohkura M, Kanaya T, Kaji K (1992) Gelation rates of poly(vinyl alcohol) solution. Polymer 33:5044–5048
167. Malik S, Jana T, Nandi AK (2001) Thermoreversible gelation of regioregular poly(3-hexylthiophene) in xylene. Macromolecules 34:274–282
168. Dikshit AK, Nandi AK (2001) Gelation mechanism of thermoreversible gels of poly(vinylidene fluoride) and its blends with poly(methyl acrylate) in diethyl azelate. Langmuir 17:3607–3615
169. Chen K, Baker AN, Vyazovkin S (2009) Concentration effect on temperature dependence of gelation rate in aqueous solutions of methylcellulose. Macromol Chem Phys 210:211–216
170. Harrington WF, Rao NV (1970) Collagen structure in solution. I. Kinetics of helix regeneration in single-chain gelatins. Biochemistry 9:3714–3724
171. Eagland D, Pilling G, Wheeler RG (1974) Studies of the collagen fold formation and gelation in solutions of a monodisperse α gelatin. Faraday Discuss 57:181–200
172. Michon C, Cuvelier G, Launay B (1993) Concentration dependence of the critical viscoelastic properties of gelatin at the gel point. Rheol Acta 32:94–103
173. Kobayashi K, Huang C, Lodge TP (1999) Thermoreversible gelation of aqueous methylcellulose solutions. Macromolecules 32:7070–7077
174. Stolin AM, Merzhanov AG, Malkin AYa (1979) Non-isothermal phenomena in polymer engineering and science: a review-2. Non-isothermal phenomena in polymer deformation. Polym Eng Sci 19:1074–1080
175. Takahashi M, Shimazaki M, Yamamoto J (2001) Thermoreversible gelation and phase separation in aqueous methyl cellulose solutions. J Polym Sci B 39:91–100
176. Guigo N, Sbirrazzuoli N, Vyazovkin S (2012) Gelation on heating of supercooled gelatin solutions. Macromol Rapid Commun 33:698–702
177. Zhuravlev E, Schmelzer JWP, Wunderlich B, Schick C (2011) Kinetics of nucleation and crystallization in poly(ε-caprolactone) (PCL). Polymer 52:1983–1997
178. Dranca I, Vyazovkin S (2009) Thermal stability of gelatin gels: effect of preparation conditions on the activation energy barrier to melting. Polymer 50:4859–4867
179. te Nijenhuis K (1981) Investigation into the ageing process in gels of gelatin/water systems by the measurement of their dynamic moduli—Part II: mechanism of the ageing process. Colloid Polym Sci 259:1017–1026
180. Teramoto A (2001) Cooperative conformational transitions in linear macromolecules undergoing chiral perturbations. Prog Polym Sci 26:667–720
181. Smeller L (2002) Pressure-temperature phase diagrams of biomolecules. Biochim Biophys Acta 1595:11–29
182. Lumry R, Eyring H (1954) Conformation changes of proteins. J Phys Chem 58:110–120

183. Lepock JR, Ritchie KP, Kolios MC, Rodahl AM, Heinz KA, Kruuv J (1992) Influence of transition rates and scan rate on kinetic simulations of differential scanning calorimetry profiles of reversible and irreversible protein denaturation. Biochemistry 31:12706–12712
184. Sanchez-Ruiz JM (1992) Theoretical analysis of Lumry-Eyring models in differential scanning calorimetry. Biophys J 61:921–935
185. Vyazovkin S, Vincent L, Sbirrazzuoli N (2007) Thermal denaturation of collagen analyzed by isoconversional method. Macromol Biosci 7:1181–1186
186. Wright NT, Humphrey JD (2002) Denaturation of collagen via heating: an irreversible rate process. Annu Rev Biomed Eng 4:109–128
187. Bischof JC, He XM (2005) Thermal stability of proteins. Ann NY Acad Sci 1066:1–22
188. Weir CE (1949) Effect of temperature on the volume of leather and collagen in water. J Res Nat Bur Stand 42:17–32
189. Wright NT (2003) On a relationship between the Arrhenius parameters from thermal damage studies. J Biomed Eng 125:300–304
190. Jacques SL (2006) Ratio of entropy to enthalpy in thermal transitions in biological tissues. J Biomed Opt 11:041108-1–041108-7
191. Miles CA, Ghelashvili M (1999) Polymer-in-a-box mechanism for the thermal stabilization of collagen molecules in fibers. Biophys J 76:3243–3252
192. Miles CA, Burjanadze TV, Bailey AJ (1995) The kinetics of the thermal denaturation of collagen in unrestrained rat tail tendon determined by differential scanning calorimetry. J Mol Biol 245:437–446
193. Liu W, Li G (2010) Non-isothermal kinetic analysis of the thermal denaturation of type I collagen in solution using isoconversional and multivariate non-linear regression methods. Polym Degrad Stab 95:2233–2240
194. Xia Z, Calderon-Colon X, Trexler M, Elisseeff J, Guo Q (2012) Thermal denaturation of type I collagen vitrified gels. Thermochim Acta 527:172–179
195. Budrugeac P, Cucos A (2013) Application of Kissinger, isoconversional multivariate nonlinear regression methods for evaluation of the mechanism and kinetic parameters of phase transitions of type I collagen. Thermochim Acta 565:241–252
196. Liu W, Tian Z, Li C, Li G (2014) Thermal denaturation of fish collagen in solution: a calorimetric and kinetic analysis. Thermochimica Acta 581:32–40
197. Cao X, Wang Z, Liu Y, Wang C, Tian Y (2010) Effect of additive on the thermal denaturation of lysozyme analyzed by isoconversional method. Acta Chim Sinica 68:194–198
198. Cao X, Tian Y, Wang Z, Liu Y, Wang C (2014) Protein denaturation kinetic processes of a simple and a complex reaction mechanism analyzed by an iso-conversional method. J Therm Anal Calorim 117:1489–1495
199. Istrate D, Popescu C, Moller M (2009) Non-isothermal kinetics of hard α-keratin thermal denaturation. Macromol Biosci 9:805–812
200. Cao X, Li J, Yang X, Duan Y, Liu Y, Wang C (2008) Nonisothermal kinetic analysis of the effect of protein concentration on BSA aggregation at high concentration by DSC. Thermochim Acta 467:99–106